https://ntrs.nasa.gov/search.jsp?R=19950024406 2020-06-16T06:38:58+00:00Z

NASA-TM-110626

NASA-TM-110626 19950024406

A WIND TUNNEL INVESTIGATION OF THE EFFECTS OF MICRO-VORTEX GENERATORS AND GURNEY FLAPS ON THE HIGH-LIFT CHARACTERISTICS OF A BUSINESS JET WING

BY
MICHELLE THERESE MARTUCCIO

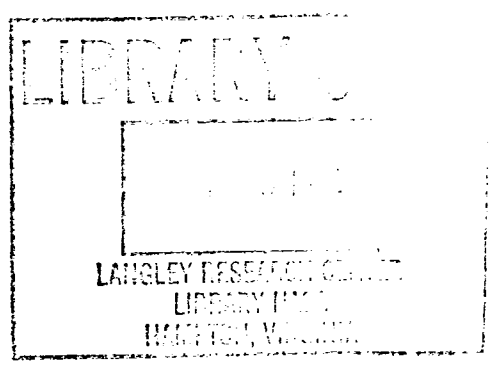
LIBRARY
LANGLEY RESEARCH CENTER
LIBRARY, NASA
HAMPTON, VIRGINIA

NASA Technical Library
3 1176 01422 7145

A Wind Tunnel Investigation of the Effects of Micro-Vortex Generators and Gurney Flaps on the High-Lift Characteristics of a Business Jet Wing

by
Michelle Therese Martuccio
B.S. May 1992, Miami University

LIBRARY COPY
9 1994
LANGLEY RESEARCH CENTER
LIBRARY NASA
HAMPTON, VIRGINIA

A Thesis submitted to

The Faculty of

The School of Engineering and Applied Science
of The George Washington University in partial satisfaction
of the requirements for the degree of Master of Science

August 1994

This research was conducted at NASA Langley Research Center

A Wind Tunnel Investigation of the Effects of Micro-Vortex Generators and Gurney Flaps on the High-Lift Characteristics of a Business Jet Wing

by
Michelle Therese Martuccio
B.S. May 1992, Miami University

A Thesis submitted to

The Faculty of

The School of Engineering and Applied Science
of The George Washington University in partial satisfaction
of the requirements for the degree of Master of Science

August 1994

This research was conducted at NASA Langley Research Center

Abstract

A study of a full-scale, semi-span business jet wing has been conducted to investigate the potential of two types of high-lift devices for improving aircraft high-lift performance. The research effort involved low-speed wind-tunnel tests of micro-vortex generators and Gurney flaps applied to the flap system of the business jet wing and included force and moment measurements, surface pressure surveys and flow visualization on the wing and flap. Results showed that the micro-vortex generators tested had no beneficial effects on the longitudinal force characteristics in this particular application, while the Gurney flaps were an effective means of increasing lift. However, the Gurney flaps also caused an increase in drag in most circumstances.

Acknowledgments

First I would like to thank the National Aeronautics and Space Administration along with the Vehicle Dynamics Branch for providing the opportunity to perform this research and complete all of the other requirements for this degree. I would also like to thank Richard White, John Lin, and Tom Moul who deserve special recognition for their knowledge and advice during the completion of this study. I am also thankful to have had the pleasure of working with Todd, Lou, Mark, Troy and Jay on the Full-Scale Business Jet Project. In addition, a very special thanks goes to Dave, Charlie, Earl, Jody, Rich, Clinton, and "Serg" for their time and patience during model changes - and for making nightshift so much fun. A big thanks goes to Stan for his exceptional work in preparing the figures in this thesis. I would also like to extend a thank you to Don Riley for his helpful comments and suggestions. Thank you also goes to Dr. Vladislav Klein for his advice as my academic advisor.

I am indebted to Dr. Phil Macklin and Dr. Richard Walker, from Miami University, for encouraging me and making "physics (and aeronautics) fun at Miami"! I also owe a debt of gratitude to Kip and Kristy for making all my years as an undergraduate great ones.

I am grateful to have old friends who are always there to listen and support me - thank you Katy, Kent and John. I am also thankful to have met some special people here from the aero club, volleyball, sailing, and the JIAFS program. I am especially grateful to Dale for always believing in me.

Of course I would not even be here without the love and support of my family - Christine, Jennette, Aimee, and Teresa - and especially the two people that have inspired me my entire life - thank you mom and dad.

Table of Contents

List of Tables

List of Figures

List of Symbols

All longitudinal forces and moments are referred to the wind axis system. Moments are presented with respect to a center of gravity location at the quarter chord of the mean aerodynamic chord of the exposed wing.

C_D	measured drag coefficient, $\frac{D}{q_\infty S}$
C_{Dfhvn}	drag coefficient due to the fuselage, horizontal and vertical tails, and nacelles
C_{Dgear}	drag coefficient due to the landing gear
C_{Dtest}	measured drag coefficient, $\frac{D}{q_\infty S}$
C_{Dtot}	total drag coefficient
C_f	micro-vortex generator location in percentage of c_f
C_L	lift coefficient, $\frac{L}{q_\infty S}$
C_{Lmax}	maximum lift coefficient
C_m	pitching moment coefficient, $\frac{M}{q_\infty S\bar{c}}$
$C_{m\alpha}$	change in pitching moment with respect to angle of attack, $\frac{\partial C_m}{\partial \alpha}$
C_p	pressure coefficient, $\frac{P_{STATIC}-P_{REF}}{q_\infty}$
c	local chord, ft
$\bar{c}$	mean aerodynamic chord, ft
c_f	local-flap-chord, ft
c_w	local-wing-chord, ft
D	drag, lbs
d	spacing between counter-rotating micro-vortex generators
g	acceleration due to gravity, 32.2 ft/sec^2

h	height of micro-vortex generator, in
h_{TR}	aircraft height at end of transition distance during takeoff, ft
L	lift, lbs
L/D	lift-to-drag ratio
l	length of micro-vortex generator, in
M	pitching moment, ft-lbs
P_{STATIC}	wing surface static pressure, lbs/in^2
P_{REF}	tunnel static pressure, lbs/in^2
q_∞	free-stream dynamic pressure, lbs/ft^2
R	radius of circular flight path assumed on takeoff, ft
r	leading-edge curvature radius of micro-vortex generator, in
S	wing area, ft^2
S_A	air distance, ft
S_B	braking distance, ft
S_{CL}	climb distance, ft
S_{FR}	free-roll distance, ft
S_G	ground distance, ft
S_L	total landing distance, ft
S_R	rotation distance, ft
S_{TO}	total takeoff distance, ft
S_{TR}	transition distance, ft
T	thrust, lbs
t	thickness of micro-vortex generator, in
V_{STALL}	stall velocity, ft/sec $\sqrt{\frac{2W_{TO}}{\rho S C_{L\,max}}}$
V_{TD}	touchdown velocity, ft/sec $1.15V_{STALL}$

V_{TO}	takeoff velocity, ft/sec $1.2V_{STALL}$
V_{50}	velocity over 50-foot obstacle during landing, ft/sec $1.3V_{STALL}$
W_L	landing weight, lbs
W_{TO}	takeoff weight, lbs
w	base width of micro-vortex generator, in
x	pressure port distance from leading edge of surface, ft
x/c	non-dimensional pressure port location, $\frac{x}{c}$
α	angle of attack, deg
β	micro-vortex generator incidence angle to the flow, deg
δ	boundary-layer thickness, in
γ	leading-edge sweep angle of micro-vortex generator, deg
λ	spacing between micro-vortex generators, in
μ_L	landing friction coefficient during braking
μ_{TO}	takeoff friction coefficient
θ_{CL}	climb angle, deg
ρ	air density, 0.002377 slugs/ft^3

Acronyms

COR	Co-Rotating
CTR	Counter-Rotating
DS	Double-Slotted
ESP	Electronically Scanned Pressure
FAR	Federal Aviation Regulation
MCARF	Multi-Component AiRFoil
MSES	Multi-Surface Euler Solver

MVG	Micro-Vortex Generator
SS	Single-Slotted
TE	Trailing Edge
UAC	United Aircraft Corporation
VG	Vortex Generator

Subscripts

max	maximum value
∞	free-stream value

1.0 Introduction

There is a world-wide demand for more efficient aircraft and increased aircraft performance. Innovative ideas for improving aerodynamic characteristics are necessary to address that demand. One area of study is that of high-lift aerodynamics. The concept of influencing flow to develop high lift has been around since the early 1900's.[1] Although the leading aerodynamicists of that time had plenty of good ideas for achieving high lift, their understanding was incomplete. Advancements in technology, greater quantitative analytic skills and years of experience combine to provide a more complete understanding than that of our predecessors. However, the complicated flow physics associated with high-lift systems still make the design of such systems a challenge.[2] Intense research in the high-lift area continues so that aircraft of the future may reap the benefits.

Many aspects of an aircraft are affected by high-lift systems. Performance, compliance with both safety and aircraft noise regulations, and system complexity are important issues. High-lift systems are used primarily to increase lift coefficients during takeoff and landing operations. If there is an increase in lift without a significant increase in drag, then the lift-to-drag ratio (*L/D*) increases. During takeoff, an increase in *L/D* allows for shorter ground-roll distances and a better rate-of-climb which affects not only aircraft performance but also reduces aircraft noise.

Aircraft noise is becoming a more important issue in today's world. The Federal Aviation Administration is enforcing more restrictive noise regulations. Aircraft built for the future will have to meet the new Stage III noise requirements under Federal Aviation Regulation (FAR) Part 36.[3] These regulations place restrictions on the amount of noise an aircraft is allowed to make during its

takeoff and landing phases based on the weight of the aircraft. Older, noisier aircraft that do not comply with the regulations are being retrofitted with new noise-reducing technology or phased out of service. These new regulations will have a significant impact on takeoff and landing operations. One idea for noise reduction is that aircraft with improved high-lift systems could climb away from the terminal area faster, thus decreasing airport and community noise. Another idea is that with increased *L/D*, aircraft could perform takeoffs at reduced thrust in order to decrease noise levels. However, such a procedure raises safety concerns. Takeoffs at reduced thrust levels prevent the aircraft from gaining altitude as quickly as it is otherwise capable. This altitude could be valuable if an emergency were to occur during the departure phase.

Current high-lift systems generally consist of very complex multi-element airfoil arrangements which usually include a leading-edge slat and two or three trailing-edge flaps. These systems already generate high lift, but it is desired to have a simpler one-flap system that can achieve the same lift as a more complex multi-flap system. A simpler system will allow for reduced weight, improved maintainability, and easier manufacturing, thus reducing the cost of operation.

The NASA Langley Research Center has been conducting analytical studies as well as wind tunnel and flight tests on the high-lift systems of transport aircraft.[4] As part of this broad research program, an investigation of a full-scale, semi-span business jet wing has been conducted in Langley's 30- by 60-Foot Tunnel. Two types of innovative high-lift devices were investigated as part of this effort -- micro-vortex generators and Gurney flaps. This paper presents and discusses the results of the micro-vortex generator and Gurney flap study.

General descriptions of micro-vortex generators and Gurney flaps and their associated flow physics are presented. This is followed by a brief discussion of micro-vortex generator and Gurney flap history along with results of previous investigations of these high-lift devices. Wind tunnel models of the business jet wing and the high-lift devices investigated are then presented. The test conditions are provided along with the experimental results and further discussion. Concluding remarks and recommendations are made.

It should be noted that this study was generic in nature and its intention was to gain knowledge in the area of high-lift aerodynamics and not necessarily to improve the specific aircraft wing being tested.

2.0 Background

The two types of high-lift devices investigated in this study are micro-vortex generators and Gurney flaps (figure 1). These two types of high-lift devices were studied because of their simplicity, potential ease of application and promising results in previous studies.[5-21]

2.1 Micro-Vortex Generators

Micro-vortex generators (MVGs) are sub-boundary layer height devices that are mounted perpendicular to an airfoil surface upstream of a flow separation region in order to prevent or delay turbulent boundary-layer separation. The MVGs generate vortices that trail downstream enhancing mixing between lower-energy air in the boundary layer near the surface and higher-energy air in the outer region of the boundary layer (figure 2). When their location on the surface is properly selected (as discussed further shortly), the MVGs continuously energize the boundary layer. The re-energization of the boundary layer counteracts the natural tendency toward boundary layer retardation and growth due to friction and adverse pressure gradients. Thus, the energized flow can withstand larger adverse pressure gradients without separating.[5,6]

In the past, vortex generators (VGs) have been used to increase mixing between higher-energy free-stream flow and lower-energy boundary-layer flow.[5-12] Vortex generators were first investigated in 1947 by Bruynes and Taylor[7] at United Aircraft Corporation (U. A. C.) as a means of improving the efficiency of a tunnel diffuser by energizing the boundary layer and thus delaying diffuser separation. The VGs introduced by Bruynes and Taylor are the type most often used. Extremely simple in concept, these vane-type

generators project normal to the surface and are set at an angle of incidence to the local flow thus acting as a lifting surface producing single trailing vortices (figure 3). Years later at U. A. C., an investigation of more complex generators (wedge, ramp, Christmas tree, etc., figure 4) was conducted but showed no advantages over the conventional vane-type generators.[8] Vane-type vortex generators have also been used to prevent or delay flow separation and therefore enhance aircraft wing lift.[5,10,11] Another application of these VGs was to reduce afterbody drag on a C-130 aircraft, thus increasing performance.[6]

All of the previously mentioned studies used VGs with a height on the order of the boundary layer thickness (δ). It has been shown that decreasing the height of the conventional vane-type vortex generators to only a fraction of δ (creating the *micro-vortex generators* mentioned earlier), can still provide sufficient mixing for enhanced lift and results in less device drag.[13,14] Studies of micro-vortex generators have recently been conducted and have shown MVGs to be effective at increasing lift and also at decreasing drag in some cases.[14] The study by Lin et al.[14] showed that MVGs can be stowed in the flap-well (figure 5) during cruise resulting in no cruise-drag penalty.

Although the idea of VGs and MVGs has been around for years, the complexity of the resulting flow physics makes theoretically modeling the flow very difficult. Most of the past investigations of VGs involved extensive experimental testing and only occasionally were complimented by theoretical work.[8,10,12] However, recently, a few studies have addressed the need for a model to assist in the optimization of new VG designs.[15,16] The existing models show the correct trends when compared to corresponding experimental data but require some further improvements before they can be effectively used for design.

Micro-vortex generator effectiveness is a function of orientation, spacing and location. There are two basic types of orientations: co-rotating (COR) and counter-rotating (CTR). When MVGs are oriented in a COR configuration, they are all set at the same incidence angle to the flow, usually equally spaced, producing vortices of equal strength that rotate in the same direction (figure 6a). Counter-rotating MVGs are set alternately at positive and negative incidence angles with respect to the flow, again generating vortices of equal strength that now rotate in opposite directions. However, counter-rotating MVGs are arranged in equally spaced pairs (figure 6b). Several studies show that counter-rotating VGs/MVGs more effectively enhance mixing,[7-9,13] while other studies favor co-rotating VGs/MVGs.[10,14]

Correct spacing is the key to establishing an effective vortex pattern.[5] Co-rotating micro-vortex generators should not be placed closer together than three times their height. In the case of co-rotating MVGs, if the vortices are generated too close together, then the low-energy air being swept out by one vortex could be swept into the surface again by the adjacent vortex. Thus when the spacing is too small, the vortices tend to weaken one another. For a CTR configuration, the spacing between each MVG pair should be at least more than four times the device height.[5]

It is necessary to place the MVGs upstream of the flow separation region in order to energize the boundary layer and prevent or delay separation. The distance upstream is determined by the strength of the vortex generated and its orientation. VGs on the order of δ in height tend to generate stronger vortices that trail downstream further than the smaller MVGs that are submerged in the boundary layer. Therefore, conventional VGs may be placed further upstream. Although counter-rotating MVGs are effective over a short distance downstream, they do not maintain their effectiveness as far downstream as co-rotating MVGs.

Therefore, for a longer effective range downstream a co-rotating MVG orientation has advantages over a counter-rotating MVG orientation.[5]

Other factors that determine the effectiveness of MVGs are shape and size. As previously mentioned, more complex vortex generators have not been shown to have any advantages over the conventional vane-type generators. The conventional vane-type generators are usually small plates or airfoils. There are several common shapes for the vane-type generators. Rectangular, delta and trapezoidal shapes (figure 7) have all been shown to be effective.[11-14] The correct size for micro-vortex generators is directly dependent on the boundary-layer thickness. MVGs that are only a fraction of δ can still provide flow mixing over a region several times their own height. Therefore, MVGs can be as small as 20% of δ in height and be effective. Typically, MVGs are not larger than 50% of δ in height.[14] MVGs on the order of 20% of δ in height have a shorter effective range compared to MVGs on the order of 50% of δ in height, but they also have less device drag.

2.2 Gurney Flaps

Gurney flaps effectively increase the camber of an airfoil. As with other trailing-edge (TE) high-lift devices, this results in an increase in maximum lift available along with a reduction in the angle of attack for zero lift. The effects of Gurney flaps on drag characteristics are not as well defined. There are some studies that show that Gurney flaps reduce drag, some show no net changes in drag and some show drag increases relative to a baseline clean-trailing-edge configuration.[17]

Liebeck presented the first description of Gurney flaps in the literature.[18] At the time of his Gurney flap study, the TE flow field of a conventional airfoil was not completely understood.[18] Figure 8a shows the proposed flow field

near the TE of a conventional airfoil operating at a moderate lift coefficient.[18] Separation bubbles occur on the upper and lower surfaces as a result of the boundary layer not being able to withstand the increase in adverse pressure gradient. The results of Liebeck's Gurney flap study showed reduced drag. In an attempt to explain these results, he hypothesized the TE flow field of an airfoil with a Gurney flap (figure 8b).[18] As the air flows over the upper surface of the flap, it is partially deflected down toward the Gurney flap. The Gurney flap helps to keep the flow attached and the effective increase in camber accelerates the flow over the upper surface. The increase in flow velocity results in a decrease in upper-surface pressure. On the lower surface, the air "sees" the corner and separates upstream thus the pressure on the lower surface is increased. The increase in pressure difference between the upper and lower surfaces results in an increase in lift. Years later, Liebeck's hypothesis was confirmed with a low Reynolds number water-tunnel study by Neuhart and Pendergraft (figure 9).[17]

This hypothesis also proposes a reduction in drag. Since the Gurney flap keeps the flow attached longer, the turning of the flow toward the Gurney flap results in a smaller wake deficit than would occur for the no Gurney flap configuration.[18] Other experimental studies showed an increase in drag at low to moderate lift coefficients. In these cases, it is possible that device drag was outweighing the benefits of the Gurney flap. The debate over the effect of Gurney flaps on drag characteristics is ongoing.

Another result of the addition of a Gurney flap to a high-lift system is an increase in nose-down pitching moment due to the increased pressure difference at the rear of the airfoil. Usually this type of increase in nose-down pitching moment can be trimmed with a conventional tail.

The history of Gurney flaps does not date back nearly as far as that of vortex generators. The Gurney flap was developed by Dan Gurney in the 1970's to produce additional "downforce" or negative lift on the inverted airfoil of race car wings. The Gurney flap and rear wing combination on race cars resulted in substantial improvements in obtainable cornering and straight-away speeds due to the increased downforce as well as reduced drag.[18] The application of Gurney flaps to airfoils on aircraft was then also investigated and experimental as well as computational work has been done.[17-21]

Several experimental investigations on race car wings (other than Dan Gurney's) have been done and found Gurney flaps to increase lift as well as drag.[17] Also, studies of Gurney flaps applied to the horizontal tails and vertical fins of various helicopter models were completed and gave similar results.[17]

Applying a Gurney flap system to an aircraft differs from the application to a race car. For an aircraft, the Gurney flap could cause a device-drag penalty and should therefore be stowed while the aircraft is in cruising flight. The possibility of stowing Gurney flaps during cruise was considered by Storms and Jang.[19] Since Gurney flaps are applied to the thin trailing edge of an airfoil, it is not easy to install a hinge and other necessary hardware. Therefore, Storms and Jang considered a miniature split-flap configuration (figure 10).[19] For testing a split-flap configuration, the Gurney flap was located a distance approximately equal to its height forward of the trailing edge. The results were comparable to the conventional trailing-edge Gurney flaps and showed no degradation in flap effectiveness. The Storms and Jang study was compared to a computational study by Jang, Ross and Cummings.[20] The experimentally measured results from reference 19 were in general agreement with the Navier-Stokes computations done in reference 20. As a result of the study in reference

20, the ability to accurately predict Gurney flap effects computationally has been somewhat successful.

Another recent experimental and computational study investigated the use of Gurney flaps in combination with conventional flaps. The Gurney flaps were placed near the trailing edge of the main airfoil element in the "cove" region (figure 11).[21] The cove is the cut-out region of the main element that the flap retracts into. The effects of the cove Gurney flaps were similar to those of the trailing-edge Gurney flaps in the previously mentioned studies. The cove Gurney flaps increased the maximum lift coefficient. They also acted to delay separation on the flap by turning the flow toward the flap. An increase in nose-down pitching moment was also evident.

Deciding on the size and location of Gurney flaps is easier than for micro-vortex generators because there are not as many variables. The thin plates mounted at trailing-edge surfaces are generally on the order of 0.5% - 2.0% local-wing-chord (c_w). Studies have shown that a Gurney flap on the order of 0.5%c_w yields most of the achievable lift increment. Increasing the Gurney flap size further does result in slightly increased lift (although the effect is not linear) but also results in a significant drag penalty. Gurney flaps are located either in the "cove" region of the main element or at the trailing edge of a flap element.

This chapter has presented several previous investigations of micro-vortex generators and Gurney flaps. While the previous two-dimensional investigations of Gurney flaps have shown that they are an effective means of increasing lift, a limit to the Gurney flap size is encountered when the potential lift benefits are outweighed by significant drag and nose-down pitching moment increases. Furthermore, previous MVG studies have shown that MVGs are effective in increasing lift and decreasing drag in some two-dimensional

circumstances. These results indicated that these two high-lift devices were effective when applied to two-dimensional airfoils. This study was done to evaluate the three-dimensional effects of micro-vortex generators and Gurney flaps on the lift, drag and pitching moment characteristics of a typical business jet wing.

3.0 Wind Tunnel Models

3.1 Full-Scale, Semi-Span Business Jet Wing

The dimensions of the full-scale, semi-span business jet wing used in this study are shown in table 1. The wing was mounted vertically in the NASA Langley 30- by 60-Foot Tunnel with a generic fuselage at the wing root (figure 12) and was centered on a turn table on the ground board so that a full angle-of-attack sweep (from -5° to 24°) could be done. Only the wing was metric (i.e., the external balance scales measured the wing longitudinal force and moment data and not that of the generic fuselage). The generic fuselage was non-metric and was there to simulate the correct flow pattern around the wing-fuselage interface.

The wing high-lift system uses Fowler-type flaps. Fowler flaps (named after H. D. Fowler) combine a slotted flap (which postpones separation by directing high-velocity air from the lower surface over the flap upper surface) with an aft translation of the flap. The aft translation of the flap allows for increased lift by effectively extending the chord of the wing.[22] The flap system has double-slotted (DS) inboard and single-slotted (SS) outboard segments and spans almost the entire trailing edge of the wing with the exception of an aileron trim surface outboard. There is not a full-sized aileron to maneuver the aircraft; therefore, a spoiler mounted flush with the airfoil surface in front of the flap system is used for roll control. A schematic of the test wing is shown in figure 13.

For the MVG and Gurney flap tests, the aft flap was fixed to the main flap so that the entire flap system was a simpler SS system. The SS flap system was hydraulically actuated and flap angles of 10°, 20° and 30° could therefore be set from the control room of the 30- by 60-Foot Tunnel. A maximum flap

deflection of 34° could be obtained by mechanically extending the push-rods and manually setting the flaps to 34°.

The wing was instrumented with 600 surface pressure ports located at nine stations along the span of the wing. These locations are numbered in figure 13. Data was taken with an Electronically Scanned Pressure (ESP) measurement system.

The cove region of the wing was "cluttered" with flap-tracks and push-rods that were necessary for the actuation of the flap system. When the flaps were deflected, there were gaps around the flap-tracks and push-rods (figure 14).

3.2 Micro-Vortex Generators

As mentioned previously, the size of MVGs depends on the boundary-layer thickness, δ. Therefore, a **M**ulti-**C**omponent **AiRF**oil analysis program, MCARF,[23] was used to predict the boundary layer on the main element as well as on the main and aft flaps. From these predictions, seven different MVG geometries were developed.* The basic MVG geometry is shown in figure 15 and the seven MVG geometries are summarized in table 2. All seven geometries are trapezoidal in shape and vary in device height (h), length (l), and leading-edge-sweep angle (γ), while base width (w), leading-edge radius curvature (r), and device thickness (t) are constant at 0.25", 0.25" and 0.016", respectively.

Separation must initially exist in order for the MVGs to be able to "clean up" the flow by keeping it attached. The location of the separation region is important to the location of the MVGs. Flow predictions on the business jet wing

* Dr. John C. Lin, Flow Modeling and Control Branch, NASA LaRC

using the Multi-Surface Euler Solver code, MSES,[24] were performed** and used to locate the MVGs. The MVGs were tested at several locations on the SS flap.

The MVG design process using MCARF and MSES was based on the manufacturer-supplied flap geometry data for a 30° deflection. After this study was completed, it was discovered that these geometry coordinates were actually for 36°. The possible impact of this discrepancy on the effectiveness of the MVGs will be discussed in a later section.

The application of the MVGs to the SS flap system was somewhat cumbersome. First the MVGs had to be mounted into a guiding strip (figure 16) which was constructed to provide the correct orientation, spacing and incidence angle to the flow. Then, using masking tape, the MVGs were held in place while the guiding strips were lined up on the flap at the location to be tested. Double-sided tape was already positioned at the location to affix the MVGs. The masking tape was removed along with the guiding strip, leaving the MVGs fastened on the surface of the flap (figure 17).

3.3 Gurney Flaps

Gurney flap size is measured as a percentage of local wing chord. Once the local wing chord was known, the size of the Gurney flaps was decided upon. Based on past results,[17-21] the Gurney flaps tested in this study were 0.5%, 1.0% and 2.0% local-wing-chord. Therefore, as the business jet wing tapered, the Gurney flaps also tapered. Figure 18 shows a Gurney flap applied to the trailing edge of the SS flap system. Different TE locations were tested and the Gurney flaps were fixed to the TE surfaces with screws.

** Mr. Jay Hardin, Vehicle Performance Branch, NASA LaRC

4.0 Wind Tunnel Tests

4.1 Test conditions

The NASA Langley 30- by 60-Foot Tunnel is an open test section, double-return tunnel (figure 19). The MVG and Gurney flap tests were conducted at a tunnel free-stream dynamic pressure of approximately 14 lb/ft^2. This corresponds to a free-stream velocity of 108.5 ft/sec. The Reynolds number, based on the mean aerodynamic chord, was 4.2 million.

Force and moment data along with surface pressure distributions were measured over an angle-of-attack range from -5° to 24°. Selected cases were supplemented with some flow visualization information on the flap region as well as on the whole wing.

The data acquisition and reduction process in the 30- by 60-Foot Tunnel uses the following devices and procedures. Forces and moments are measured by a set of external balance "scales" located beneath the ground board. Tunnel dynamic pressure is measured using a static pressure port located upstream and corrected for tunnel blockage based on previously-completed tunnel surveys. The instrumentation signals are filtered (1 Hz) and sampled at 10 samples per second for 20 seconds. These data are read by a NEFF interface into an HP 9000/400 workstation. All data are reduced on-line and available to the test engineer via plots or printouts. Pressure data are read by a PSI 8400 electronic scanner (ESP) system. Still photographs for flow visualization were taken with a Hasselblad camera. The yarn tufts were approximately four inches long with four inches spaced between them. The uncertainty on the force and moment data was ±3% at 95% reliability while the uncertainty on the pressure data was ±6% at 95% reliability.

Micro-vortex generators were tested at four different local-flap-chord locations: 7%, 15%, 20% and 30% (figure 20). Most of the tests were run with the maximum flap deflection of 34°, although a few cases were run with flaps set at 30° (see table 3). The Gurney flaps were tested in four different configurations (figures 21-24). Configuration 1 was tested at flap deflections of 10°, 20° and 30°. The 10° and 30° flap deflections represent takeoff and landing configurations, respectively, for the aircraft. The other three configurations were only tested at flap deflections of 20° and 30°. All the Gurney flap cases are summarized in table 4.

Results from the MVG cases studied will be presented in the order given in table 3. For the MVG cases, the results will include longitudinal force and moment data (F, M) and selected flow visualization information (T).

Gurney flap results will be presented in the order given in table 4. Longitudinal force and moment data (F, M) will be presented for all of the Gurney flap results along with some surface pressure distributions (P). The Gurney flaps showed no apparent effect on upper-surface flow; therefore, no flow visualization information is presented for the Gurney flaps.

4.2 Results and Discussion

This section summarizes the results of the MVG and Gurney flap tests. First, a comparison of the effects of the various MVG configurations is made, followed by a brief discussion and explanation of the results. The MVG results are shown in figures 26-42. Then, the effects of the various Gurney flap configurations are compared, results are discussed and a short performance analysis is done. Figures 43-79 show the Gurney flap results.

4.2.1 *Micro-vortex generators*

Prior to testing any MVG geometry, some flow visualization was done on the baseline wing (no MVGs) with the maximum flap deflection of 34°. Figure 25a shows that for a low angle of attack, $\alpha = 0°$, the flow over the main element is fully attached while the flow over the SS flap element contains a great deal of separation. At this α, it is apparent that the flap-tracks, gaps and push-rods necessary for flap extension cause "pockets" of separation behind them. At $\alpha = 6°$ (figure 25b), the flow over the main element is still clean, and the flow on the SS flap element is still mostly separated. Around $\alpha = 18°$ (figure 25c), the onset of the stall can be seen on the inboard section of the wing, as would be expected. By $\alpha = 24°$ (figure 25d), the flow over the whole wing is fully separated. The flow visualization information helped characterize the flow over the full-scale, semi-span business jet wing. Because of the large amounts of flow separation that appeared in the flap region (due to the flap-tracks, gaps and push-rods) even at low α, it was decided that MVG geometry 6, the largest MVG (based on height and length), should be tested first.

Figures 26 and 27 show the effects of MVG 6 orientation on the longitudinal force and moment data. First a COR orientation was tested and when it had no apparent effect, a CTR orientation (with all other variables remaining the same) was tested. These figures show that, for the configurations tested, neither the COR nor the CTR orientation significantly affected lift, drag or pitching moment on the wing. Note that the data in figure 27 (as well as in the other pitching moment coefficient figures) is for a wing only and shows an unstable ($C_{m\alpha} > 0$) slope as a result. The flow visualization pictures of the tufted SS flap in figure 28 compare the baseline wing with no MVGs to the COR-orientation case. The flow visualization confirms that the MVG configurations tested in these cases had little or no effect on flow separation.

Next, MVG 6 was tested at 30%c_f with an angle of incidence to the flow of 23°. It was hoped that the larger incidence angle would allow MVG 6 to produce vortices strong enough to show some desired effects, and that moving the MVGs further downstream to 30%c_f might be beneficial. Moving the MVGs to 30%c_f would assure that the vortices were stronger when they reached the separation region. This configuration, however, was also unable to noticeably influence the flow (figures 29 and 30).

Since moving the MVG location further downstream from 20% to 30%c_f had no noticeable effect, the next case moved the MVGs to 15% local-flap-chord. However, MVG 5 was tested instead. MVG 5 has the same height (h) as MVG 6 but is shorter (l). At locations (C_f) further upstream, the surface had more curvature and MVG 5 was more applicable to these locations because of its shorter length. Results similar to the previous cases were obtained (figures 31 and 32).

It was decided that no variation of the MVG geometry, orientation, location, etc. was going to be effective because of the separation caused by the flap-tracks and push-rods. Therefore, a model modification was made. For the rest of the MVG tests, the flap-tracks, gaps and push-rods were taped in an attempt to clean up the flow. Figure 33 shows that taping the wing produces an increase in lift and a decrease in drag. Figure 34 compares the moment characteristics of the untaped and taped wing. The effects of taping can also be seen in the flow visualization pictures in figure 35.

The next three cases were run with MVG 5 even further upstream at 7%c_f and $\beta = 23°$, varying spacing and flap deflection (see table 3). Figures 36 and 37 show that varying spacing from 1" to 2" had no significant effect. Figures 38 and 39 show the difference between a 30° flap deflection and the 34° flap deflection used in all of the previous cases. As would be expected, the 30° flap

deflection does not produce as much lift or drag or cause as much of a nose-down pitching moment. Comparing the baseline wing at 30° to the wing with MVG 5 at 30°, shows that the MVGs cause a decrease in lift.

The final two cases studied were for MVG 5 moved to 20%c_f with a COR orientation, $\beta = 23°$ and a flap deflection of 30° while varying spacing. These configurations again showed little effect on separation, similar to the other 30° tests already mentioned (figures 40 and 41). Due to time constraints and the fact that the MVGs tested thus far appeared to have no effect on flow separation control, the other MVG geometries were not tested.

The MVG configurations studied were tested with flap deflections of 34° and 30° which represent a landing configuration for the aircraft. Evaluation of MVG effectiveness on separation control was based mainly on lift enhancement and drag reduction. None of the MVG configurations showed an increase in lift, or a decrease in drag. The flow visualization presented in figure 28 is representative of most of the MVGs studied.

A possible explanation for the lack of MVG effectiveness is based on the previously mentioned discrepancy concerning the flap deflection geometry used in the MSES predictions. Note that these discrepancies were discovered during the analysis of results *after* testing. When MSES was run (*prior* to testing) for what was thought to be a 30° flap deflection, a 36° flap geometry was actually being run. These predictions did not show much separation, so MSES was run for a larger flap deflection. The larger flap deflection (thought to be 35°) was actually 41° (which is unattainable on the model). These MSES predictions did indicate enough separation to warrant the use of MVGs. Therefore, *during* testing, a flap deflection of 34° (maximum attainable on the model) was used to assure that there was separation. However, there was not sufficient separation at 34° caused by adverse pressure gradients due to airfoil

shape. Most of the separation on the flap that did occur was because of the flap extension hardware (MSES was unable to predict the separation regions caused by the flap-tracks, gaps and push-rods). The large amount of flap extension hardware per foot of flap caused "pockets" of separation (figure 42). The MVGs designed for this study were unable to affect the flow in these regions. The small regions of flow between these "pockets" of separation were already mostly attached. Therefore, the MVGs did not have sufficient separation in these regions to show any significant effects. Taping the flap-tracks, gaps and push-rods in an attempt to minimize their effects did result in "cleaner" flow compared to the untaped wing. However, the MVGs still did not have a noticeable effect because again, there was not (aerodynamic) separation to "clean up".

4.2.2 *Gurney flaps*

For clarity, the results from the various Gurney flap configurations will be presented grouped by configuration beginning with Configuration 1 (figure 21), followed by Configurations 2 (figure 22), 3 (figure 23) and 4 (figure 24). Table 4 summarizes the different cases in this manner.

The tape on the flap-tracks, gaps and push-rods of the wing was removed for the Gurney flap runs. The flap region of the wing remained tufted, however, the Gurney flaps showed little effect in the flow visualization tests. Therefore, no flow visualization results are presented.

Configuration 1 consists of the Gurney flap at the TE of the SS flap (figure 21). All three Gurney flap sizes (0.5%, 1.0% and 2.0%) were tested in this configuration. Figures 43 and 44 show how the Gurney flaps effect the lift coefficient (C_L), drag coefficient (C_D) and lift-to-drag ratio (L/D) at a takeoff flap deflection of 10°. The 2.0% Gurney flap was not tested at 10°. The Gurney

flaps show an increase in C_L throughout the alpha range and also an increase in C_D for a given C_L at low to moderate lift coefficients. However, figure 43 shows that the 0.5% Gurney flap yields a significant increase in lift coefficient over the baseline while only a modest increase in drag coefficient compared to the 1.0% Gurney flap. Figure 44 shows that both the 0.5% and 1.0% Gurney flaps decrease *L/D*. The expected increase in nose-down pitching moment caused by the Gurney flaps is shown in figure 45.

Similar results can be seen in figures 46 through 48 for a flap deflection of 20°. With the addition of the 2.0% Gurney flap results in these figures, it is more apparent that as the Gurney flap size increases, the increase in C_L over the baseline (no Gurney flap) also increases. However, the larger Gurney flap significantly increases C_D for a given C_L and further decreases *L/D*. Also, the larger Gurney flap further increases the nose-down pitching moment.

A 30° flap deflection corresponds to a landing configuration. These results are shown in figures 49-51. The Gurney flaps increase C_L throughout the alpha range prior to stall along with increasing C_D for a given C_L and decreasing *L/D*. Again the addition of Gurney flaps result in an expected increase in nose-down pitching moment.

The 0.5% Gurney flap has yielded the largest increase in C_L for the smallest increase in C_D thus far. Therefore, this configuration will be used to show how the Gurney flaps effect pressure distributions at the TE of the SS flap. Figures 52 and 53 show results for 10° and 30° flap deflections, respectively, taken at the 1440 pressure location on the wing (figure 13). As mentioned in an earlier section, the Gurney flaps affect the pressure at the TE of the airfoil. These results show that the Gurney flaps decrease C_p on the upper surface while increasing C_p on the lower surface, thus increasing the pressure

difference between the upper and lower surfaces. This increase results in the previously mentioned increases in C_L and nose-down pitching moment.

Looking at C_m for the angle of attack compatible with landing (about $\alpha=4\frac{1}{2}°$, an aircraft characteristic provided by the manufacturer) in figure 51, shows that the increase in nose-down pitching moment caused by the 0.5% Gurney flap when compared to the SS baseline is on the order of 0.03. The study in reference 25 can be used to find a corresponding horizontal tail deflection for $\Delta C_m = 0.03$. Reference 25 is a study of a typical business jet and its results are used here to give an approximation for the tail deflection required to trim the increase in nose-down pitching moment caused by the 0.5% Gurney flap. According to reference 25, this $\Delta C_m = 0.03$ corresponds to about a 2° horizontal tail deflection. Therefore, the small increase in nose-down pitching moment could be easily trimmed with a conventional tail. Later in this section Gurney flap results will be compared to DS flap (with no Gurney flap) results.

The next cases presented are for Configuration 2, which consists of the 1.0% Gurney flap mounted forward of the trailing edge of the SS flap (figure 22). This configuration was tested at flap deflections of 20° and 30°. Mounting the Gurney flap forward of the TE of the SS flap represents a "split-flap" configuration. It would be easier to employ such a split-flap than to put a Gurney flap at the thin TE of a flap. The split-flap was studied to see how its effects compare to the Gurney flap at the TE of the SS flap (Configuration 1). Figures 54-56 and 57-59 show this comparison for flap deflections of 20° and 30° respectively. The curves are nearly identical. However, for both 20° and 30°, the 1.0% Gurney flap in Configuration 1 shows a slight increase in C_L over the 1.0% Gurney flap in Configuration 2 and slightly more C_D for a given C_L. Both configurations decrease *L/D*, however, Configuration 2 does not have as

large a decrease as Configuration 1. Configuration 2 also does not have as large an increase in nose-down pitching moment as Configuration 1.

Configuration 3 studies the 0.5% Gurney flap in the cove region (figure 23). As with Configuration 2, these tests were performed at 20° and 30° flap deflections. This configuration was investigated to see if it showed any advantages over mounting the 0.5% Gurney flap at the TE of the SS flap. The 0.5% Gurney flap in the cove decreases C_L slightly compared to the baseline at a flap deflection of 20° - unlike the other configurations tested thus far (figure 60). The two C_L versus C_D curves are very similar (figure 60), although at low drag coefficients it appears that the cove Gurney flap has slightly less C_D for a given C_L than the baseline wing. Also for a given C_L, Configuration 3 has less drag than the 0.5% Gurney flap Configuration 1. The 0.5% Gurney flap in the cove also results in an increase in *L/D* (figure 61) as well as a decrease in nose-down pitching moment (figure 62) compared to the baseline and Configuration 1.

When the SS flap is deflected 30°, the 0.5% cove Gurney flap shows an almost identical C_L-curve to the baseline throughout the alpha range prior to stall. The 0.5% cove Gurney flap shows a slight increase in C_{Lmax} over the baseline (figure 63). Although the 0.5% Gurney flap at the TE of the SS flap shows an increase in C_L over both the baseline and the cove Gurney flap, it also results in more C_D for given C_L (figure 63). The cove Gurney flap results in less C_D for a given C_L compared to the baseline at a flap deflection of 30° (figure 63) and a higher *L/D* curve (figure 64). Figure 65 shows that the cove Gurney flap decreases nose-down pitching moment, which is a different result than expected based on results from the Gurney flaps mounted at the TE of the SS flap. The inset plot in figure 65 shows the surface pressure coefficient versus x/c position on the flap for the 0.5% cove Gurney flap and the baseline.

The Gurney flap in the cove decreases positive pressure on the lower surface of the flap. At a 30° flap deflection, the decrease in positive pressure on the lower surface means less force pushing on the flap in the drag direction. Because the flap is behind and below the center of gravity of the wing, this effect appears as a decrease in nose-down pitching moment compared to that of the baseline.

The last Gurney flap configuration is Configuration 4 (figure 24). These cases consisted of the 0.5% cove Gurney flap and the 1.0% Gurney flap at the TE of the SS flap in combination. Again, only flap deflections of 20° and 30° were tested. This investigation proposed combining the increase in C_L from the 1.0% TE Gurney flap with the decrease in C_D from the 0.5% cove Gurney flap. Figures 66-68 and 69-71 show the results of Configurations 1, 3, and 4 plotted against the baseline for flap deflections of 20° and 30°, respectively. The 0.5% and 1.0% Gurney flaps in combination (Config. 4) result in slightly less C_L than the 1.0% alone (Config. 1, figures 66 and 69). Figures 66 and 69 also show that for a given C_L, Configuration 4 has slightly less C_D than Configuration 1. Configuration 3 (the 0.5% Gurney flap in the cove alone) is the only configuration to show an increase in *L/D* over the baseline (figures 67 and 70). However, Configuration 4 does increase *L/D* over Configuration 1. Figures 68 and 71 show that the two Gurney flaps in combination (Config. 4) do not increase the nose-down pitching moment as much as the 1.0% alone at the TE of the SS flap (Config. 1).

As previously mentioned, the effect of Gurney flaps on drag characteristics has not been consistent from one study to the next. In this study, Gurney flaps applied to the TE of the SS flap increased drag. They also were effective in increasing lift characteristics in this configuration. Unlike the micro-vortex generators, the Gurney flaps were not dependent on flow separation existing and their effectiveness was not inhibited by the separation caused by

the flap extension hardware. The effective increase in camber as a result of the Gurney flaps is the reason for the increases in lift. Similar to the description in Section 2.2, Gurney flaps caused the flow velocity over the upper surface of the airfoil to increase and reduced the flow velocity over the lower surface. This resulted in the noted increase in pressure difference between the upper and lower surfaces of the flap, which, in turn, resulted in an increase in lift and nose-down pitching moment on the wing. Because there was not much separation on the flap due to adverse pressure gradients (mentioned earlier), the Gurney flaps did not reduce drag by reducing the wake region behind the flap. Any reduction in the wake region the Gurney flaps may have caused was outweighed by the drag increase due to the forward facing flat plate area of the Gurney flaps. The larger the Gurney flap size, the larger the increase in drag.

The results obtained when the 0.5% Gurney flap was mounted in the cove region differed from the results for the Gurney flaps at the TE of the SS flap. It is likely that the Gurney flap in the cove region restricted air flowing through the gap between the main wing element and the flap by decreasing the gap size. The airflow which would normally flow through the gap would then move along the flap lower surface, resulting in a slightly more negative surface pressure distribution. The result would be the noted drag decrease.

It is of interest to see how a SS flap with Gurney flaps compares to a conventional DS flap without Gurney flaps. Figures 72-74 and 75-77 compare a SS flap with no Gurney flap and a DS flap with no Gurney flap to the 0.5% and 1.0% Gurney flaps in Configuration 1 for flap deflections of 10° and 30°, respectively. At a flap deflection of 10°, when the DS system is simplified to a SS system, lift is lost. Adding Gurney flaps to the SS flap system produces more lift than the DS flap with no Gurney flaps, as well as more drag (figure 72). The Gurney flap configurations decrease *L/D* compared to the baseline cases

(SS and DS flaps without Gurney flaps) at a 10° flap deflection (figure 73). They also increase the nose-down pitching moment compared to the DS flap at 10° deflection (figure 74). At low angles of attack, where the increase is more significant, the increase in nose-down pitching moment caused by the larger 1.0% Gurney flap is still only on the order of 0.04. Using reference 25 again, $\Delta C_m = 0.04$ also corresponds to about a 2° horizontal tail deflection. Therefore, the increase in nose-down pitching moment caused by the 1.0% Gurney flap could be trimmed (earlier in this section this was shown for the 0.5% Gurney flap).

Figure 75 shows that at a 30° flap deflection, the simplified SS system produces significantly less lift than that achievable with the DS system. Adding Gurney flaps to the SS flap at this flap deflection provides lift comparable to that achieved with the DS flap system. The 0.5% Gurney flap has less drag than the DS flap at 30° deflection. The 0.5% Gurney flap even shows an increase in *L/D* over the DS flap (figure 76). Although the 0.5% Gurney flap increases the nose-down pitching moment when compared to the baseline SS flap at 30° deflection, it does not increase nose-down pitching moment as much as the baseline DS flap (figure 77).

5.0 Performance Analysis

A short performance analysis for takeoff and landing operations of a typical business jet aircraft was done to evaluate the effectiveness of the Gurney flaps when they are mounted at the TE of the SS flap. Following reference 26, the total takeoff distance over a 50-foot obstacle was divided into four segments (figure 78a) and the total landing distance from a 50-foot obstacle was divided into three segments (figure 78b). The following equations from reference 26 were used to compute each of these distances. The total takeoff distance (S_{TO}) to clear a 50-foot obstacle is the sum of the ground distance (S_G), rotation distance (S_R), transition distance (S_{TR}), and climb distance (S_{CL}):

$$S_G = \frac{1.44(W/S)_{TO}}{g\rho C_{L\,max}\left[\frac{T}{W} - \frac{D}{W} - \mu_{TO}\left(1 - \frac{L}{W}\right)\right]} \qquad (1)$$

where $D = \frac{1}{2}\rho V^2 S C_{Dtot}$ and $C_{Dtot} = C_{Dtest} + C_{Dgear} + C_{Dfhvn}$

$$S_R = 3V_{TO} \qquad (2)$$

$$S_{TR} = R \sin\theta_{CL} \qquad (3)$$

where $R = \frac{V_{TO}^2}{0.15g}$ and $\sin\theta_{CL} = \frac{T - D}{W_{TO}}$

$$S_{CL} = \frac{50 - h_{TR}}{\tan \theta_{CL}} \tag{4}$$

where $h_{TR} = R(1 - \cos \theta_{CL})$

Similarly, the total landing distance (S_L) over a 50-foot obstacle is the sum of the air distance (S_A), free-roll distance (S_{FR}), and braking distance (S_B):

$$S_A = \frac{L}{D}\left[\frac{V_{50}^2 - V_{TD}^2}{2g} + 50\right] \tag{5}$$

$$S_{FR} = 3V_{TD} \tag{6}$$

$$S_B = \frac{W_L}{g\mu_L \rho S\left(\frac{C_{Dtot}}{\mu_L} - C_L\right)} ln\left[1 + \frac{\rho}{2}\frac{S}{W_L}\left(\frac{C_{Dtot}}{\mu_L} - C_L\right)V_{TD}^2\right] \tag{7}$$

Constants in equations 1-7 were fixed at the values given in table 5. Furthermore, tables 6a-d provide all needed variables for equations 1-7. Takeoff and landing distances for several configurations are found in tables 7 and 8, respectively. Figure 79 shows the takeoff and landing performance analysis for DS and SS flaps with no Gurney flaps along with the 0.5% and 1.0% Gurney flaps in Configuration 1. The zero on the x-axis corresponds to configurations without Gurney flaps (baselines). Takeoff distances for the SS and DS baseline cases differ by less than 100 feet. Adding a 0.5% Gurney flap

to the SS flap decreases takeoff distance by about 3.5% compared to the DS flap baseline and 5% compared to the SS flap baseline. The 1.0% Gurney flap decreases takeoff distance by about 5% compared to the DS flap baseline and 6.6% compared to the SS flap baseline. For the baseline cases, landing distance differs more than for the takeoff distances. The addition of the 0.5% Gurney flap to the SS flap decreases the landing distance by 4.7% - to almost the same distance achieved with the DS flap. The larger 1.0% Gurney flap does not have more of a benefit than the 0.5% during landing. This performance analysis shows that the SS flap with the 0.5% Gurney flap can achieve a better takeoff distance and a comparable landing distance to that of the DS flap system.

6.0 Concluding Remarks

Micro-vortex generators were applied to a single-slotted flap system of a full-scale, semi-span business jet wing at flap deflections of 34° and 30°. Two trapezoidal shaped, vane-type micro-vortex generators, with the same height but different lengths, were investigated in several different configurations.

Three sizes of Gurney flaps were tested on a single-slotted flap system of a full-scale, semi-span business jet wing at flap deflections of 10°, 20° and 30°. Four different applications of the Gurney flap concept were investigated.

6.1 Micro-vortex generators

The micro-vortex generators tested showed no significant lift enhancement or drag reduction. The wing used for the micro-vortex generator tests had unexpected flow separation due to the flap extension hardware rather than undesirable separation due to the presence of adverse pressure gradients. This is a possible reason the micro-vortex generators were unable to affect flow separation.

6.2 Gurney flaps

The following conclusions are made about the effects of Gurney flaps on high-lift characteristics:

1) In general, Gurney flaps are an effective means of increasing the maximum lift coefficient. However, they do increase drag and decrease the lift-to-drag ratio in most cases.

2) Results for Gurney flaps applied to the trailing edge of a single-slotted flap (Configuration 1) show:

a) The larger the Gurney flap size, the more lift and drag result,

although the increases are not linear. Gurney flaps in this configuration also reduce the lift-to-drag ratio.

b) The small increase in nose-down pitching moment that results from the addition of a Gurney flap can be easily trimmed with moderate deflections of a conventional horizontal tail surface.

c) 0.5% and 1.0% Gurney flaps decrease the takeoff distance to clear a 50-foot obstacle compared to a double-slotted flap system. The landing distance over a 50-foot obstacle is comparable for the 0.5% and 1.0% Gurney flaps and the double-slotted flap system.

2) When the 1.0% Gurney flap is mounted approximately one inch forward of the trailing edge (Config. 2), the results are comparable to the 1.0% Gurney flap in Configuration 1. The data of Configuration 2 shows less of a decrease in the lift-to-drag ratio and less of an increase in the nose-down pitching moment compared to the data of Configuration 1.

3) Results for the 0.5% Gurney flap in the cove region of the main wing element (Configuration 3) indicated:

a) No significant lift enhancement.

b) A noticeable decrease in drag compared to the baseline single-slotted flap.

c) A slight increase in the lift-to-drag ratio.

d) Less of an increase in nose-down pitching moment than when compared to results of the baseline single-slotted flap.

4) Combining the 0.5% cove Gurney flap with the 1.0% Gurney flap at the trailing edge of the single-slotted flap (Configuration 4) results in:

a) Less lift and drag than the 1.0% Gurney flap alone (Config. 1).

b) An increase in the lift-to-drag ratio compared to Configuration 1 but a decrease compared to the baseline.

c) Less nose-down pitching moment increase than Configuration 1.

The application of high-lift devices to the three-dimensional wing of a typical business jet aircraft shows that, in this study, Gurney flaps are an effective high-lift device, yet micro-vortex generators are not. The performance analysis indicates that Gurney flaps mounted at the trailing edge of the single-slotted flap improve takeoff and landing distances compared to a conventional double-slotted flap system.

7.0 Recommendations

7.1 Micro-vortex generators

In the past, studies have shown MVGs to be an effective means of controlling boundary-layer separation. Although in this study the micro-vortex generators were not effective, it should not be concluded that they will not work in other cases. Further investigations of MVGs applied to three-dimensional wings should be done. First, it is necessary to answer questions about what type of airfoil configurations MVGs would have beneficial effects on. Also, more studies could help identify effective MVG configurations. For example, what orientation is best in a certain situation. Further investigations would allow for a data base on MVGs to build and could aid in the development of theoretical three-dimensional models needed to accurately predict MVG performance. Theoretical models would benefit the experimental design stage and the interpretation of experimental results.

Vortex generators are already successfully applied to several types of aircraft. The idea of micro-vortex generators used to develop high lift shows promise and the idea of stowing MVGs during cruise is worth further investigation also.

7.2 Gurney flaps

The high-lift systems of today are effective at improving the low-speed performance characteristics of transport aircraft. It is, however, necessary to further increase performance for the next generation of aircraft. The possibility of adding Gurney flaps to high-lift systems exists because of their simplicity and significant impact on the aerodynamic performance of airfoils. Now that the benefits of Gurney flaps are known, the actual application to an aircraft wing

needs to be considered. The question of whether or not a Gurney flap needs to be retracted in cruise needs to be answered. It is possible that the benefit from the decrease in angle of attack for zero lift could outweigh the drag-device penalty. If it is found that the Gurney flaps would need to be retracted in cruise, then the "split-flap" configuration should be further investigated. A configuration not tested in this study that should be looked at is a split-flap in the cove. Most of the configurations in this study were not tested at a 10° flap deflection. Gurney flap configurations that seem promising should be tested at landing as well as takeoff flap deflections to see which Gurney flap configurations benefit both phases of operation. Once there is a solid data base for Gurney flaps, some configurations should be tested in flight.

References

1. Smith, A. M. O.: High-Lift Aerodynamics. AIAA Paper No. 74-939, August 1974.

2. Brune, G. W. and McMasters, J. H.: Computational Aerodynamics Applied to High-Lift Systems. *Progress in Aeronautics and Astronautics: Applied Computational Aerodynamics,* Vol. 125, AIAA, Washington D.C., 1989, pp. 389-433.

3. Federal Aviation Administration, Department of Transportation, 14 CFR, Part 36 - Noise Standards: Aircraft Type and Airworthiness Certification, pp. 700-772, revised as of January 1993.

4. Yip, L. P., Vijgen, P. M. H. W., Hardin, J. D., and van Dam, C. P.: In-Flight Pressure Distributions and Skin-Friction Measurements on a Subsonic Transport High-Lift Wing Section. AGARD CP-415, October, 1992.

5. Pearcey, H. H.: Shock-Induced Separation and Its Prevention by Design and Boundary Layer Control. *Boundary Layer and Flow Control,* Vol. 2, ed. G. V. Lachman, Pergamon Press, Oxford, England, 1961, pp. 1166-1344.

6. Calarese, W., Crisler, W. P., and Gustafson, G. L.: Afterbody Drag Reduction by Vortex Generators. AIAA Paper No. 85-0354, January 1985.

7. Taylor, H. D.: The Elimination of Diffuser Separation by Vortex Generators. United Aircraft Corporation Research Department Report R-4012-3, June 1947.

8. Grose, R. M.: Theoretical and Experimental Investigation of Various Types of Vortex Generators. United Aircraft Corporation Research Department Report R-15362-5, March 1954.

9. Tanner, L. H., Pearcey, H. H., and Tracy, C. M.: Vortex Generators; Their Design and Their Effects on Turbulent Boundary Layers. National Physical Laboratory, Preliminary Report, January 1954.

10. Gould, D. G.: The Use of Vortex Generators to Delay Boundary Layer Separation; Theoretical Discussion Supported by Tests on a CF-100 Aircraft. National Aeronautical Establishment Laboratory Report LR-183, December 1956.

11. Gadetskiy, V. M., Serebriyskiy, Ya. M., and Fomin, V. M.: Investigation of the Influence of Vortex Generators on Turbulent Boundary Layer Separation. NASA TT F-16,056, December 1974.

12. Breidenthal, Jr., R. E., and Russell, D. A.: Aerodynamics of Vortex Generators. NASA CR-182511, December 1987.

13. Lin, J. C., Howard, F. G., and Selby, G. V.: Small Submerged Vortex Generators for Turbulent Flow Separation Control. *Journal of Spacecraft,* Vol. 27, No. 5, October 1990, pp. 503-507.

14. Lin, J. C., Robinson, S. K., McGhee, R. J., and Valarezo, W. O.: Separation Control on High Reynolds Number Multi-Element Airfoils. AIAA Paper No. 92-2636, June 1992.

15. Griffin, D. A.: Investigation of a Model for Predicting Separation Control with Vortex Generators. AIAA Paper No. 93-0009, January 1993.

16. Barber, T. J., Mounts, J. S., and McCormick, D. C.: Boundary Layer Energization by Means of Optimized Vortex Generators. AIAA Paper No. 93-0445, January 1993.

17. Neuhart, D. H. and Pendergraft, Jr., O. C.: A Water Tunnel Study of Gurney Flaps. NASA TM 4071, November 1988.

18. Liebeck, R. H.: Design of Subsonic Airfoils for High Lift. *Journal of Aircraft,* Vol. 15, No. 9, September 1978, pp. 547-561.

19. Storms, B. L. and Jang, C. S.: Lift Enhancement of an Airfoil Using a Gurney Flap and Vortex Generators. AIAA Paper No. 93-0647, January 1993.

20. Jang, C. S., Ross, J. C., and Cummings, R. M.: Computational Evaluation of an Airfoil with a Gurney Flap. AIAA Paper No. 92-2708-CP, June 1992.

21. Ross, J. C., Storms, B. L., and Carrannanto, P. G.: Lift-Enhancing Tabs on Multi-Element Airfoils. AIAA Paper No. 93-3504, August 1993.

22. Hoerner, S. F. and Borst, H. V.: *Fluid-Dynamic Lift,* Hoerner Fluid Dynamics, New Jersey, 1975, p. 5-2.

23. Brune, G. W. and Manke, J. W.: An Improved Version of the NASA-Lockheed Multi-Element Airfoil Analysis Computer Program. NASA CR-145323, March 1978.

24. Drela, M.: A User's Guide to MSES V1.2. MIT Computational Fluid Dynamics Laboratory, July 1991.

25. Coe, Jr., P. L., Turner, S. G., and Owens, D. B.: Low-Speed Wind-Tunnel Investigation of the Flight Dynamic Characteristics of an Advanced Turboprop Business/Commuter Aircraft Configuration. NASA TP-2982, April 1990.

26. Nicolai, L. M.: Takeoff and Landing Analysis. *Fundamentals of Aircraft Design*, METS, Inc., Xenia, Ohio, 1975, chpt. 10.

27. Dunham, D. M., Gentry, Jr., G. L., Manuel, G. S., Applin, Z. T., and Quinto, P. F.: Low-Speed Aerodynamic Characteristics of a Twin-Engine General Aviation Configuration with Aft-Fuselage-Mounted Pusher Propellers. NASA TP-2763, 1987.

Tables

Table 1. Dimensions of the full-scale, semi-span business jet wing tested

Wing area (exposed semi-span)	98.246 ft^2
Wing span (exposed semi-span)	18.839 ft
Mean aerodynamic chord (exposed)	6.0833 ft

Table 2. Micro-vortex generator geometries

MVG geometry	Height, h (inches)	Length, l (inches)	Leading-edge sweep angle, γ(degrees)
1	0.200	0.750	30.0
2	0.200	0.816	22.6
3	0.200	0.682	45.0
4	0.150	0.948	22.6
*5	0.250	0.761	22.6
*6	0.250	1.020	22.6
7	0.150	0.612	22.6

*Micro-vortex generator geometries tested

Table 3. Micro-vortex generator cases

Case	MVG geometry	MVG orientation	C_f (%)	β (deg)	λ (in)	δ_f (deg)	Wing taped	Data type	Fig #s
1	6	COR	20	16	1	34	no	F,M,T	26-28
2	6	CTR	20	16	2, d=1	34	no	F,M	26,27
3	6	COR	30	23	1	34	no	F,M	29,30
4	5	COR	15	23	1	34	no	F,M	31,32
5	5	COR	7	23	1	34	yes	F,M	36,37
6	5	COR	7	23	2	34	yes	F,M	36-39
7	5	COR	7	23	2	30	yes	F,M	38,39
8	5	COR	20	23	1	30	yes	F,M	40,41
9	5	COR	20	23	2	30	yes	F,M	40,41

Note: F = force data, M = moment data, T = flow visualization information

Table 4. Gurney flap cases

Configuration	Gurney flap size (% c_w)	SS flap angle, δ_f (deg)	Data type	Figure #s
1	0.5	10	F,M,P	43-45,52
	1.0		F,M	43-45
	0.5	20	F,M	46-48
	1.0		F,M	46-48
	2.0		F,M	46-48
	0.5	30	F,M,P	49-51,53
	1.0		F,M	49-51
	2.0		F,M	49-51
2	1.0	20	F,M	54-56
	1.0	30	F,M	57-59
3	0.5	20	F,M	60-62
	0.5	30	F,M	63-65
4	0.5 & 1.0	20	F,M	66-68
	0.5 & 1.0	30	F,M	69-71

Note: F = force data, M = moment data, P = surface pressure data

Table 5. Performance analysis equation constants

Gravity, g	32.2 ft/s^2
Density, ρ	0.002377 slug/ft^3
Wing area, S	241.4 ft^2
Takeoff weight, W_{TO}	16,100 lbs
Landing weight, W_L	15,700 lbs
Thrust, T	5800 lbs
Takeoff coefficient of friction, μ_{TO}	0.02
Landing coefficient of friction, μ_L	0.4
Drag coefficient due to landing gear (reference 26), C_{Dgear}	0.21
Drag coefficient due to fuselage, horizontal and vertical tails, and nacelles (reference 27), C_{Dfhvn}	0.02

Table 6a. Takeoff and landing variables for the baseline wing with a single-slotted flap

Dist.	C_{Lmax}	V	C_L	L	C_{Dtest}	C_{Dtot}	D	R	θ_{CL}	h_{TR}
S_G	1.6582	$0.7V_{TO}$ 154.53	$@\alpha=0°$ 0.5530	3788.7	$@\alpha=0°$ 0.0225	0.2525	1729.8			
S_R	1.6582	V_{TO} 220.75								
S_{TR}	1.6582	V_{TO} 220.75	$0.8C_{Lmax}$ 1.3266		$@C_L=1.3$ 0.0608	0.2908	4066.2	10,089	6.182°	
S_{CL}	1.6582	V_{TO} 220.75	$0.8C_{Lmax}$ 1.3266		$@C_L=1.3$ 0.0608	0.2908	4066.2	10,089	6.182°	58.672
S_A	2.0097	V_{50} 217.23 V_{TD} 192.17	$@L=W_L$ $V=V_{50}$ 1.1596	15,700	$@C_L=1.2$ 0.0957	0.3257	4409.4			
S_{FR}	2.0097	V_{TD} 192.17								
S_B	2.0097	V_{TD} 192.17	$@\alpha=0°$ 1.0757		$@\alpha=0°$ 0.0845	0.3145				

Table 6b. Takeoff and landing variables for the baseline wing with a double-slotted flap

Dist.	C_{Lmax}	V	C_L	L	C_{Dtest}	C_{Dtot}	D	R	θ_{CL}	h_{TR}
S_G	1.6870	$0.7V_{TO}$ 153.20	$@\alpha=0°$ 0.6142	4136.2	$@\alpha=0°$ 0.0233	0.2533	1705.7			
S_R	1.6870	V_{TO} 218.86								
S_{TR}	1.6870	V_{TO} 218.86	$0.8C_{Lmax}$ 1.3496		$@C_L=1.3$ 0.0632	0.2932	4030.0	9917.2	6.312°	
S_{CL}	1.6870	V_{TO} 218.86	$0.8C_{Lmax}$ 1.3496		$@C_L=1.3$ 0.0632	0.2932	4030.0	9917.2	6.312°	60.113
S_A	2.1839	V_{50} 208.39 V_{TD} 184.34	$@L=W_L$ $V=V_{50}$ 1.2601	15,700	$@C_L=1.3$ 0.1162	0.3462	4313.4			
S_{FR}	2.1839	V_{TD} 184.34								
S_B	2.1839	V_{TD} 184.34	$@\alpha=0°$ 1.2558		$@\alpha=0°$ 0.1162	0.3462				

Table 6c. Takeoff and landing variables for the 0.5% Gurney flap at the trailing edge of the single-slotted flap

Dist.	C_{Lmax}	V	C_L	L	C_{Dtest}	C_{Dtot}	D	R	θ_{CL}	h_{TR}
S_G	1.7571	$0.7V_{TO}$ 150.12	$@\alpha=0°$ 0.7078	4576.5	$@\alpha=0°$ 0.0298	0.2598	1679.7			
S_R	1.7571	V_{TO} 214.45								
S_{TR}	1.7571	V_{TO} 214.45	$0.8C_{Lmax}$ 1.4057		$@C_L=1.4$ 0.0704	0.3004	3963.9	9521.6	6.548°	
S_{CL}	1.7571	V_{TO} 214.45	$0.8C_{Lmax}$ 1.4057		$@C_L=1.4$ 0.0704	0.3004	3963.9	9521.6	6.548°	62.119
S_A	2.1830	V_{50} 208.43 V_{TD} 184.38	$@L=W_L$ $V=V_{50}$ 1.2596	15,700	$@C_L=1.3$ 0.1047	0.3347	4172.3			
S_{FR}	2.1830	V_{TD} 184.38								
S_B	2.1830	V_{TD} 184.38	$@\alpha=0°$ 1.1867		$@\alpha=0°$ 0.1047	0.3347				

Table 6d. Takeoff and landing variables for the 1.0% Gurney flap at the trailing edge of the single-slotted flap

Dist.	C_{Lmax}	V	C_L	L	C_{Dtest}	C_{Dtot}	D	R	θ_{CL}	h_{TR}
S_G	1.7995	$0.7V_{TO}$ 148.34	$@\alpha=0°$ 0.7850	4955.8	$@\alpha=0°$ 0.0376	0.2676	1689.7			
S_R	1.7995	V_{TO} 211.91								
S_{TR}	1.7995	V_{TO} 211.91	$0.8C_{Lmax}$ 1.4396		$@C_L=1.4$ 0.0744	0.3044	3922.5	9297.2	6.697°	
S_{CL}	1.7995	V_{TO} 211.91	$0.8C_{Lmax}$ 1.4396		$@C_L=1.4$ 0.0744	0.3044	3922.5	9297.2	6.697°	63.435
S_A	2.1652	V_{50} 209.29 V_{TD} 185.14	$@L=W_L$ $V=V_{50}$ 1.2494	15,700	$@C_L=1.2$ 0.1154	0.3454	4340.0			
S_{FR}	2.1652	V_{TD} 185.14								
S_B	2.1652	V_{TD} 185.14	$@\alpha=0°$ 1.2312		$@\alpha=0°$ 0.1154	0.3454				

Table 7. Takeoff performance analysis, $\delta f = 10°$

Configuration	S_G	S_R	S_{TR}	S_{CL}	S_{TO}
Baseline wing SS flap	3186	662	1087	0	4935
Baseline wing DS flap	3106	657	1090	0	4853
0.5% Gurney flap at TE of SS flap	2956	643	1086	0	4685
1.0% Gurney flap at TE of SS flap	2888	636	1084	0	4608

Table 8. Landing performance analysis, $\delta f = 30°$

Configuration	S_A	S_{FR}	S_B	S_L
Baseline wing SS flap	745	577	1595	2917
Baseline wing DS flap	716	553	1511	2780
0.5% Gurney flap at TE of SS flap	740	553	1488	2781
1.0% Gurney flap at TE of SS flap	716	555	1512	2783

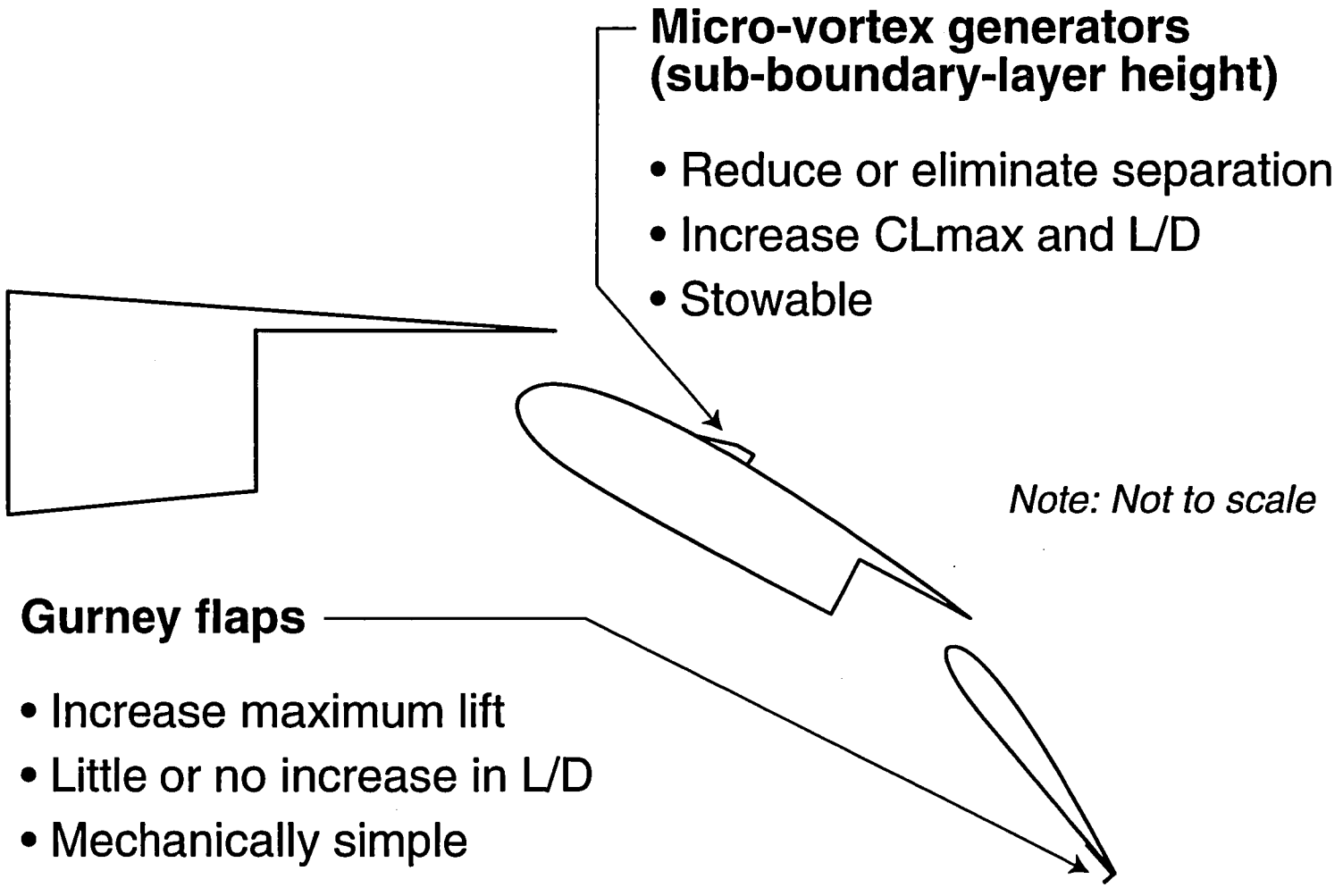

Figure 1. Micro-vortex generators and Gurney flaps.

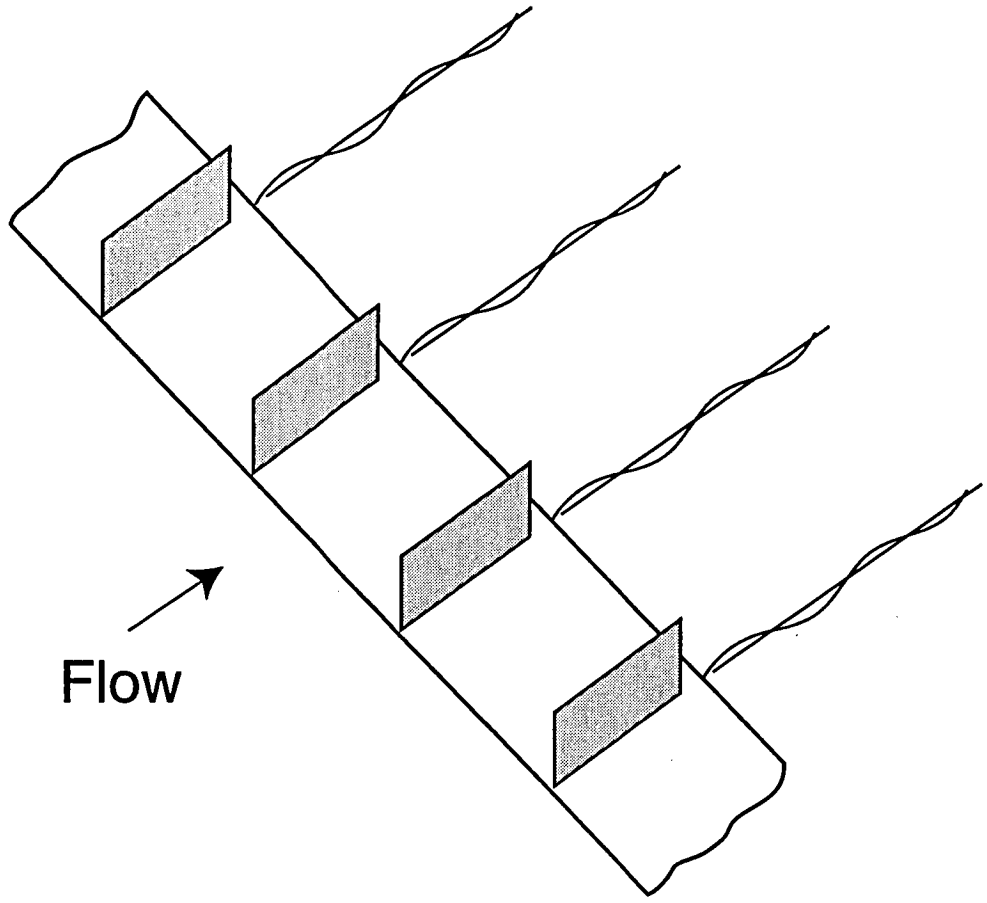

Figure 2. Vane-type micro-vortex generators producing vortices to enhance mixing between lower-energy boundary-layer flow and higher-energy boundary-layer flow.

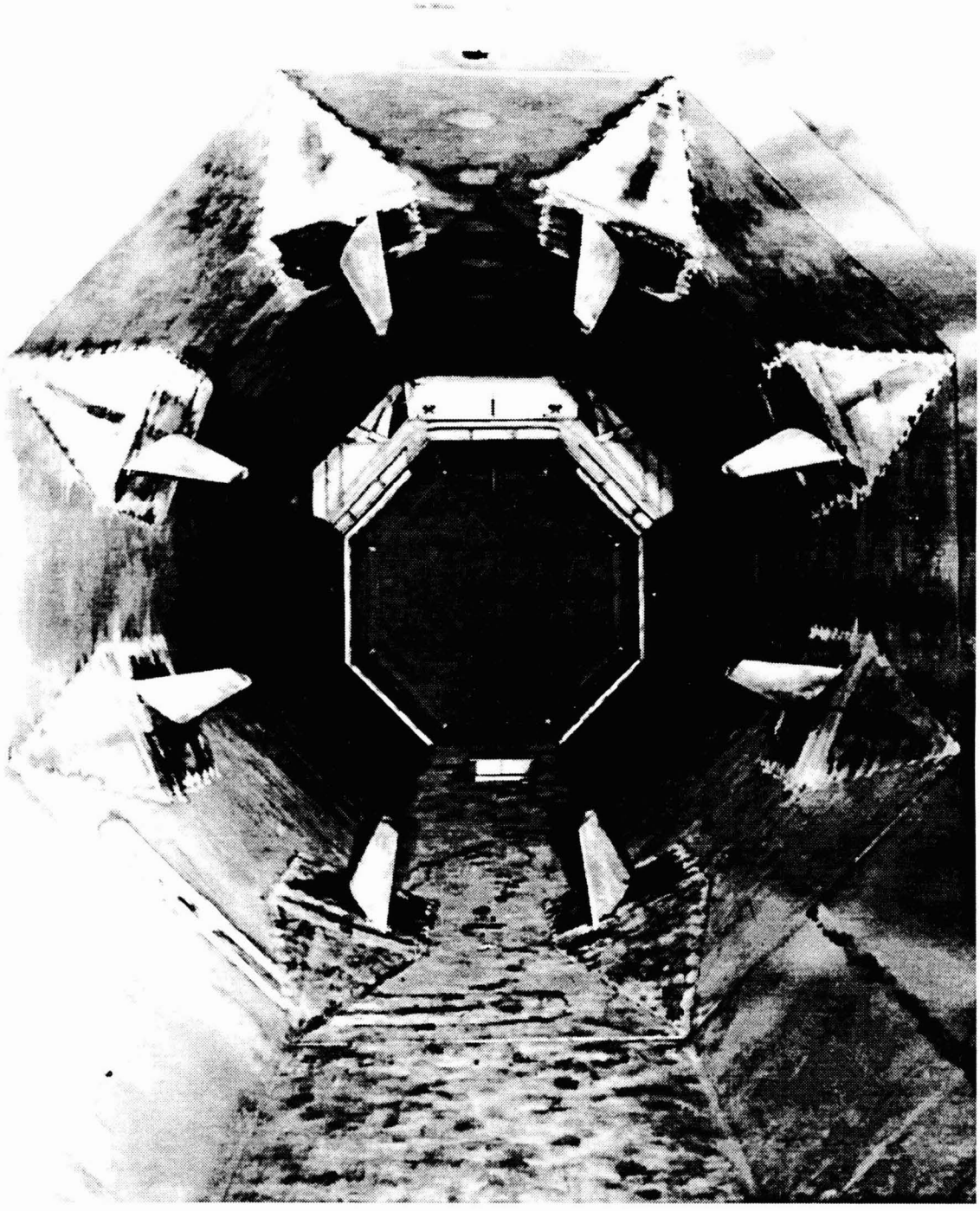

Figure 3. Conventional vane-type vortex generators (reference 7).

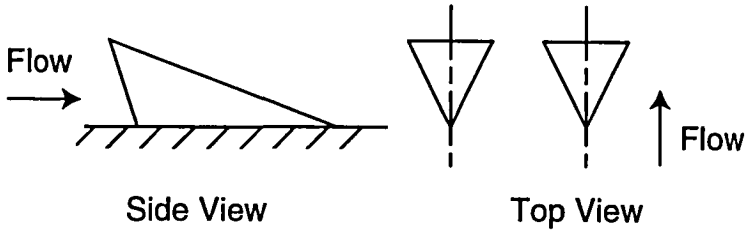

(a) Wedge-type vortex generator

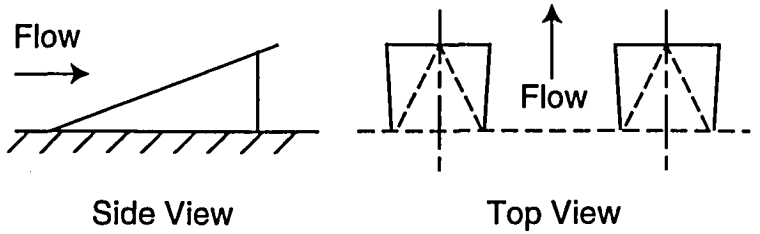

(b) Ramp-type vortex generator

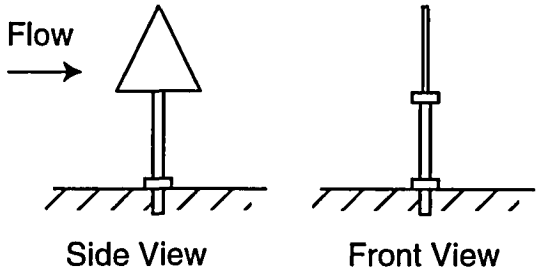

(c) Christmas tree vortex generator

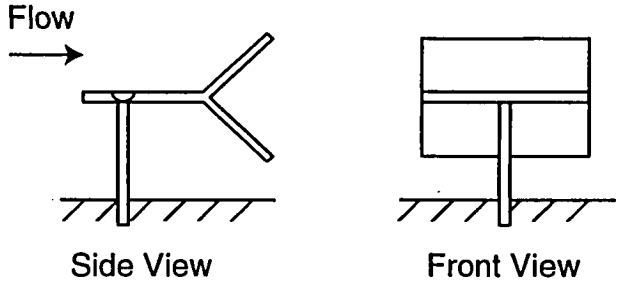

(d) Flap-type vortex generator

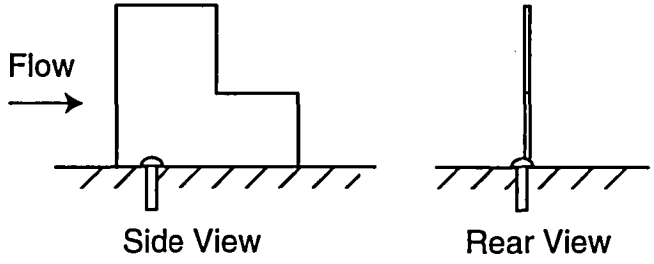

(e) Stepped chord vortex generator

Figure 4. Complex vortex generators (reference 8).

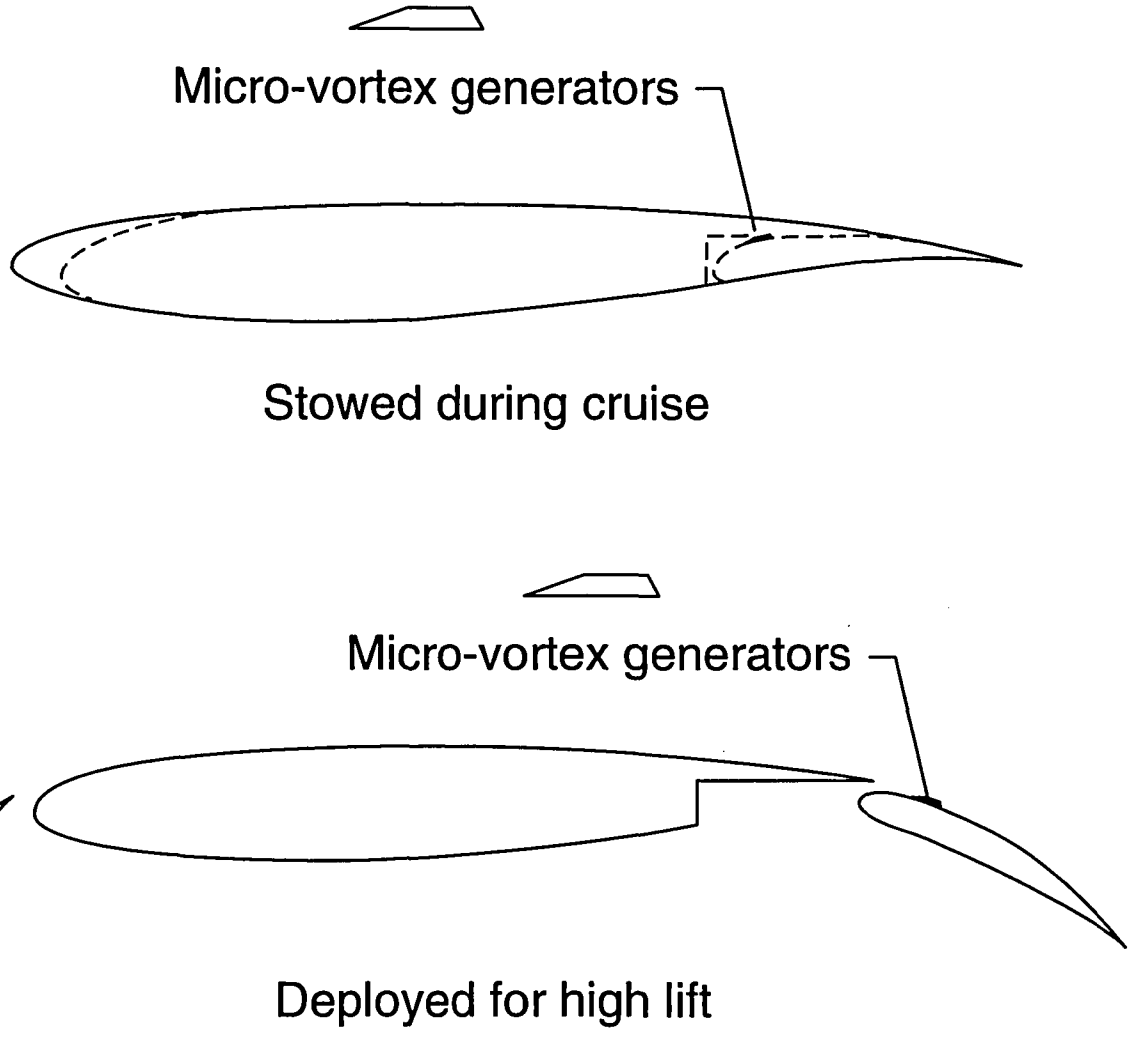

Figure 5. The concept of stowing micro-vortex generators in the flap-well during cruise (reference 14).

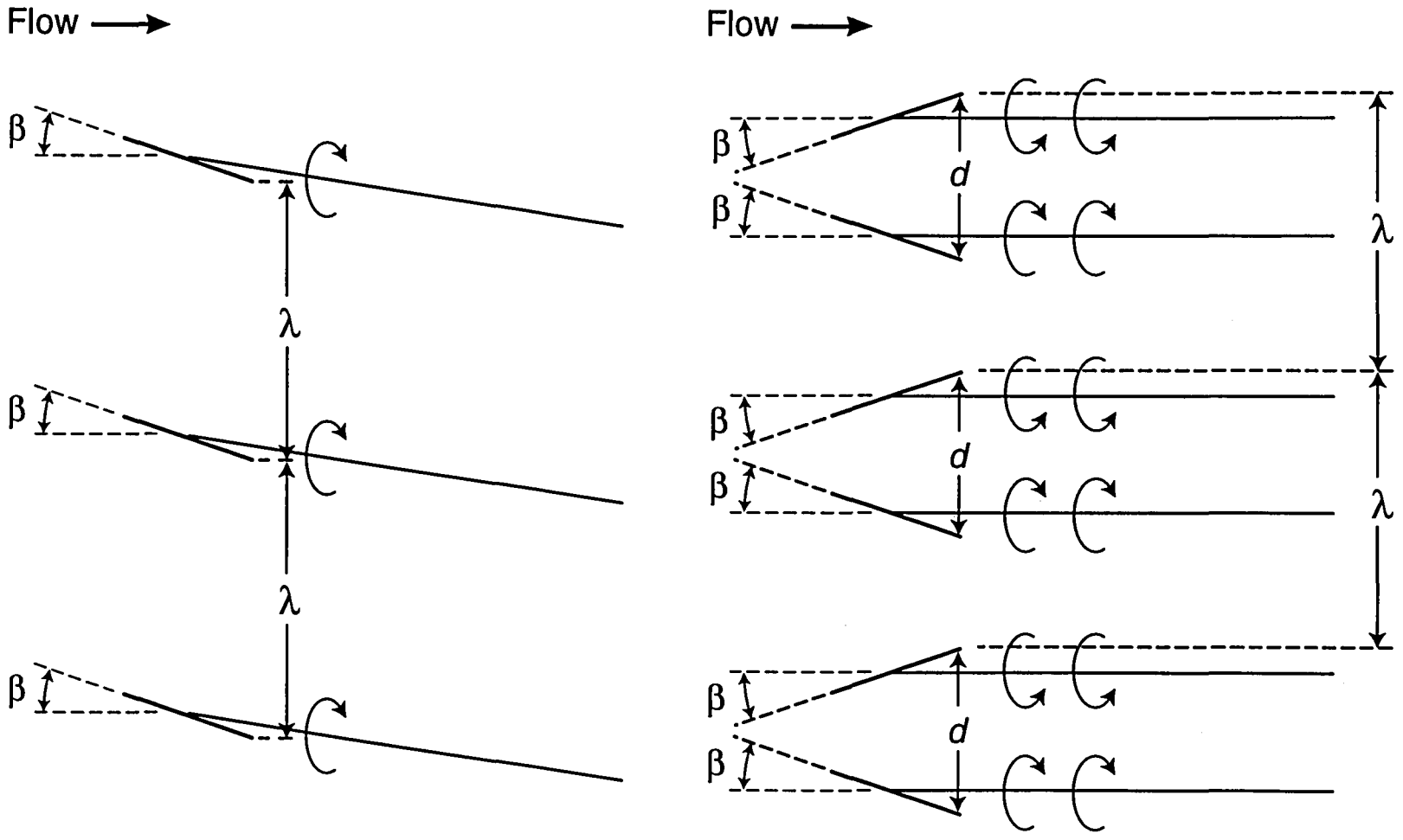

Figure 6. Micro-vortex generator orientation.

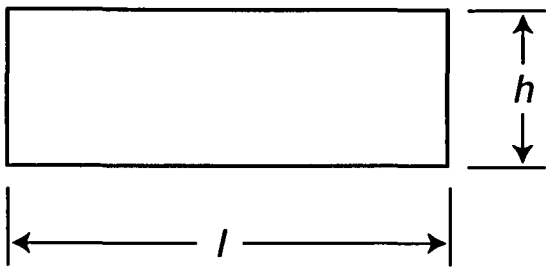

(a) Rectangular

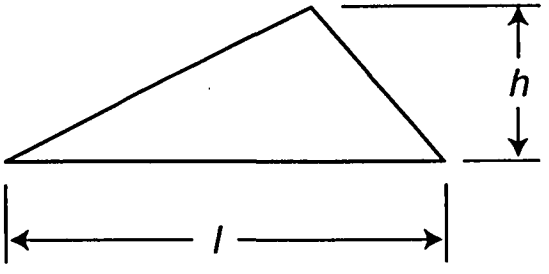

(b) Delta

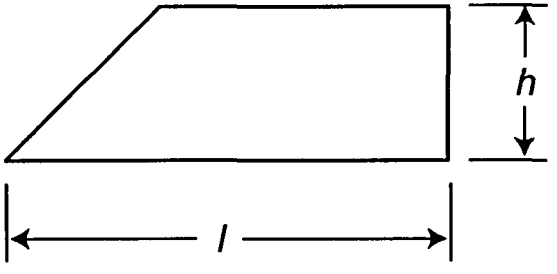

(c) Trapezoidal

Figure 7. Side views of vane-type micro-vortex generator shapes.

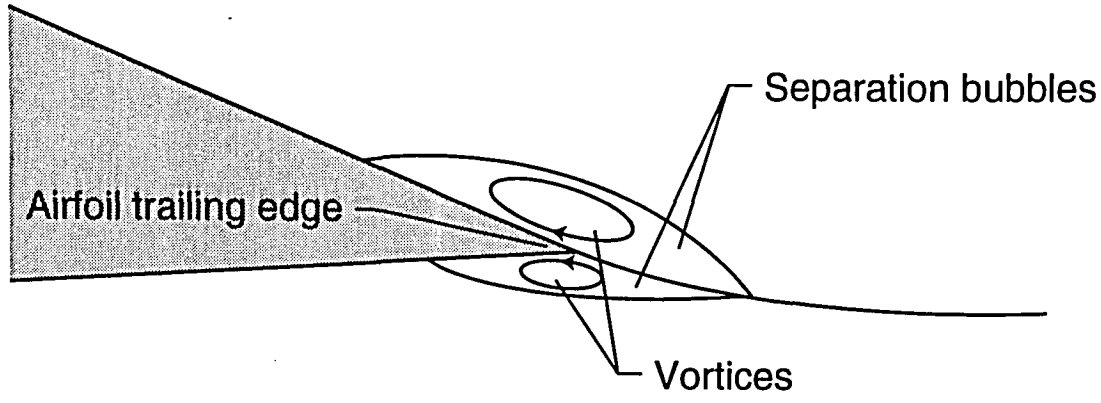

(a) Conventional airfoil with no Gurney flap

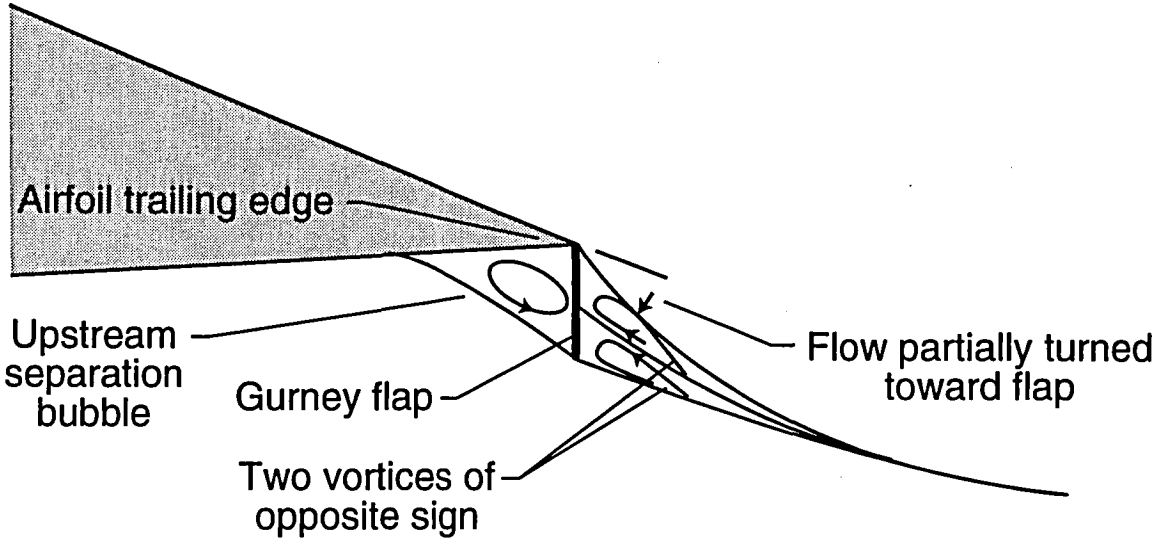

(b) Airfoil with Gurney flap

Figure 8. Liebeck's hypothesized flow fields at the airfoil trailing edge without and with a Gurney flap (reference 18).

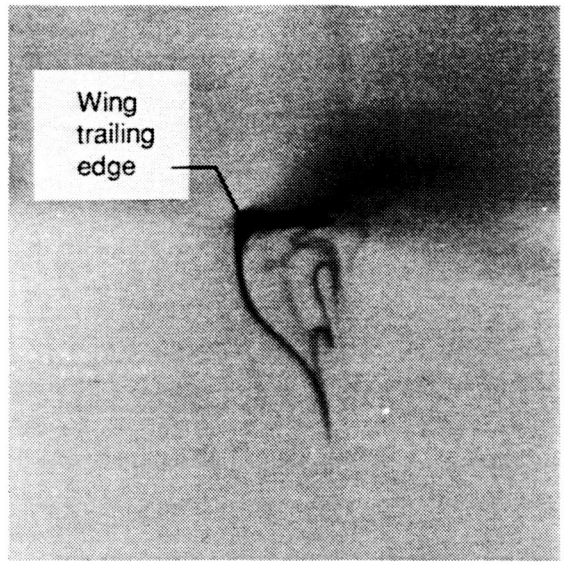

(a) Lower-surface vortex shedding

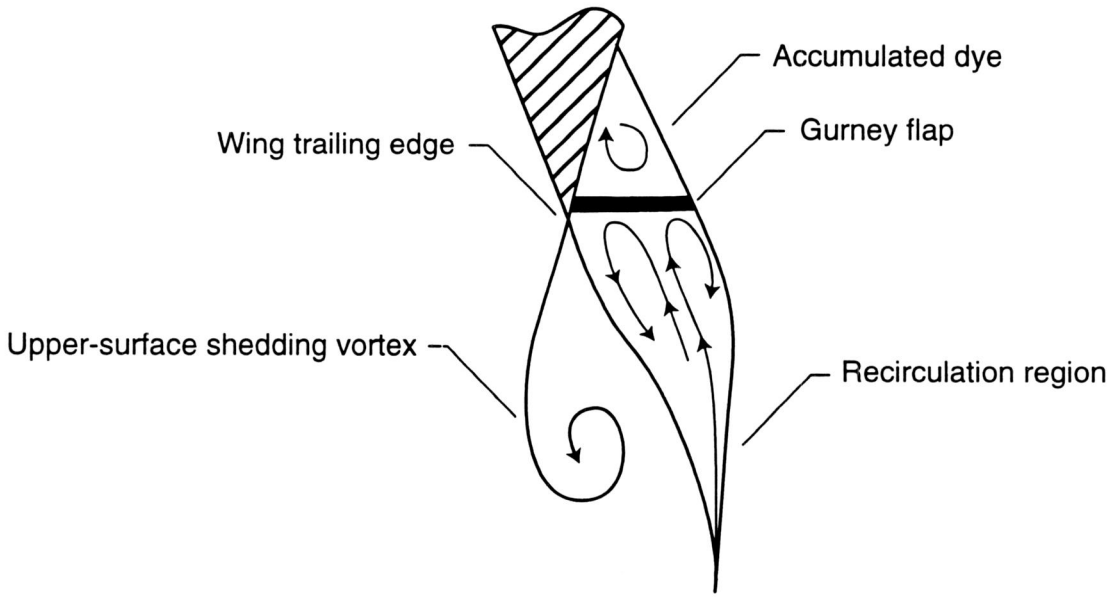

(b) Flow inside recirculation region

Figure 9. Trailing-edge flow field near Gurney flap from the water-tunnel study by Neuhart and Pendergraft (reference 17).

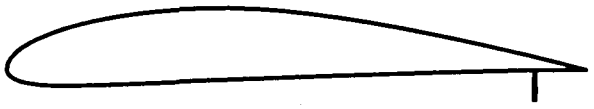

Figure 10. Split-flap configuration (reference 19).

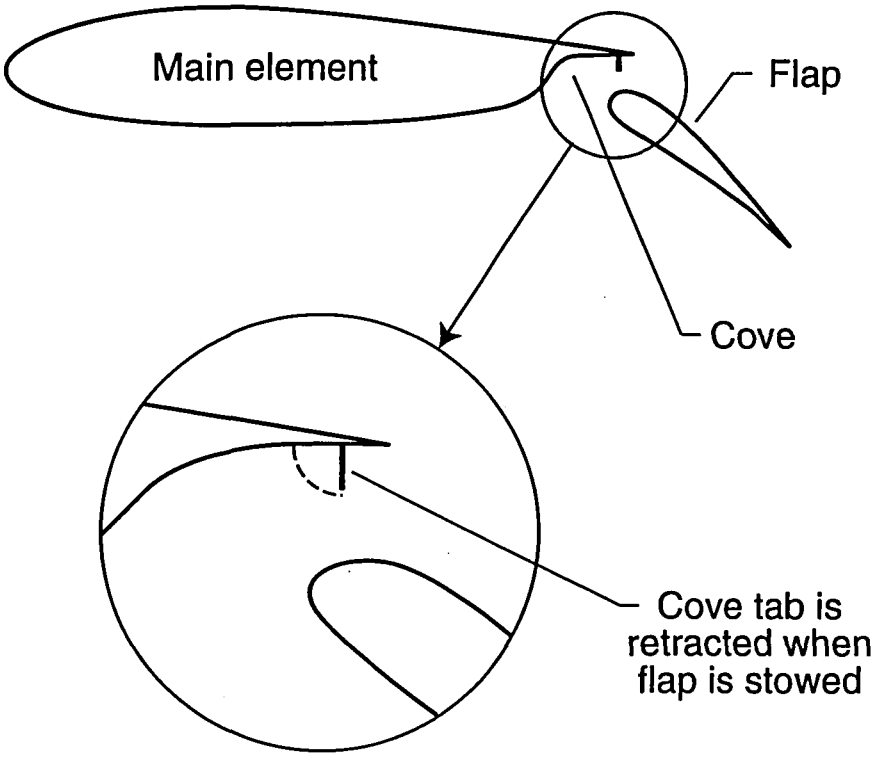

Figure 11. Gurney flap mounted at trailing edge of main element in the cove region (reference 21).

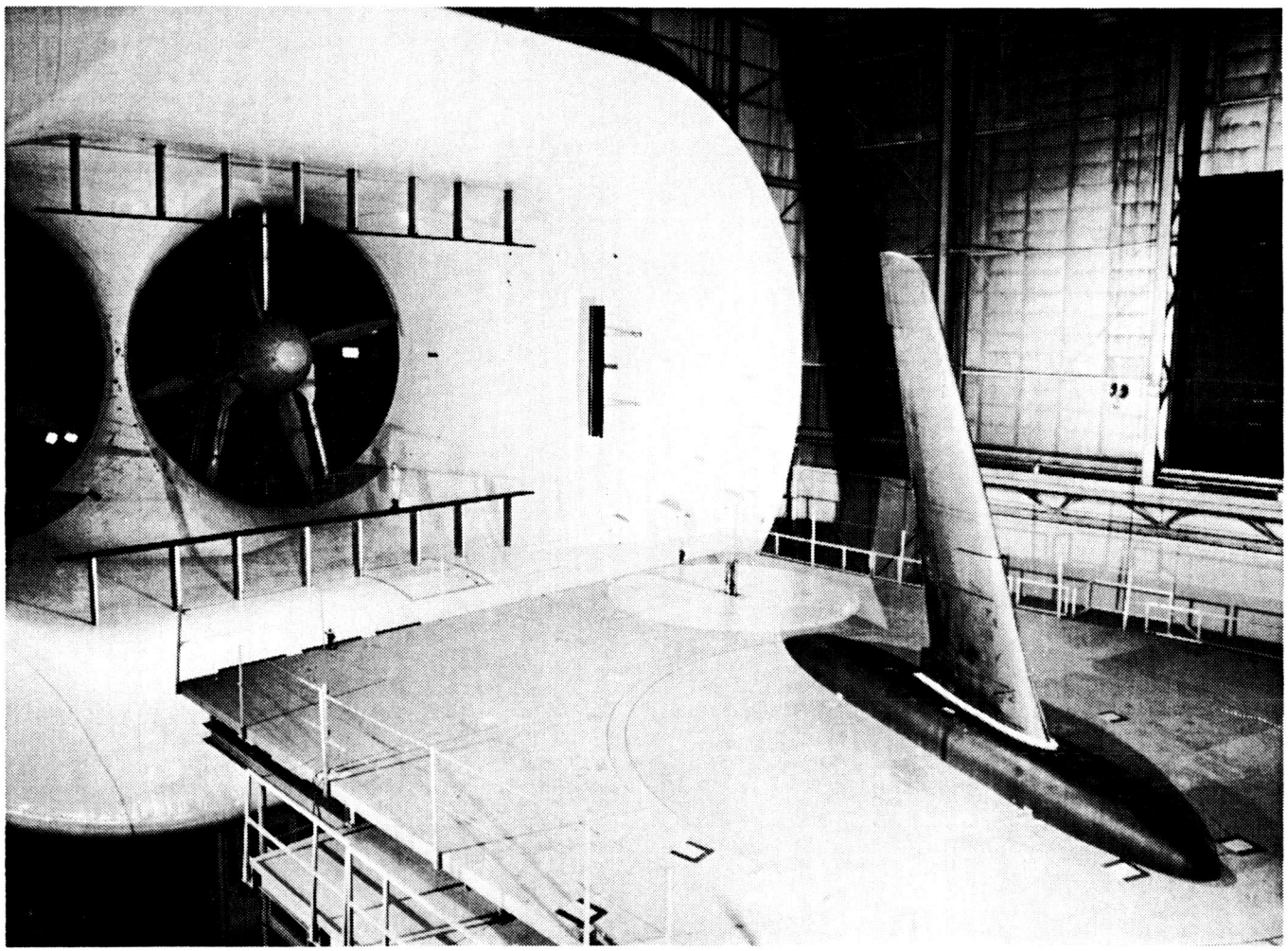

Figure 12. Photograph of full-scale, semi-span business jet wing mounted in NASA Langley's 30- by 60-Foot Tunnel.

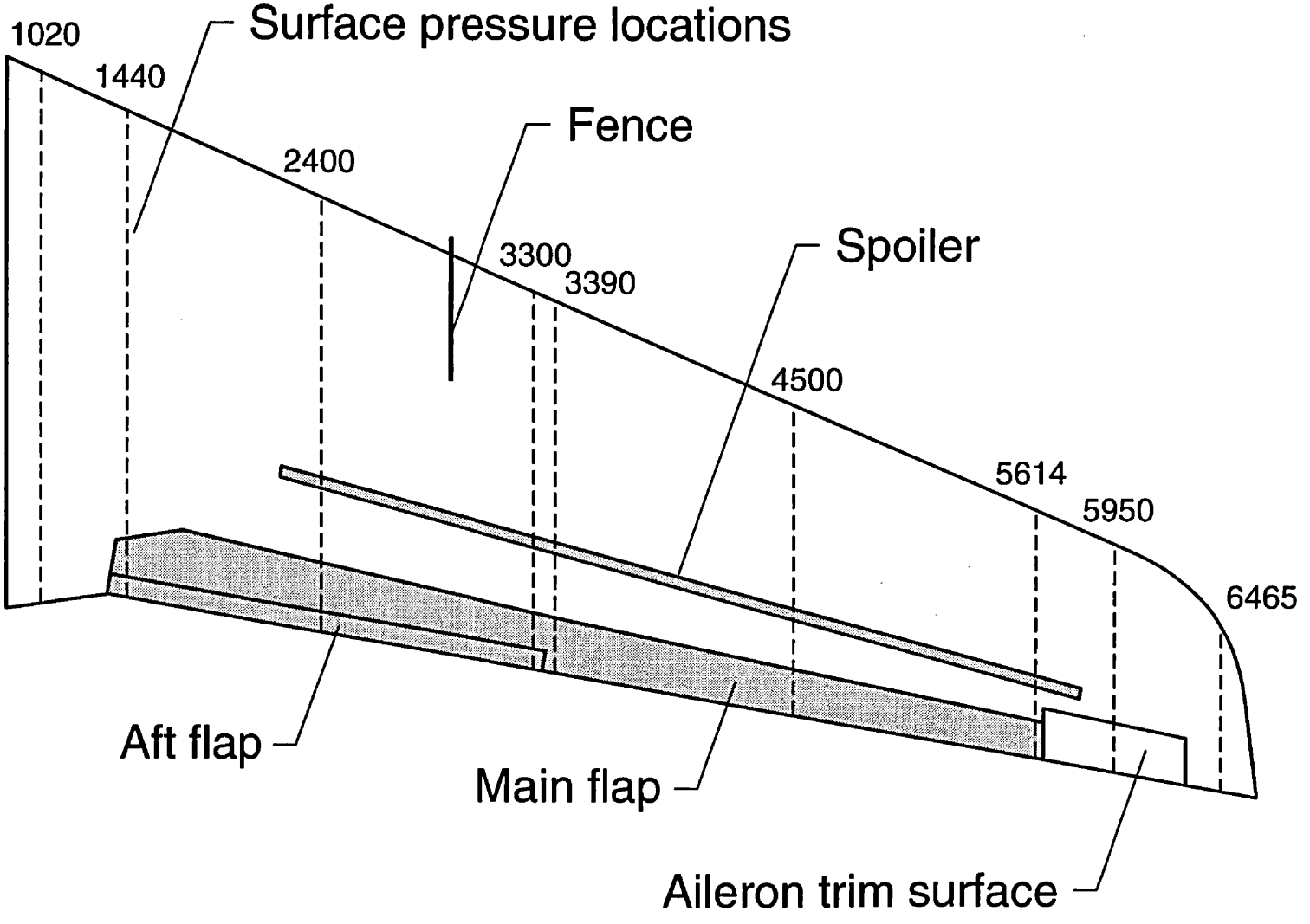

Figure 13. Schematic of the business jet wing.

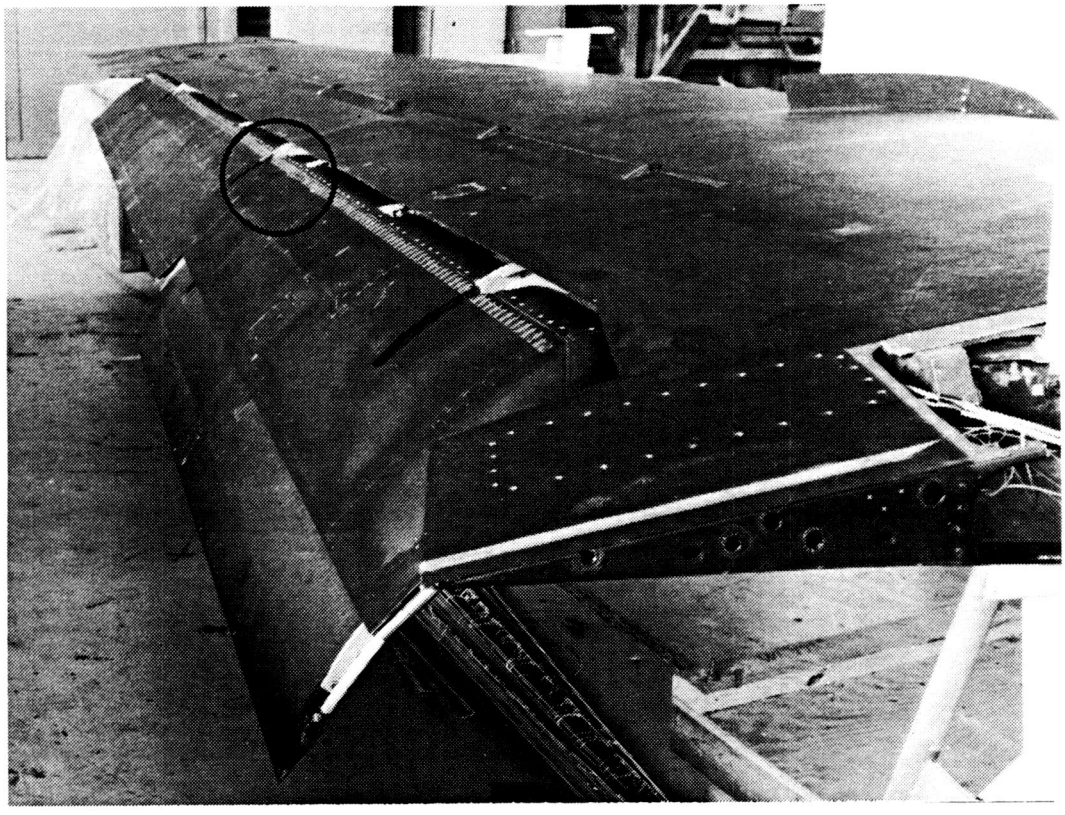

(a) Flap-tracks, (gaps) and push-rods.

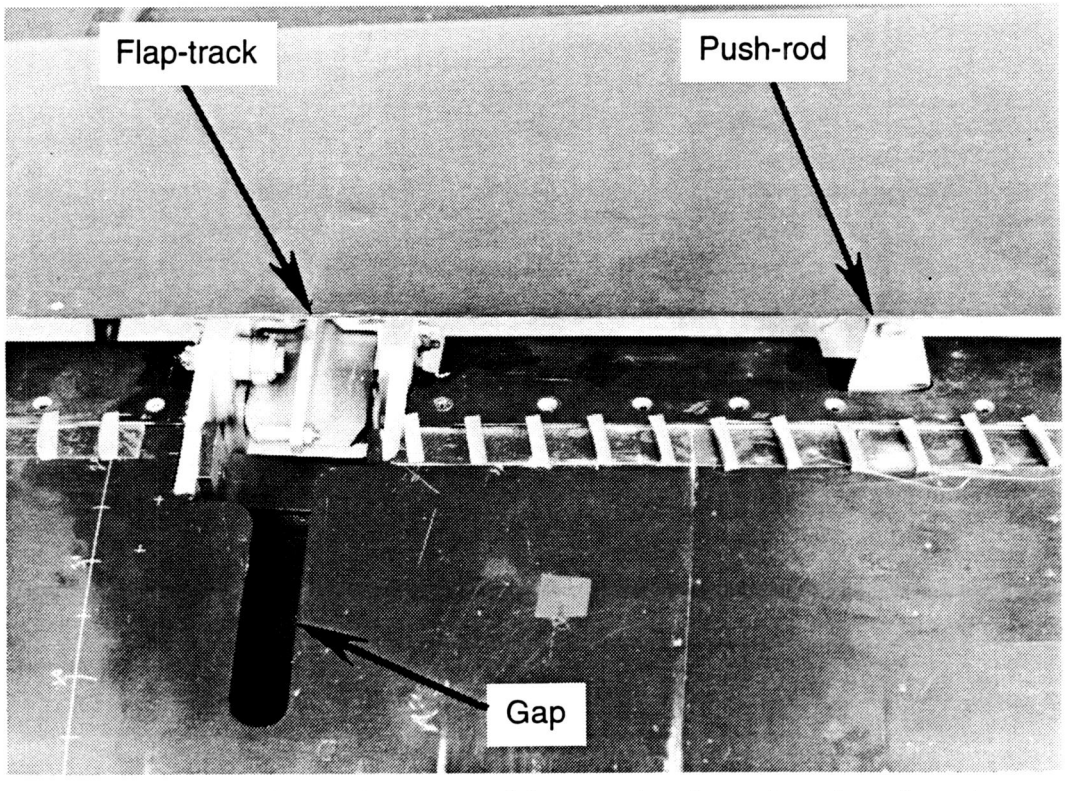

(b) Details of the middle set of flap-tracks, (gaps) and push-rods.

Figure 14. Photographs of flap-tracks, gaps and push-rods on wing.

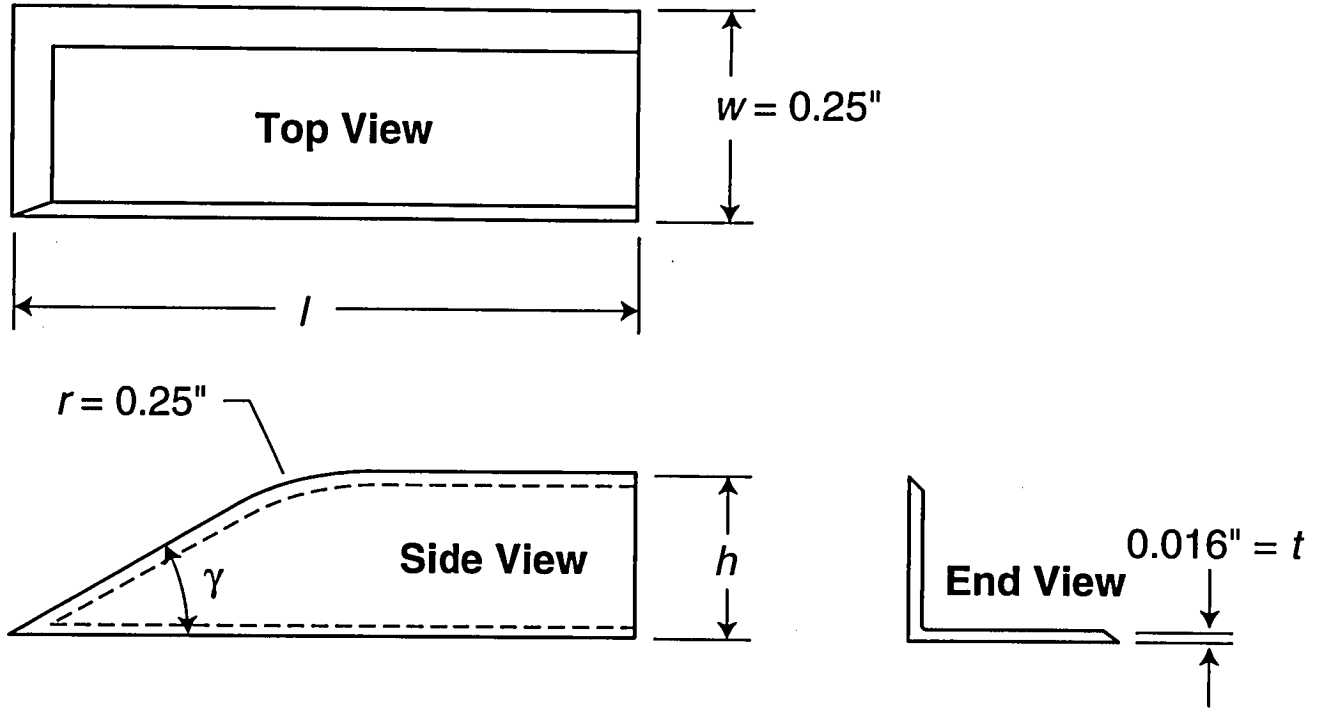

Figure 15. The basic micro-vortex generator geometry designed for this study (Note: not to scale).

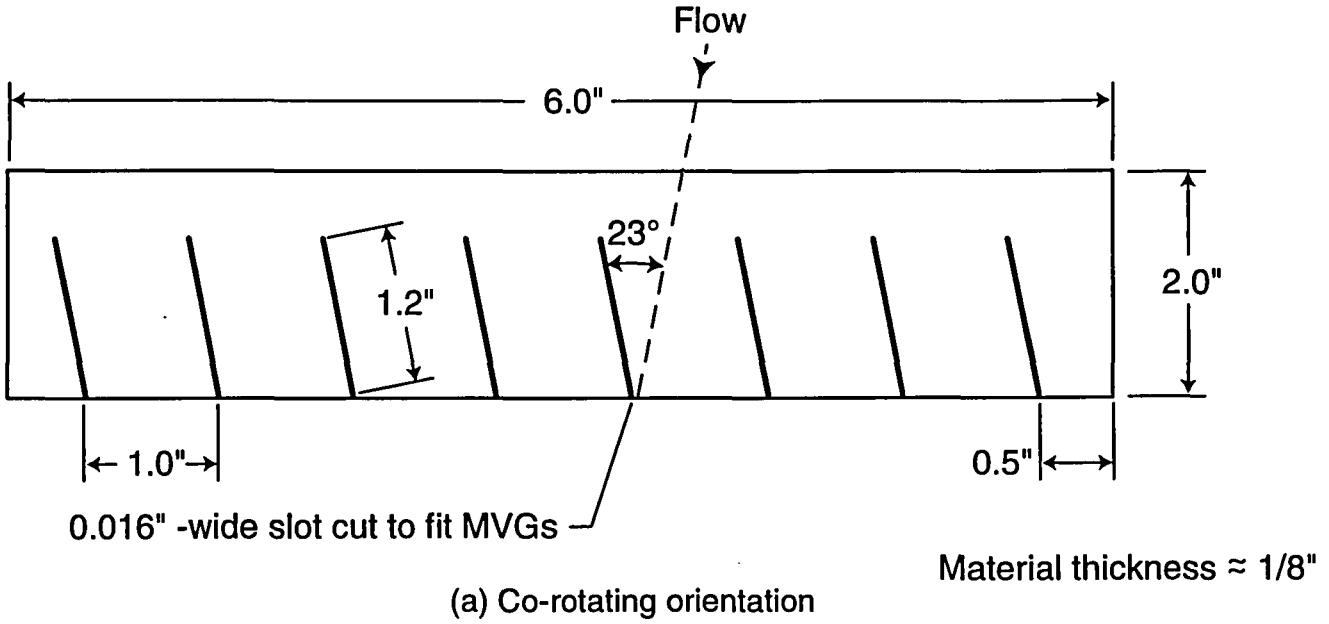

(a) Co-rotating orientation

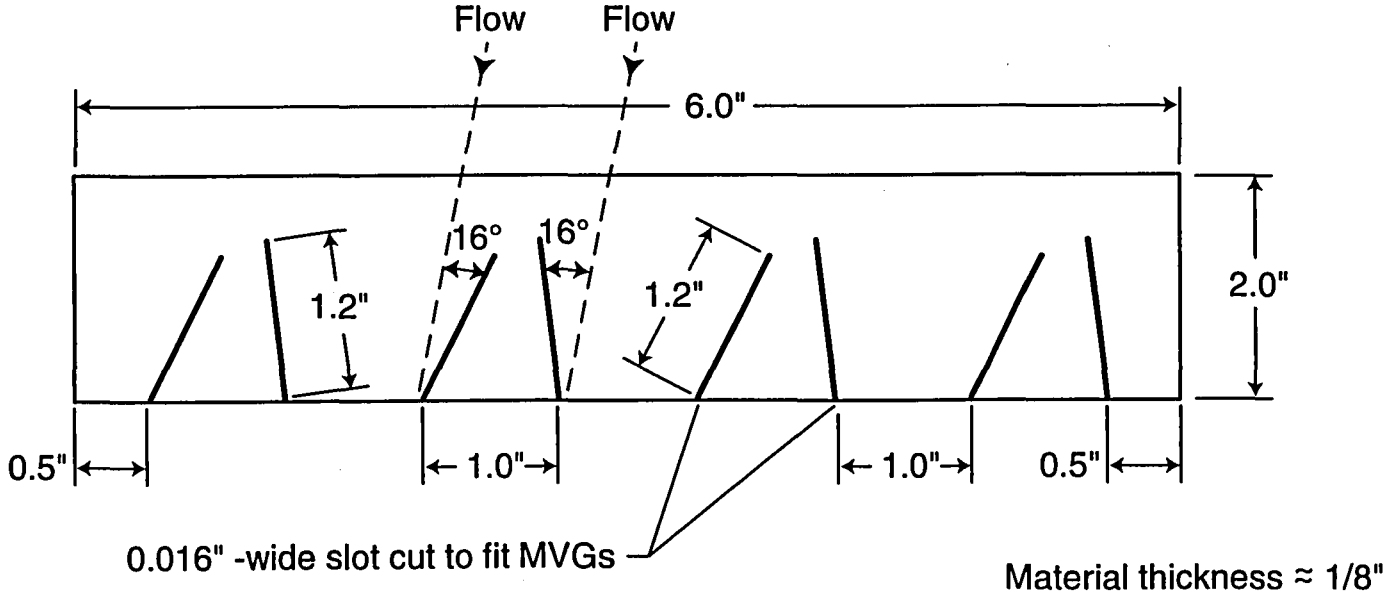

(b) Counter-rotating orientation

Figure 16. Micro-vortex generator mounting guide strips (Note: not to scale).

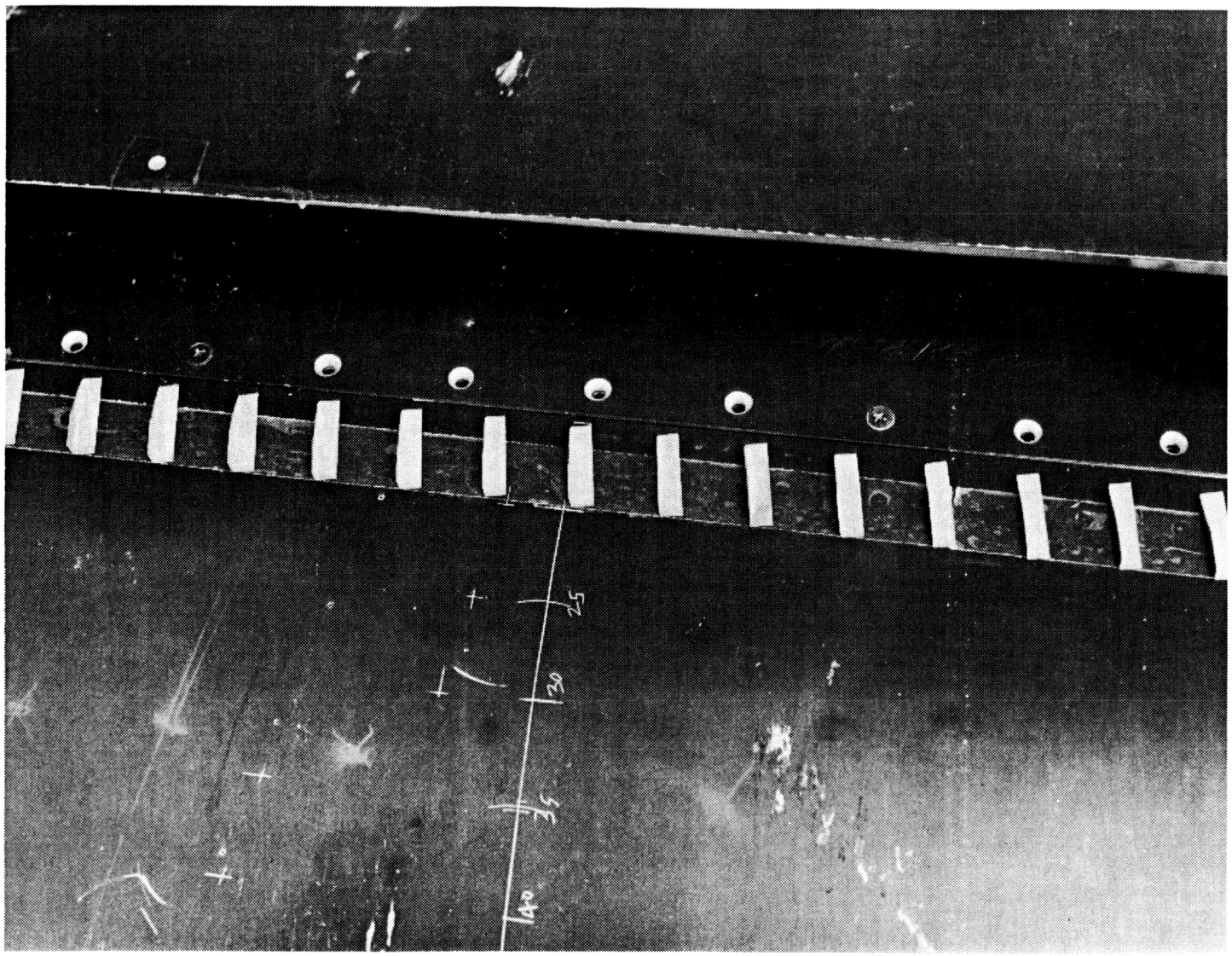

Figure 17. Photograph of micro-vortex generators mounted on flap.

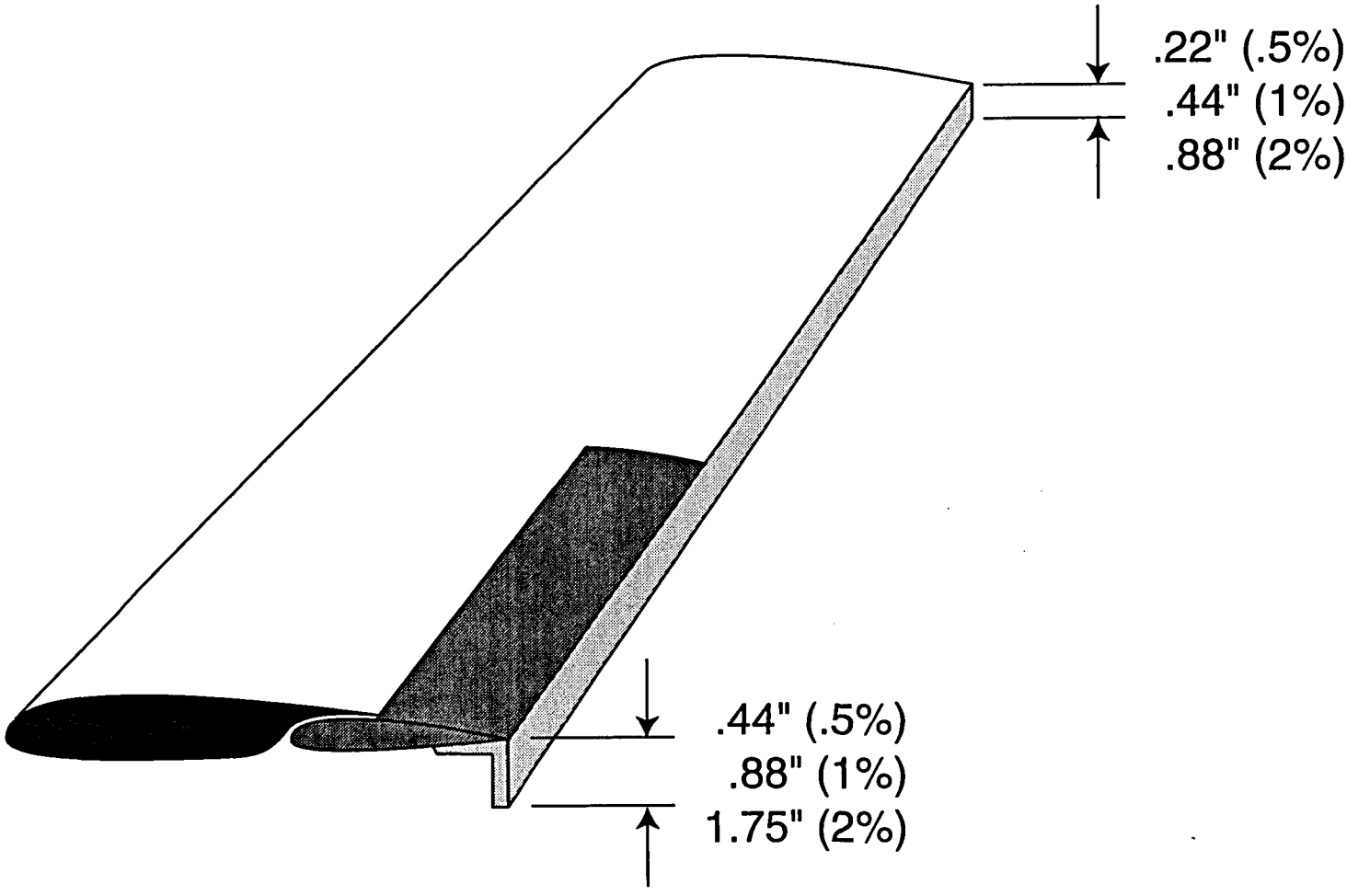

Figure 18. Gurney flaps applied to the trailing edge of the single-slotted flap system.

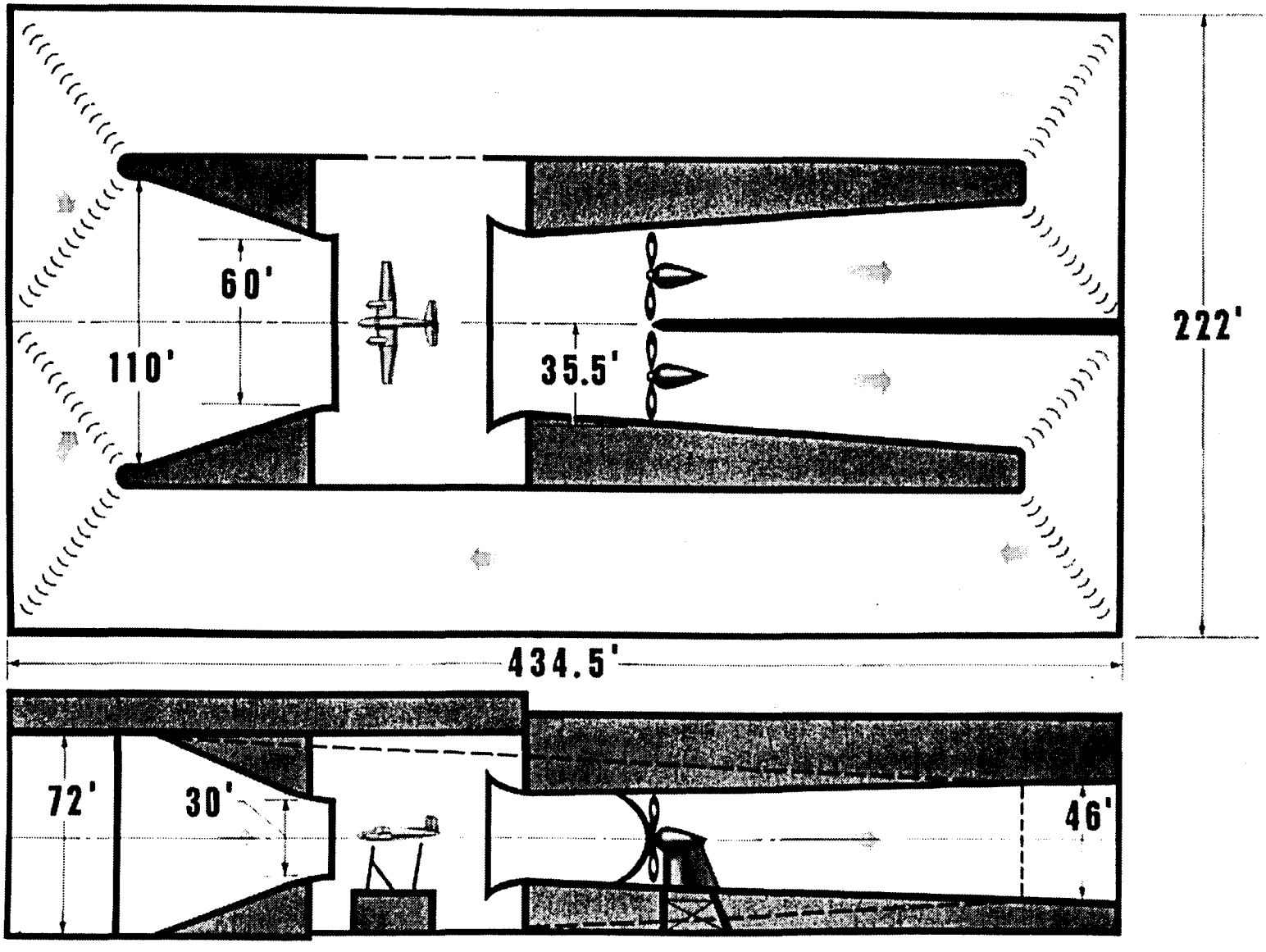

Figure 19. NASA Langley's 30- by 60-Foot Tunnel.

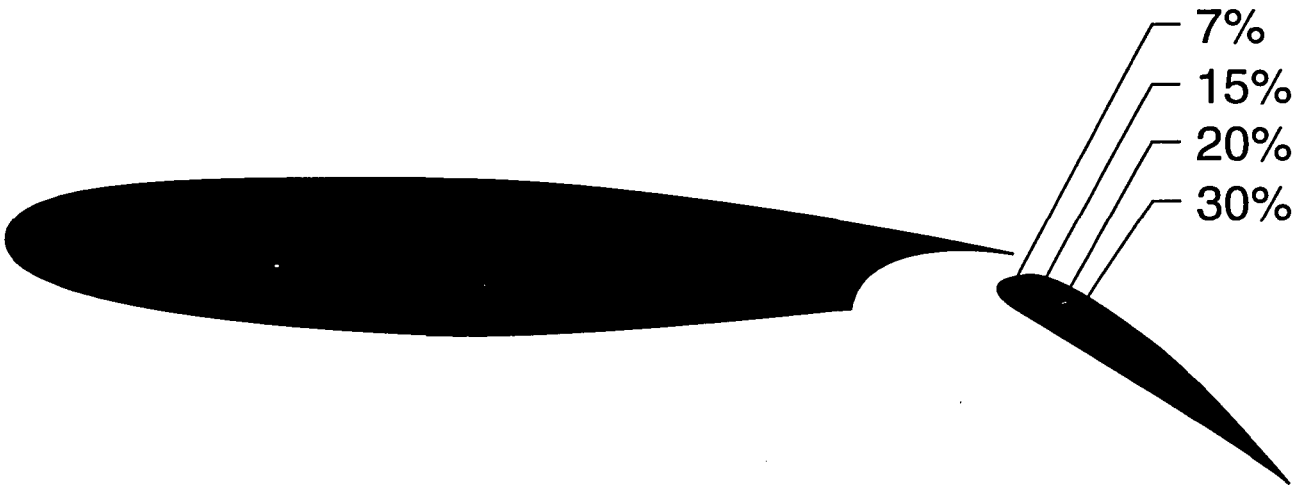

Figure 20. Micro-vortex generator locations tested on the single-slotted flap.

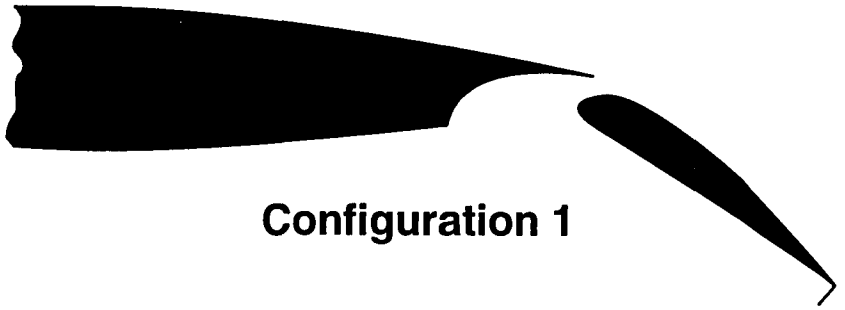

Figure 21. 1.0% Gurney flap applied to the trailing edge of the single-slotted flap.

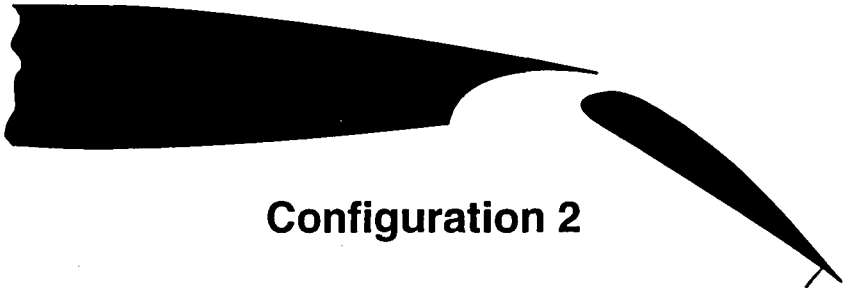

Figure 22. 1.0% Gurney flap mounted approximately one inch forward of the trailing edge of the single-slotted flap.

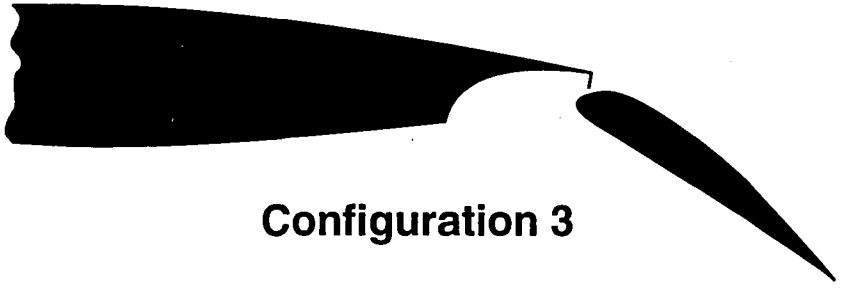

Figure 23. 0.5% Gurney flap applied to the trailing edge of the main airfoil element (in the cove region).

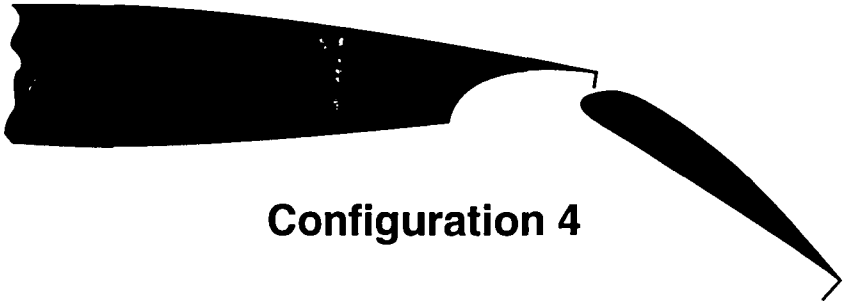

Figure 24. 0.5% Gurney flap applied to the trailing edge of the main airfoil element (cove) and the 1.0% Gurney flap applied to the trailing edge of the single-slotted flap.

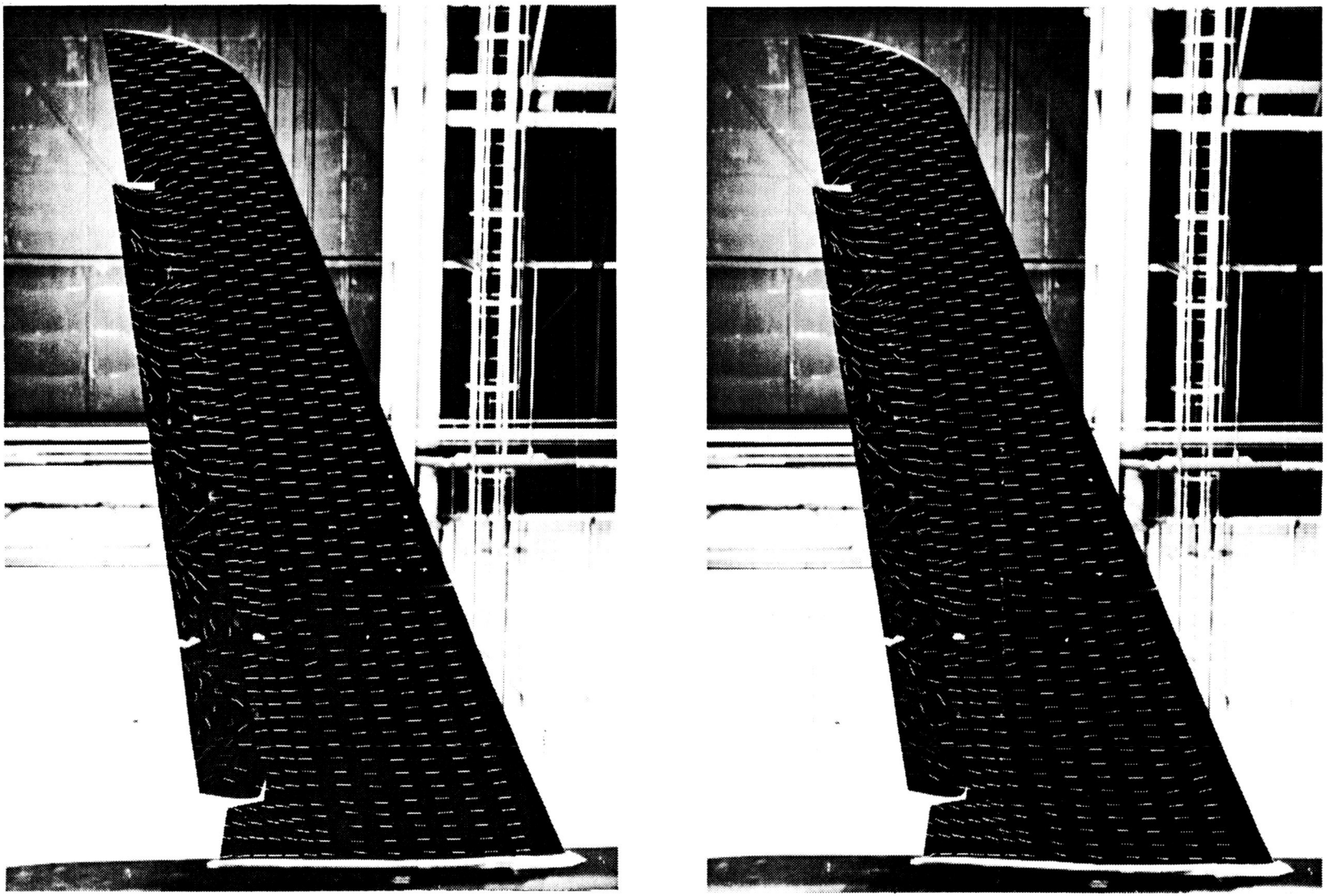

(a) $\alpha = 0°$ (b) $\alpha = 6°$

Figure 25. Flow visualization of the full-scale, semi-span business jet wing at $\delta_f = 34°$.

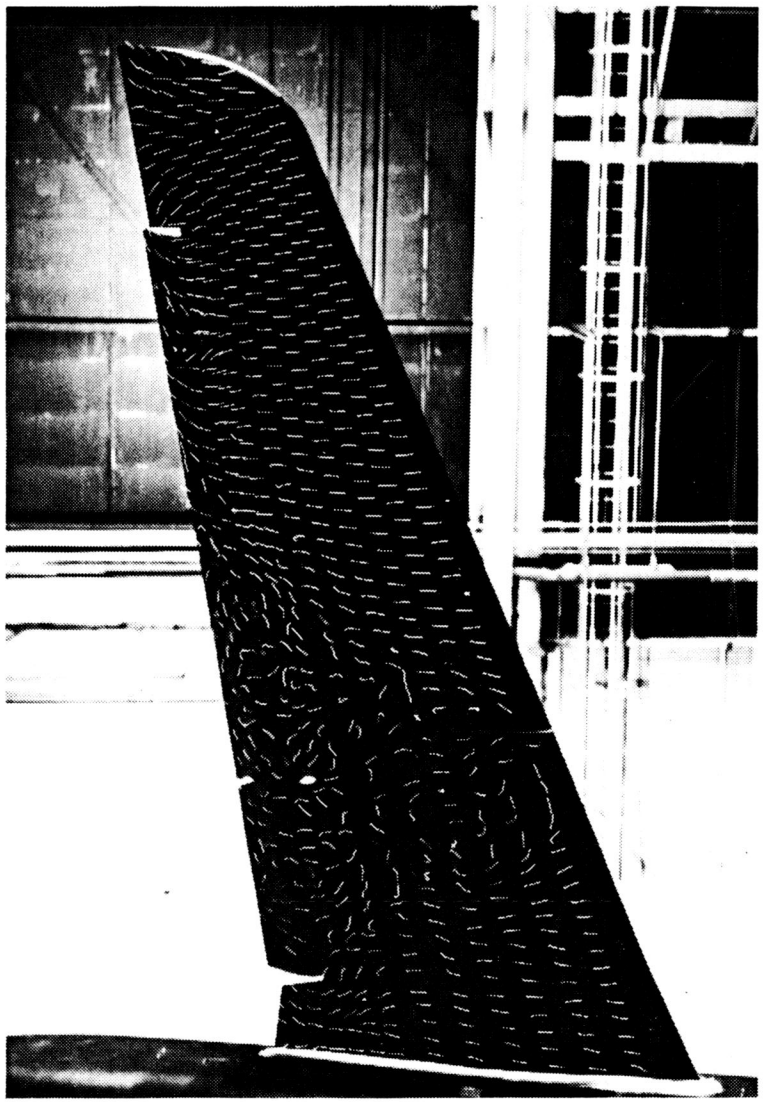

(c) $\alpha = 18°$

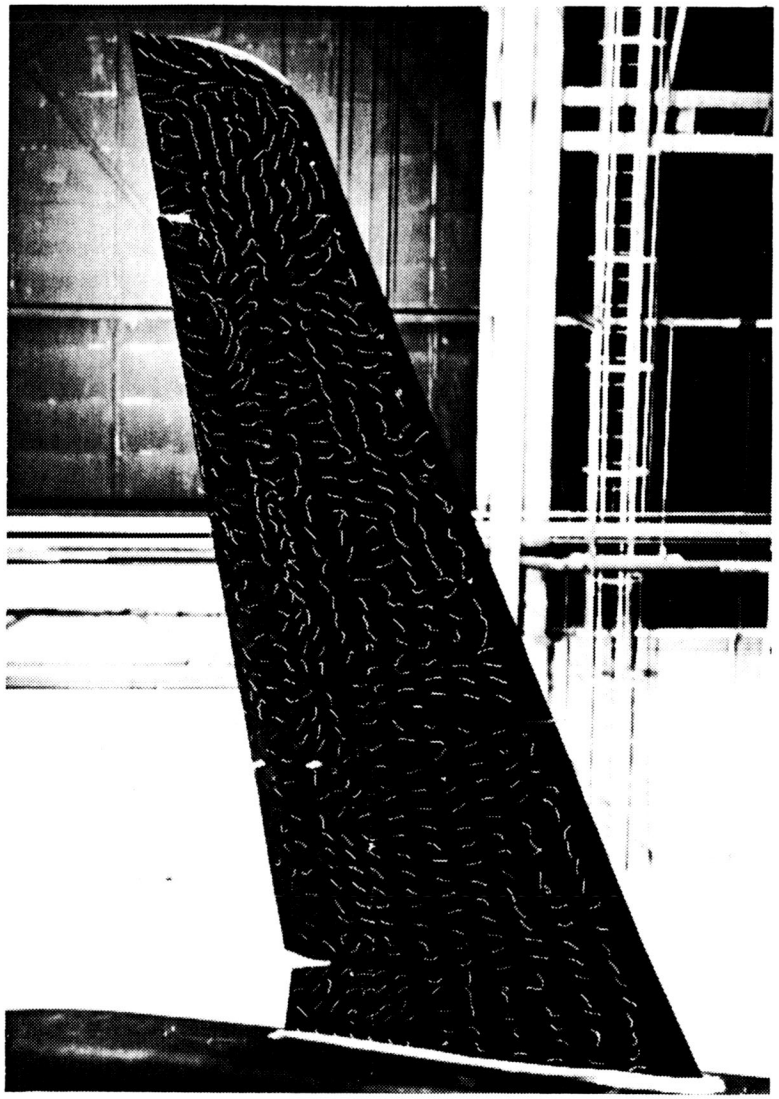

(d) $\alpha = 24°$

Figure 25. Concluded.

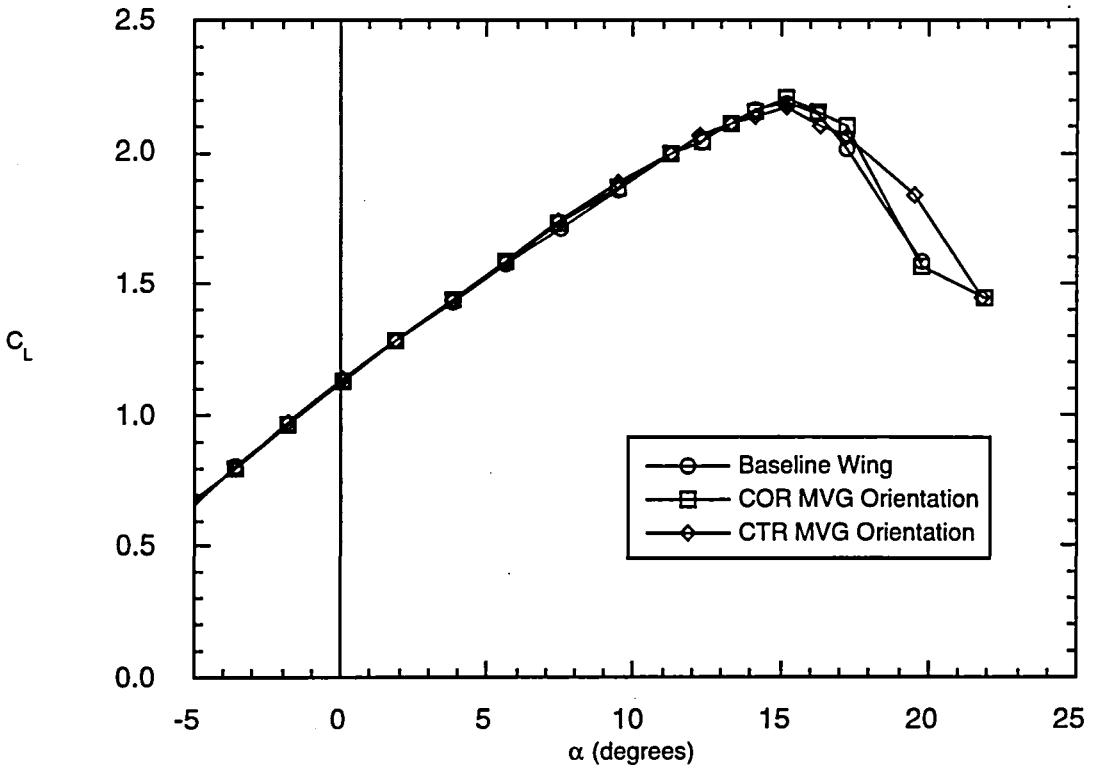

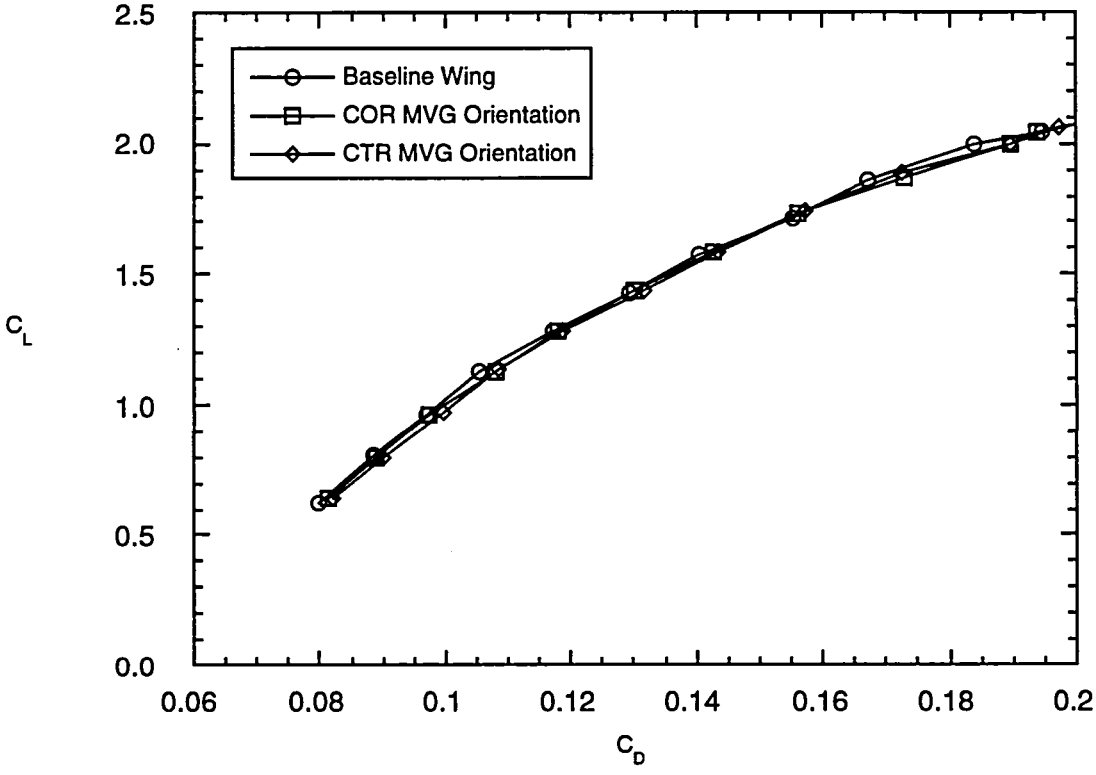

Figure 26. Effect of MVG 6 orientation on the lift and drag coefficients; $C_f = 20\%c_f$, $\beta = 16°$, $\lambda = 1"$ (COR), $\lambda = 2"$ (CTR), $d = 1"$ (CTR), $\delta_f = 34°$.

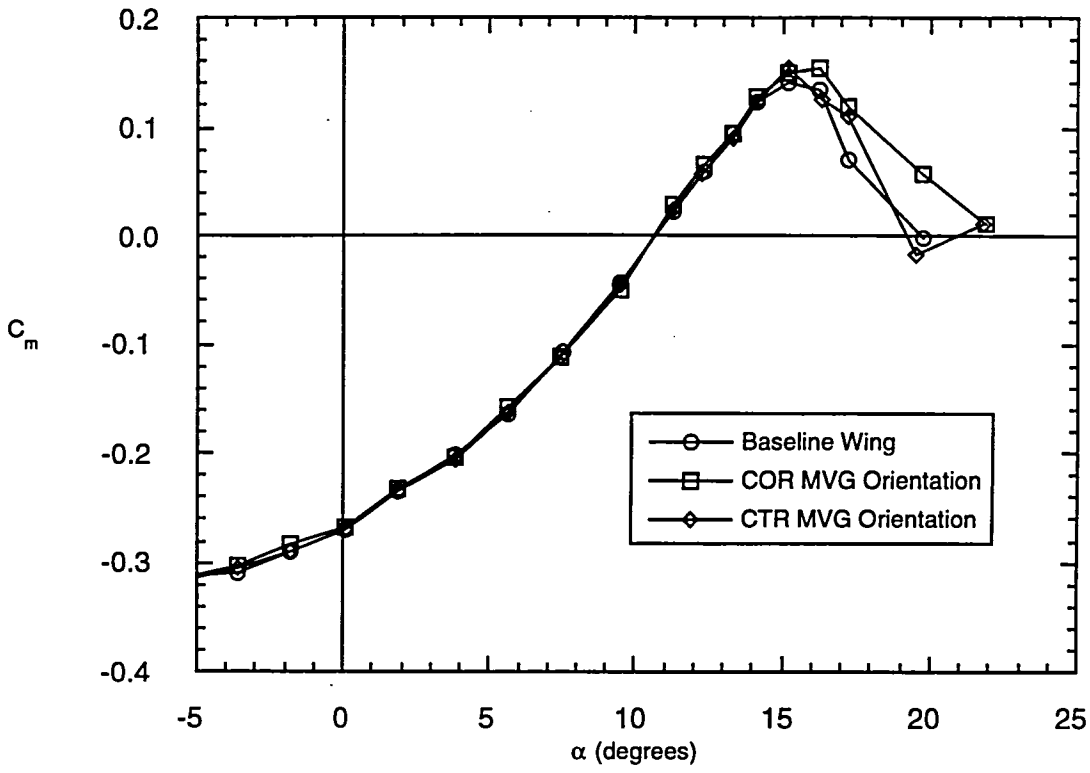

Figure 27. Effect of MVG 6 orientation on pitching moment coefficients; $C_f = 20\%c_f$, $\beta = 16°$, $\lambda = 1"$ (COR), $\lambda = 2"$ (CTR), $d = 1"$ (CTR), $\delta_f = 34°$.

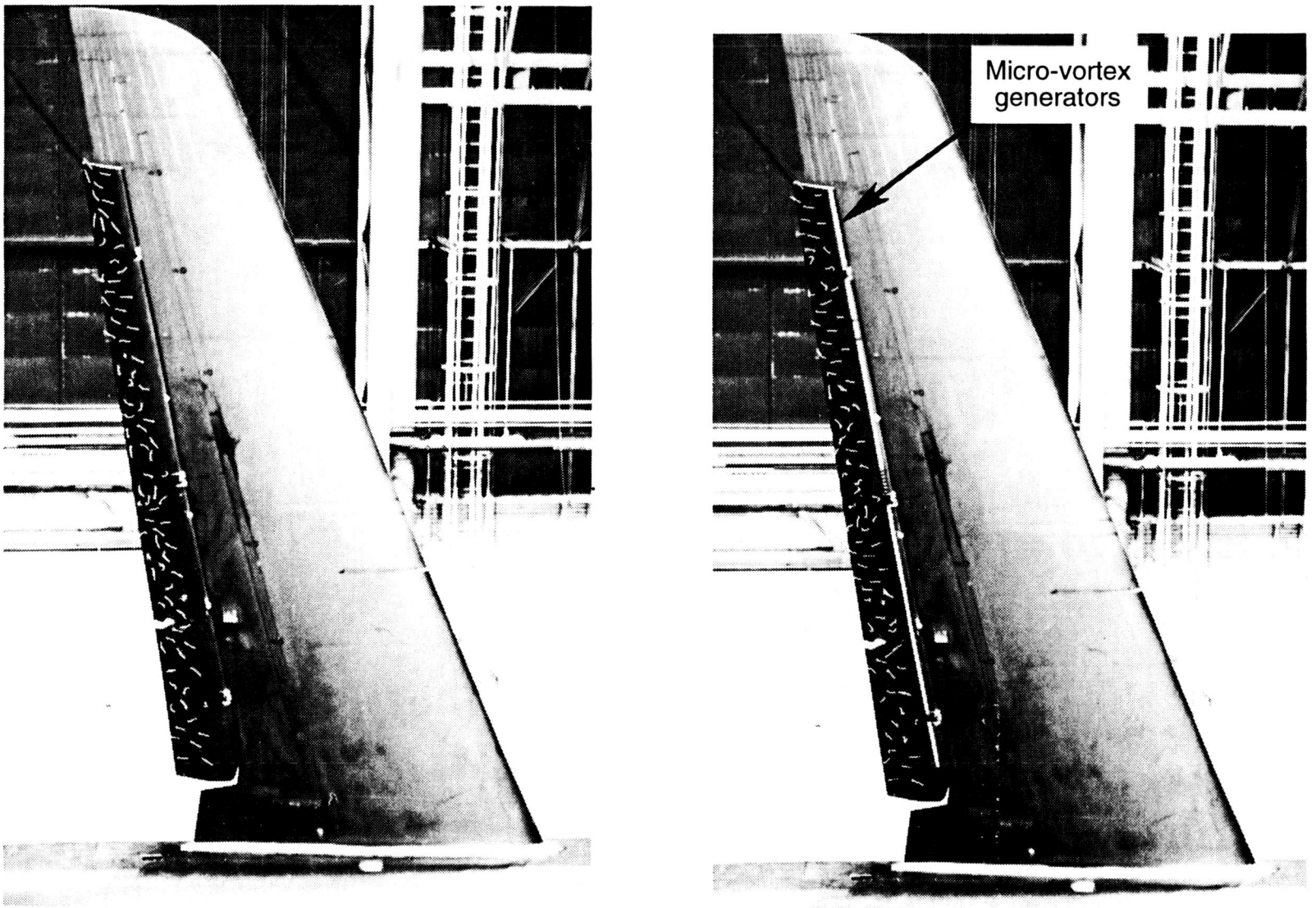

(a) Baseline wing, no micro-vortex generators.

(b) MVG 6, COR orientation, C_f = 20%c_f, β = 16°, λ = 1".

Figure 28. Flow visualization of the single-slotted flap element; δ_f = 34°, α = 4°.

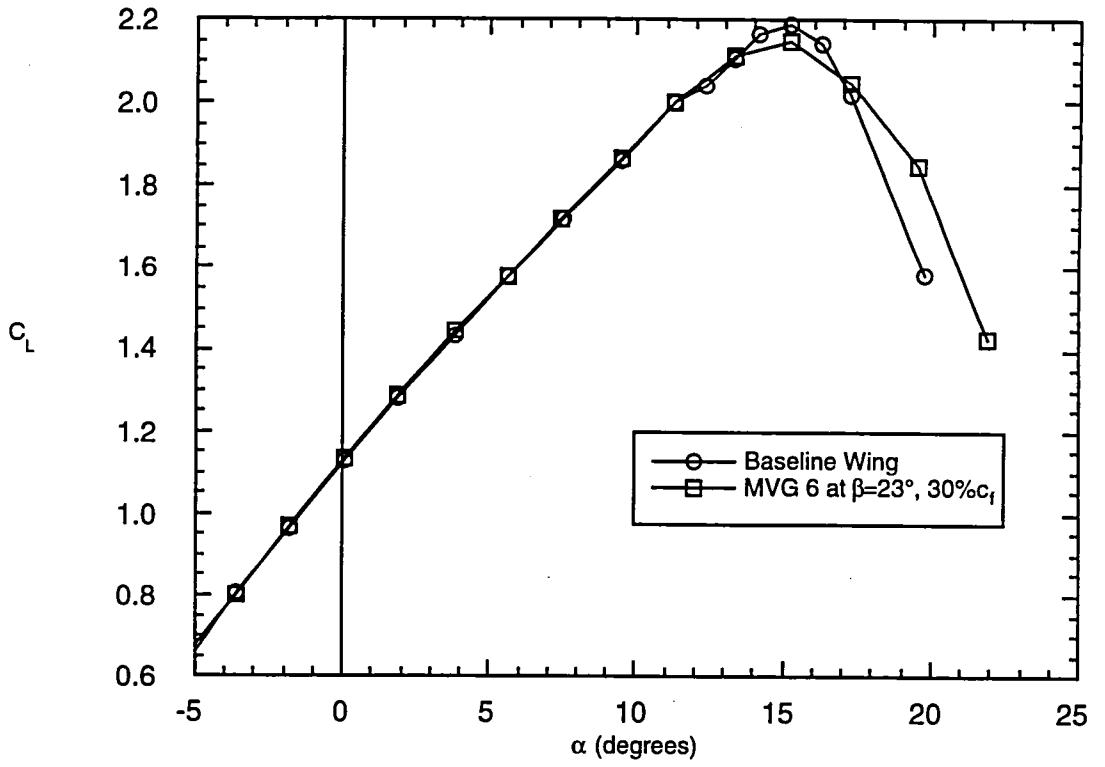

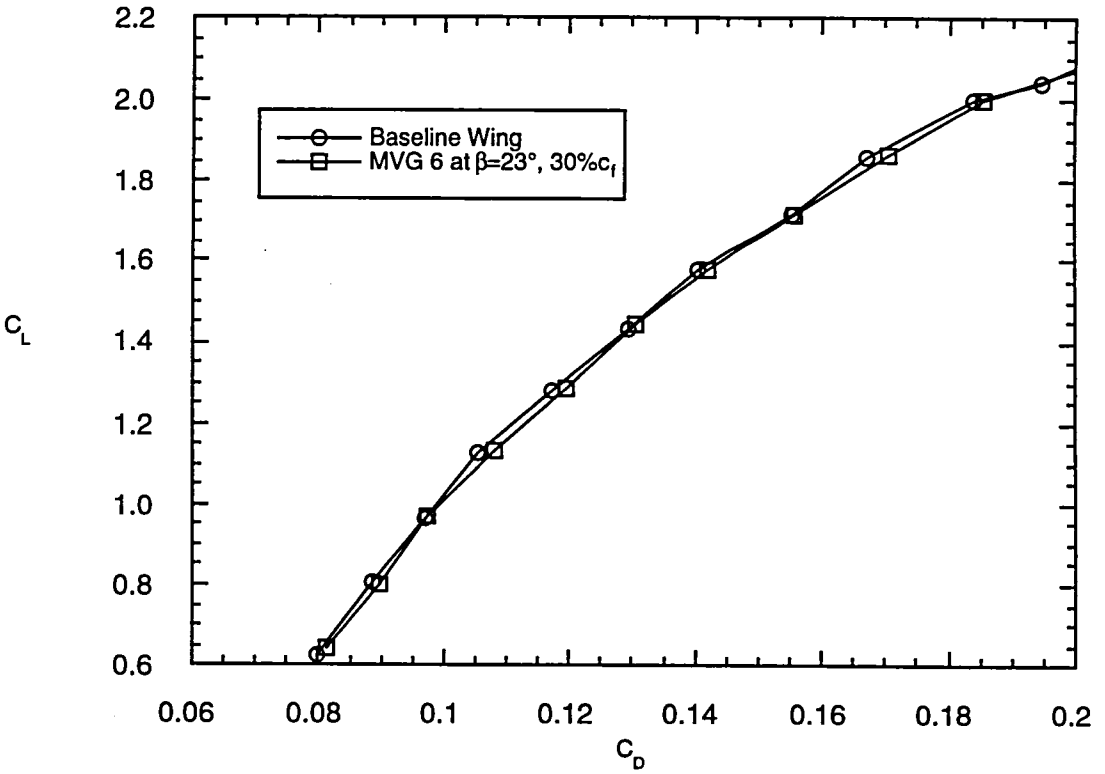

Figure 29. Effect of β and C_f on the lift and drag coefficients; COR orientation, $\lambda = 1"$, $\delta_f = 34°$.

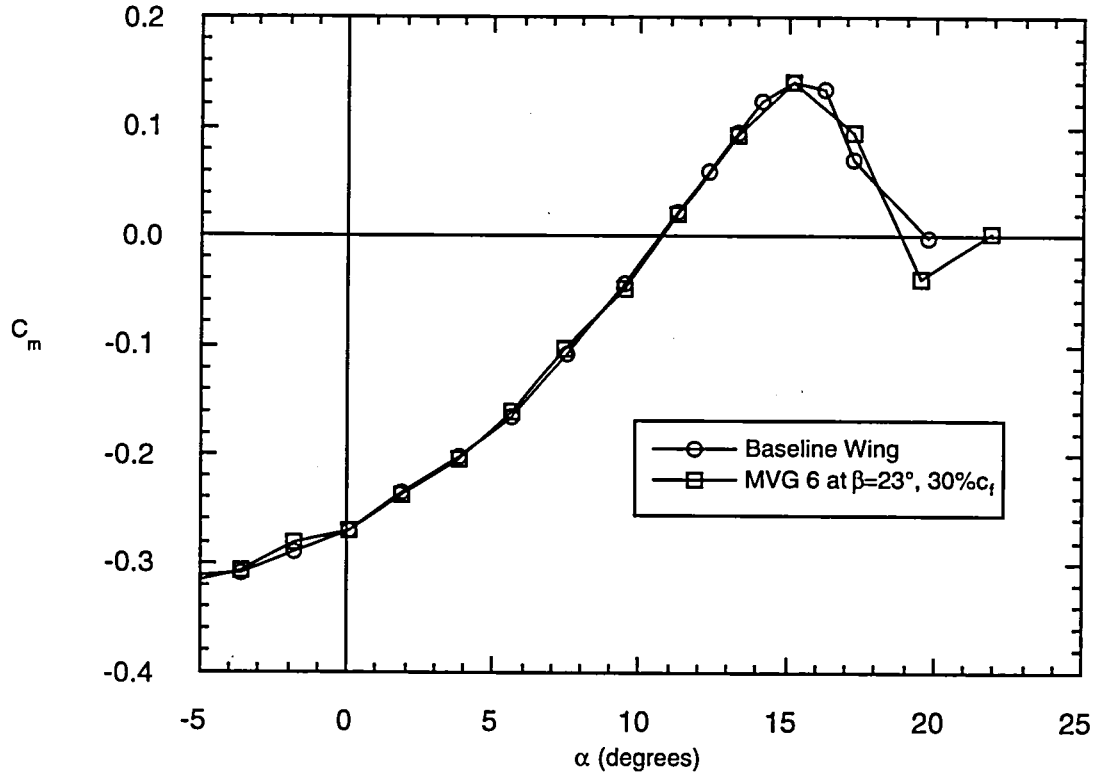

Figure 30. Effect of β and C_f on the pitching moment coefficient; COR orientation, $\lambda = 1"$, $\delta_f = 34°$.

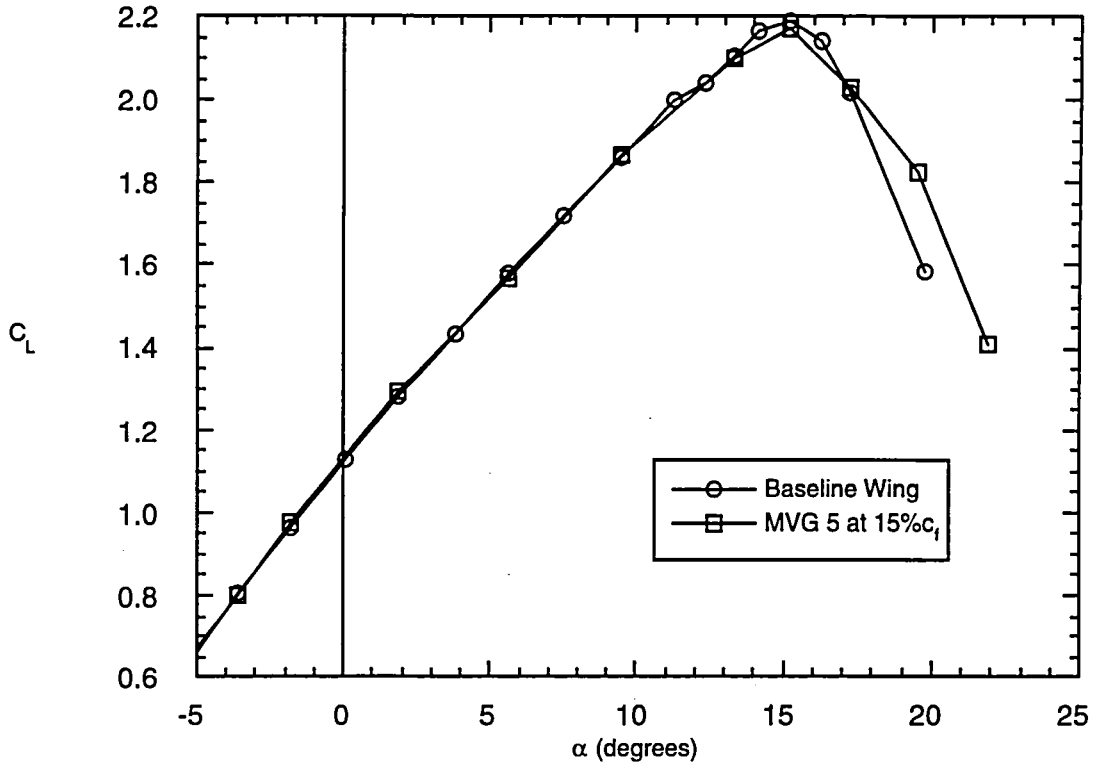

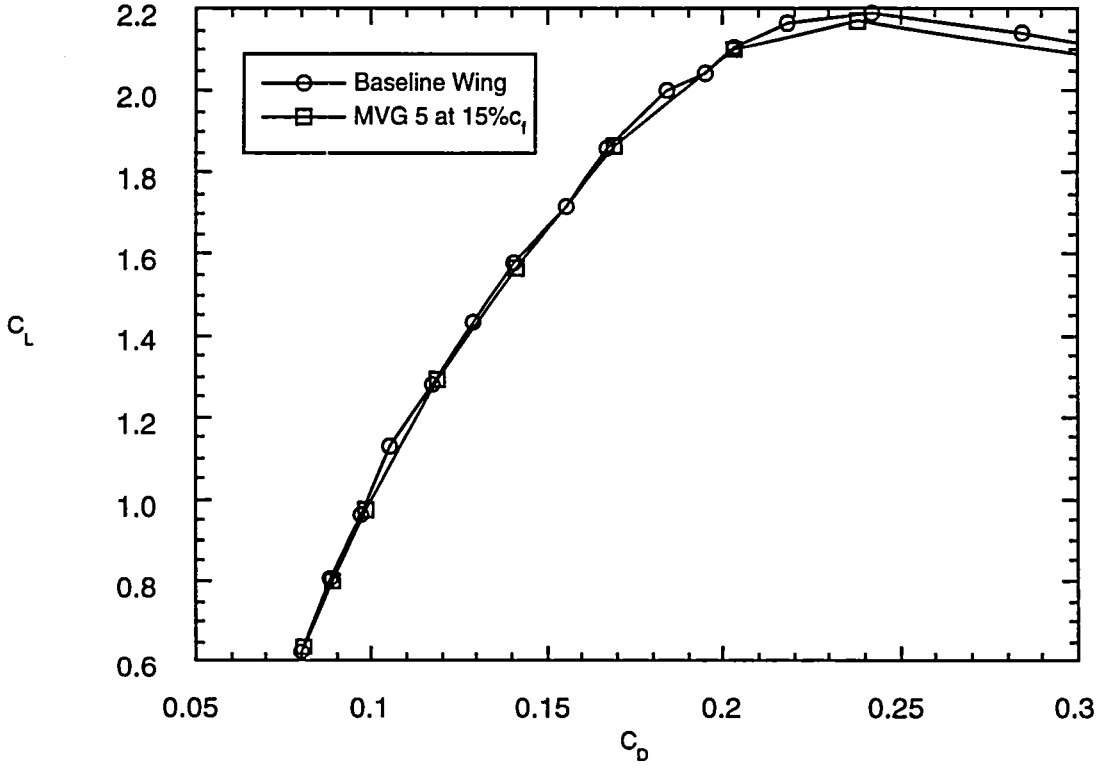

Figure 31. Effect of C_f on the lift and drag coefficients; COR orientation, $\beta = 23°$, $\lambda = 1"$, $\delta_f = 34°$.

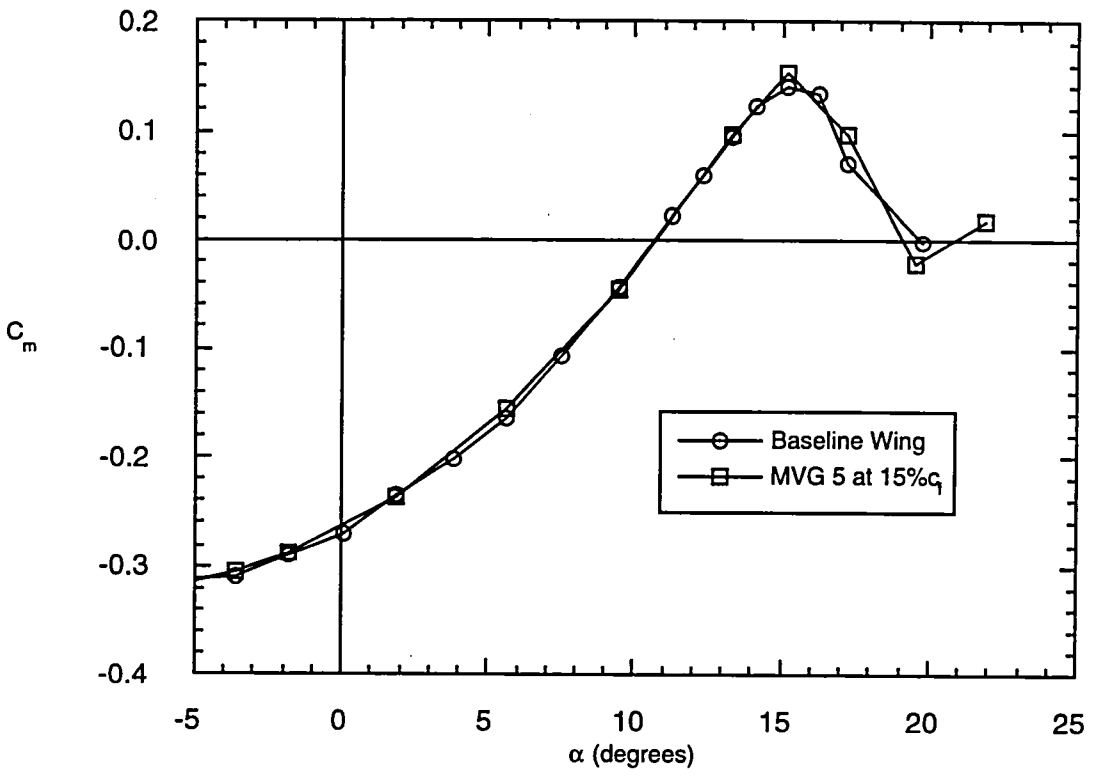

Figure 32. Effect of C_f on the pitching moment coefficient; COR orientation, $\beta = 23°$, $\lambda = 1"$, $\delta_f = 34°$.

This Page Intentionally Left Blank

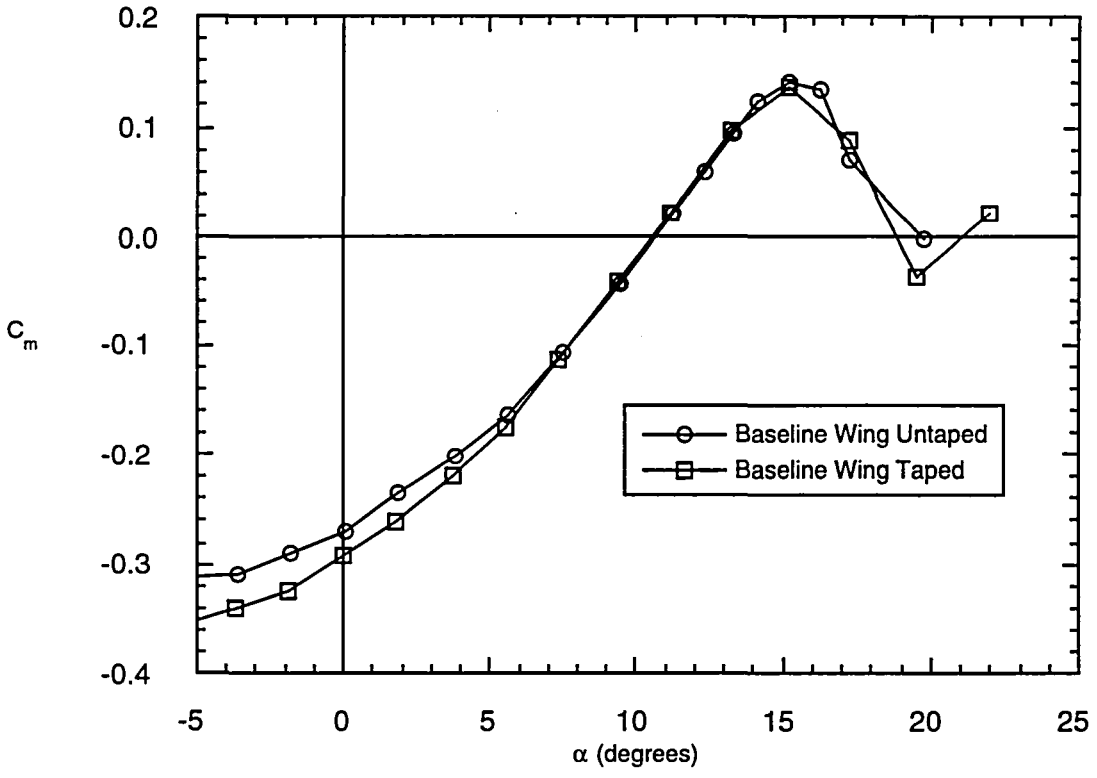

Figure 34. Effect of taping the flap-tracks, gaps and push-rods on the pitching moment coefficient; no MVGs, $\delta_f = 34°$.

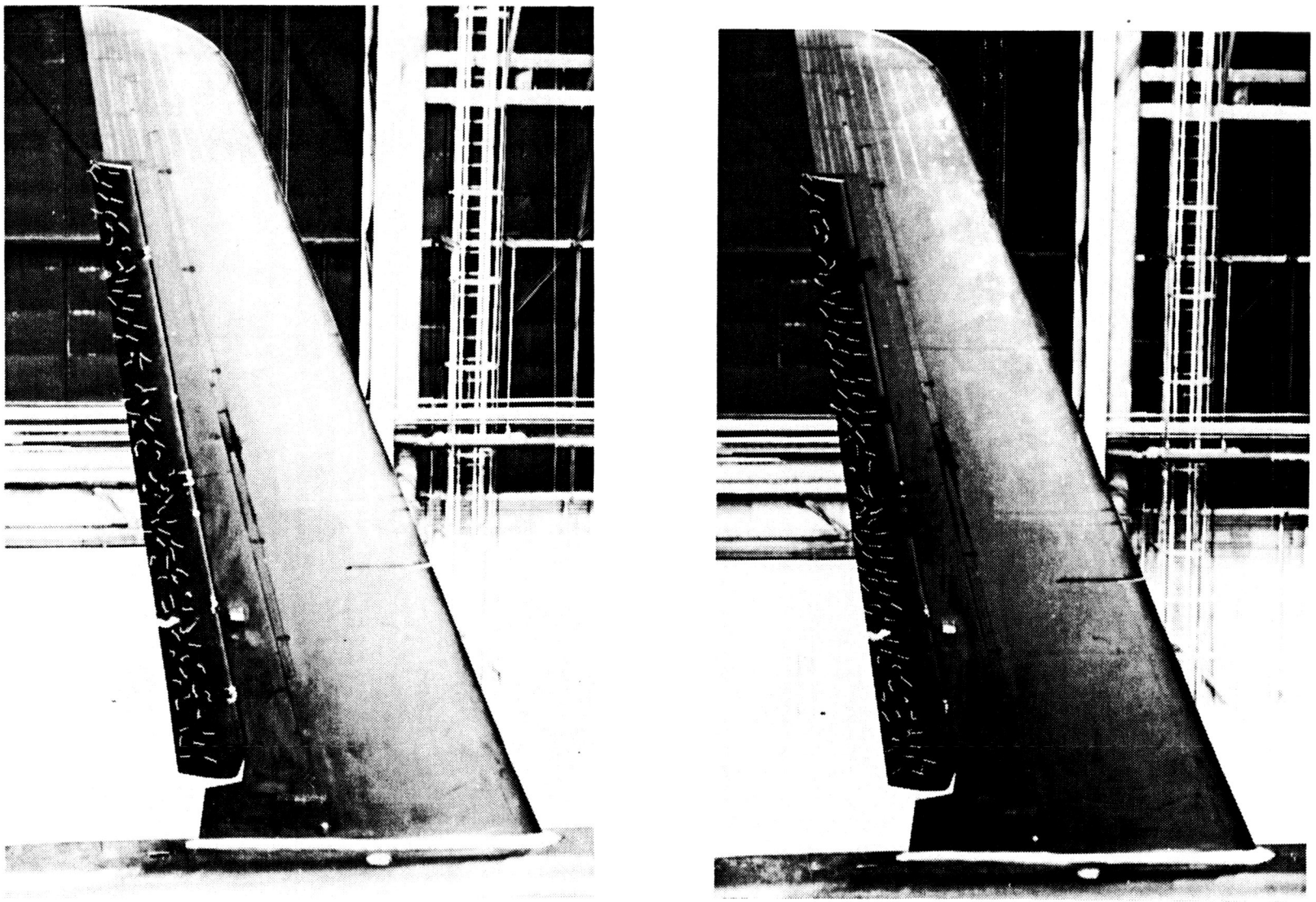

(a) Baseline wing untaped

(b) Baseline wing taped

Figure 35. Flow visualization of the single-slotted flap with flap-tracks, gaps and push-rods untaped and taped; $\delta_f = 34°$, $\alpha = 0°$.

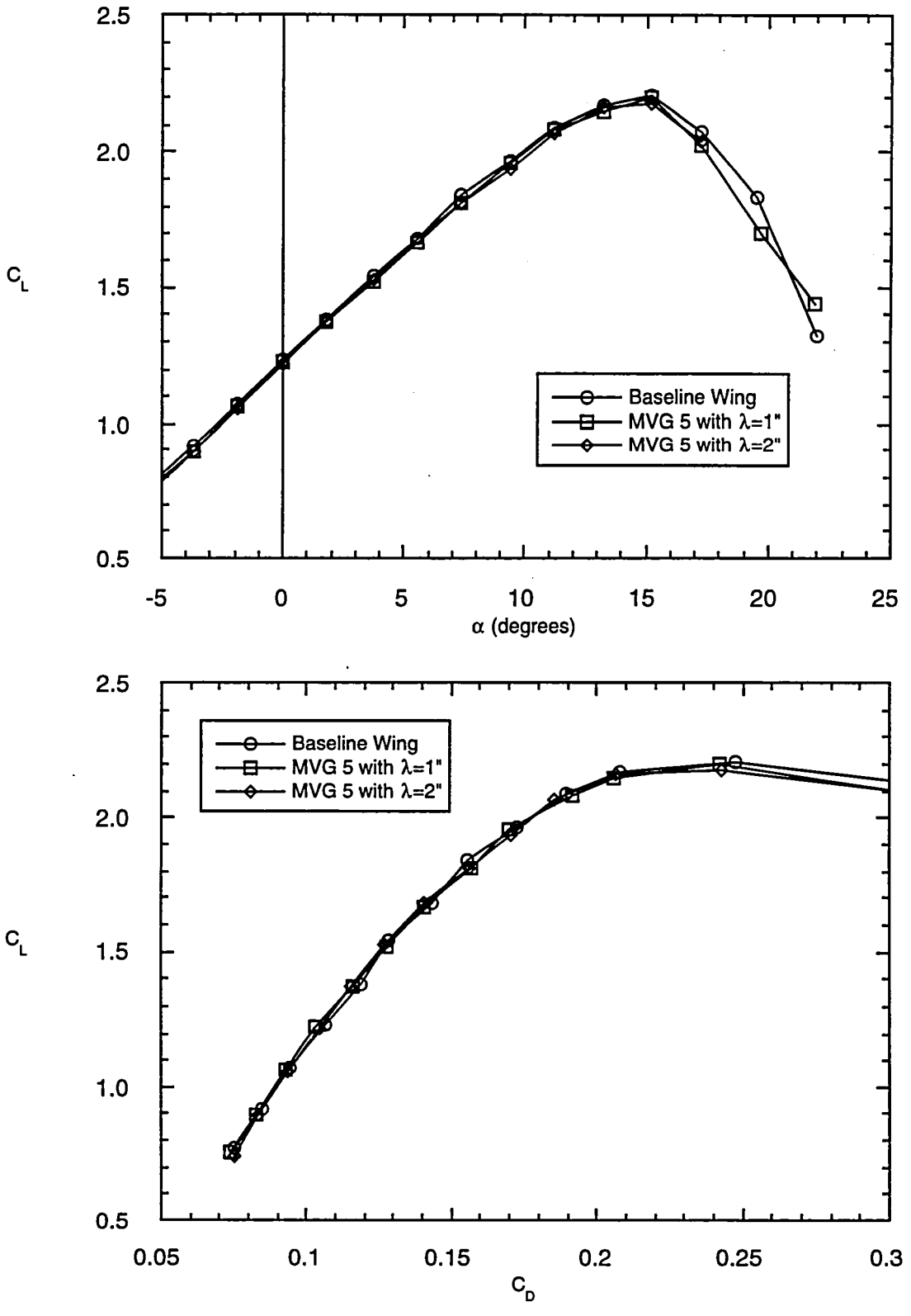

Figure 36. Effect of spacing on the lift and drag coefficients; COR orientation, $C_f = 7\%c_f$, $\beta = 23°$, $\delta_f = 34°$, wing taped.

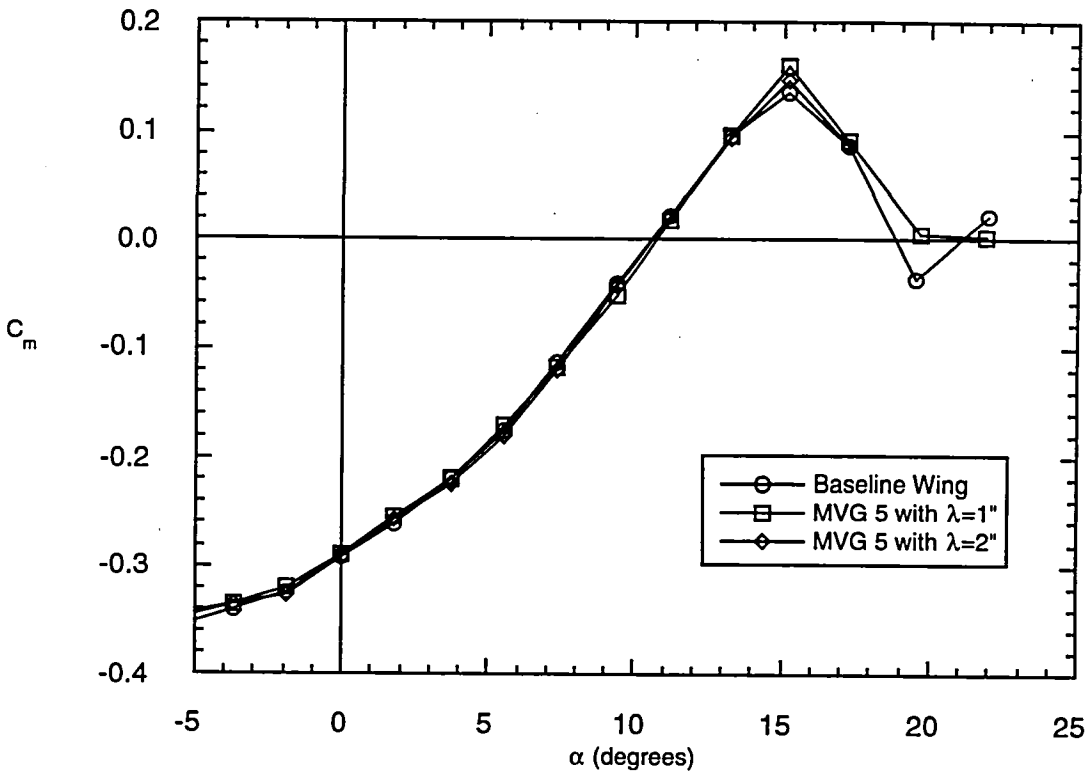

Figure 37. Effect of spacing on the pitching moment coefficient; COR orientation, $C_f = 7\%c_f$, $\beta = 23°$, $\delta_f = 34°$, wing taped.

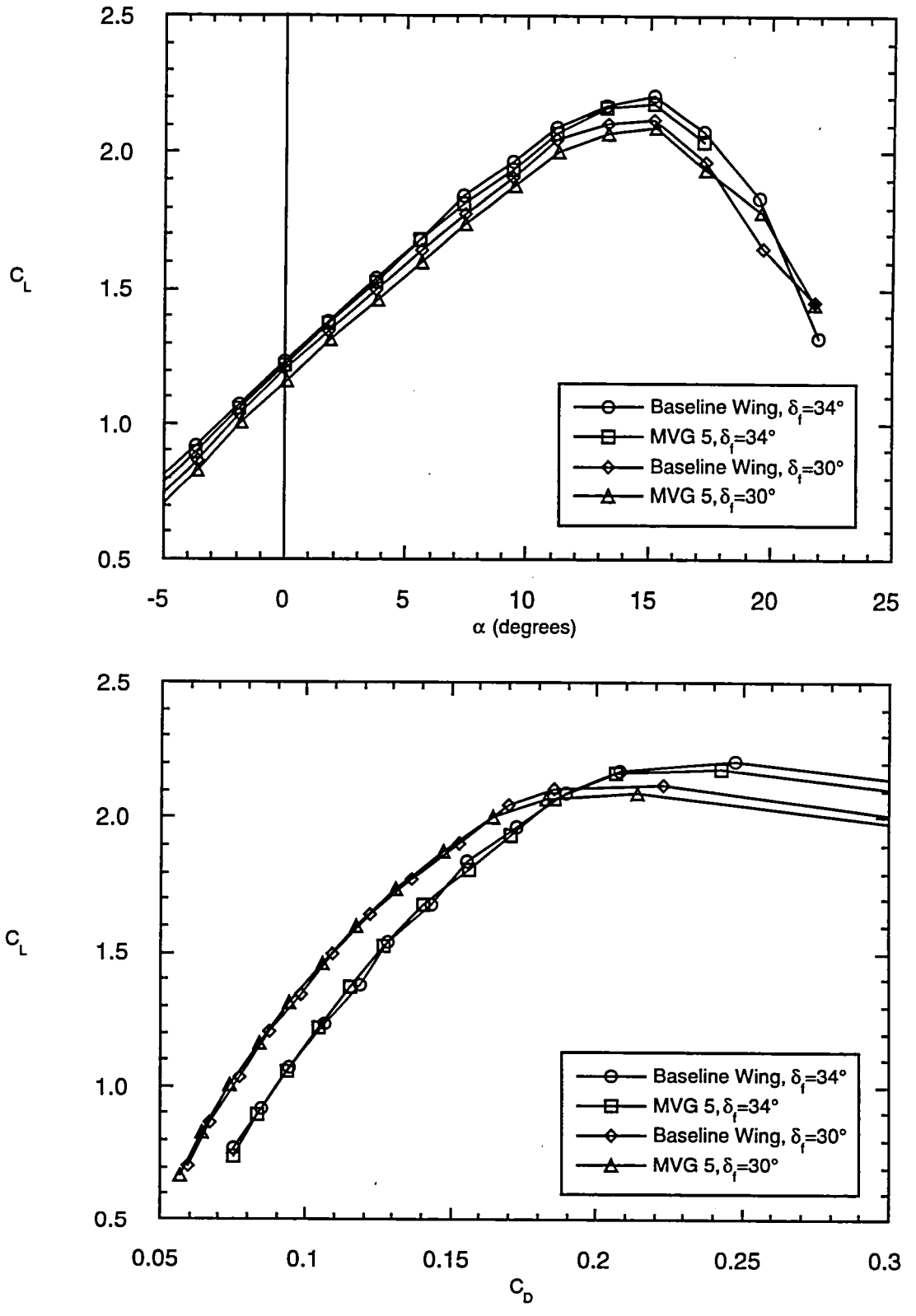

Figure 38. Effect of flap deflection on the lift and drag coefficients; COR orientation, $C_f = 7\%c_f$, $\beta = 23°$, $\lambda = 2"$, wing taped.

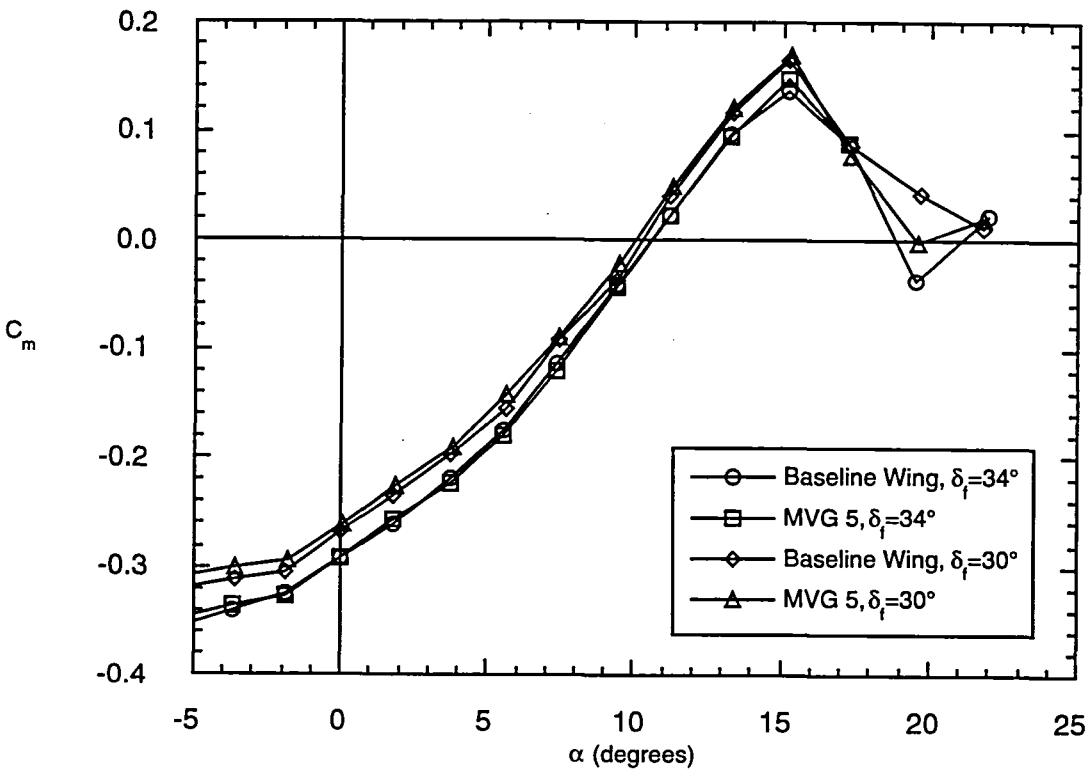

Figure 39. Effect of flap deflection on the pitching moment coefficient; COR orientation, $C_f = 7\%c_f$, $\beta = 23°$, $\lambda = 2"$, wing taped.

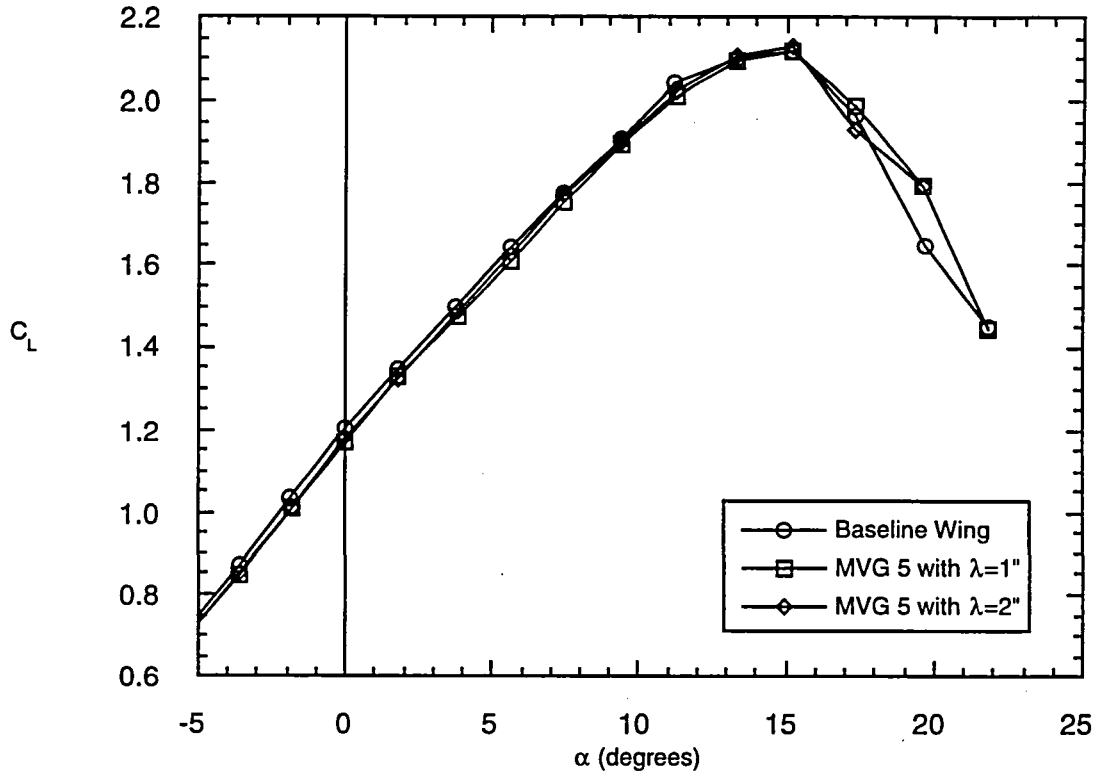

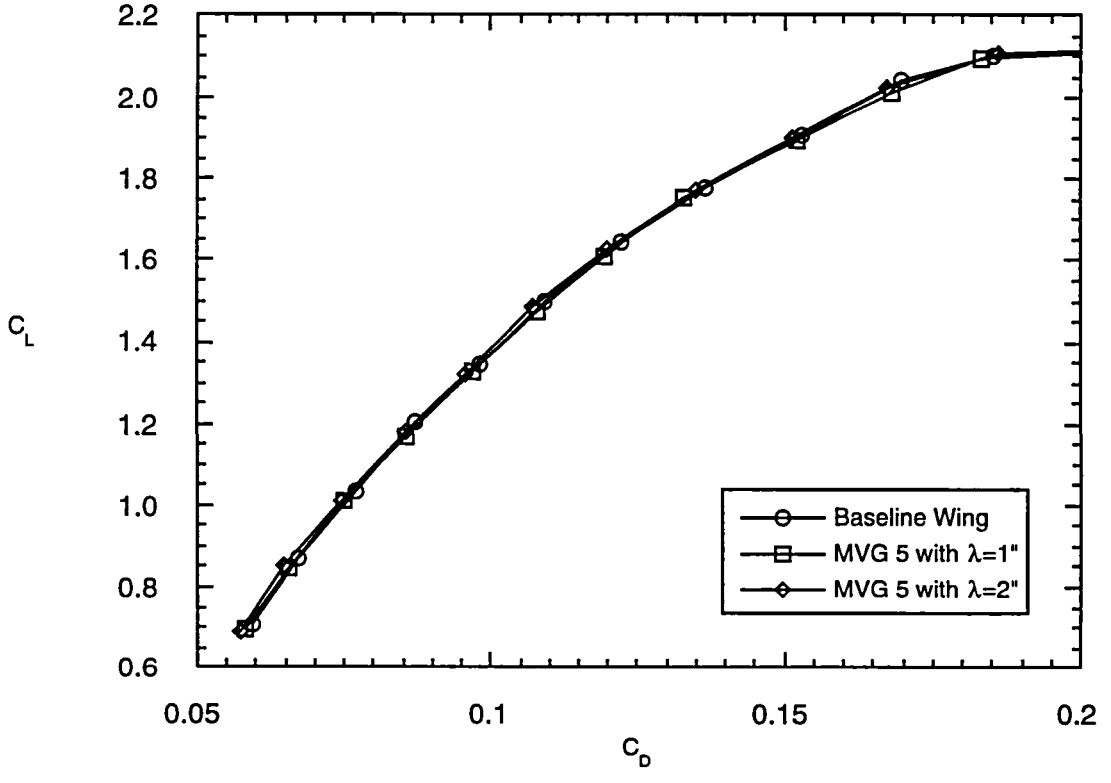

Figure 40. Effect of spacing on the lift and drag coefficients; COR orientation, $C_f = 20\%c_f$, $\beta = 23°$, $\delta_f = 30°$, wing taped.

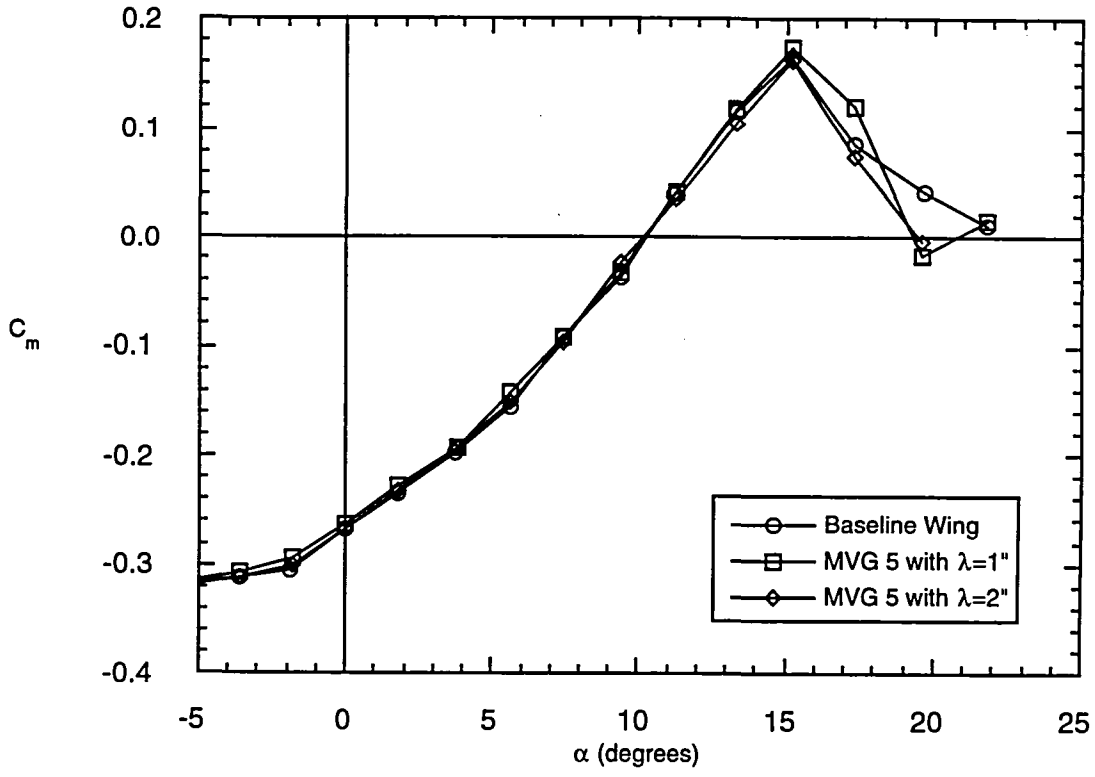

Figure 41. Effect of spacing on the pitching moment coefficient; COR orientation, $C_f = 20\%c_f$, $\beta = 23°$, $\delta_f = 30°$, wing taped.

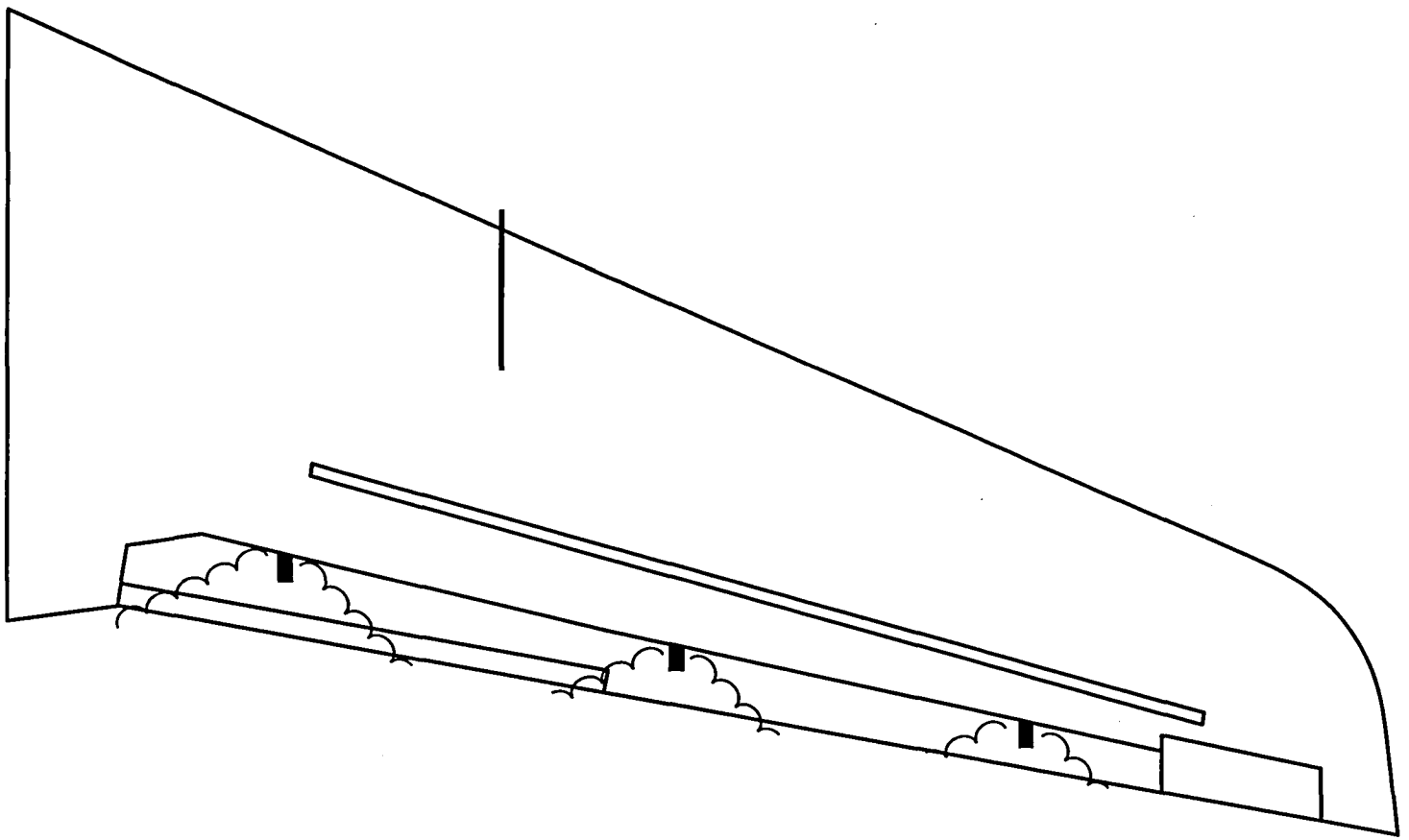

Figure 42. Schematic of wing with "pockets" of separation in single-slotted flap region.

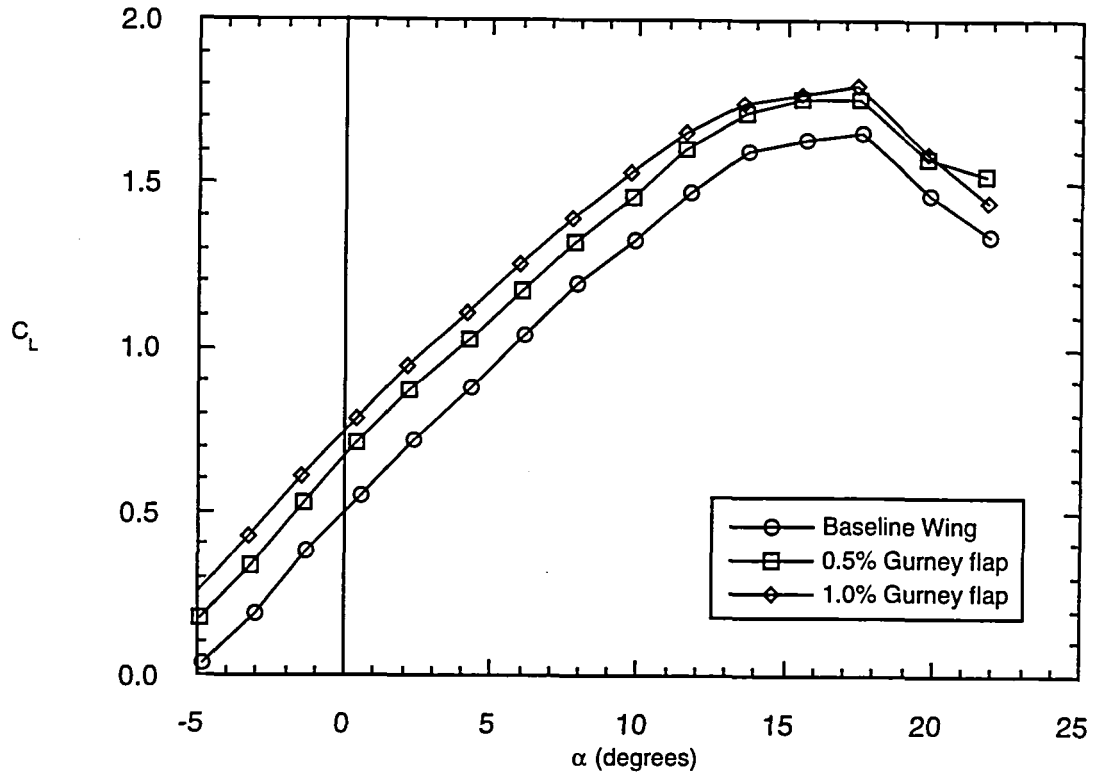

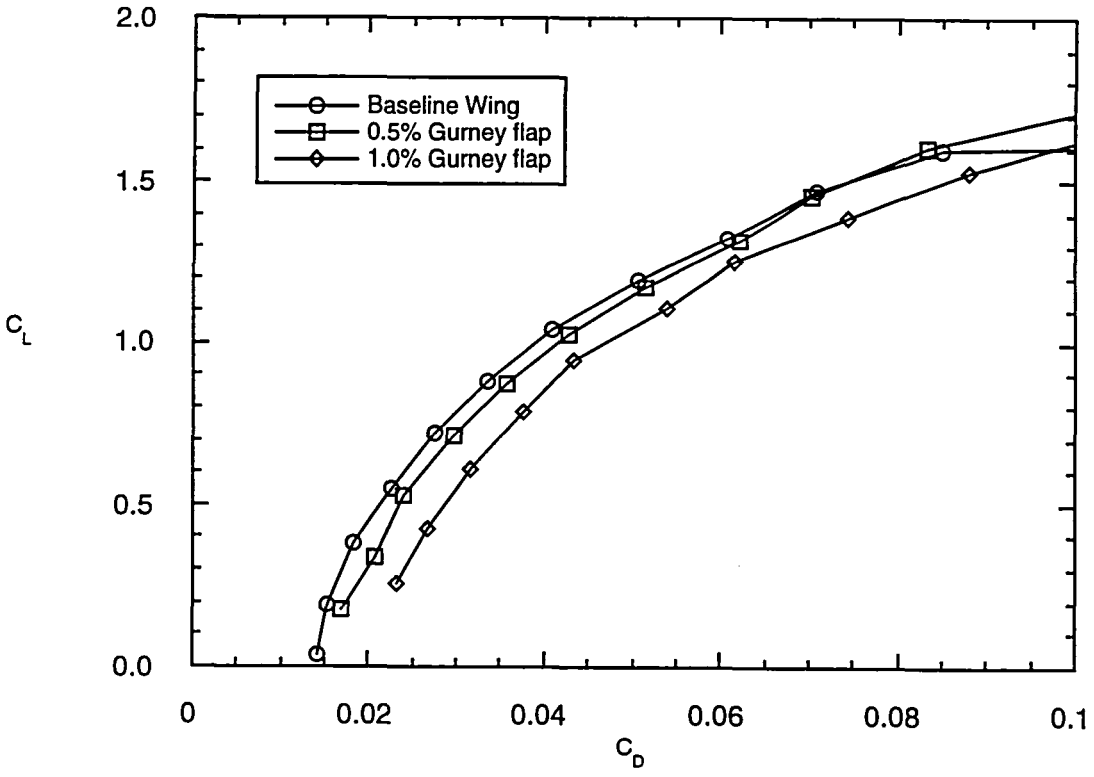

Figure 43. Effect of Gurney flap Configuration 1 on the lift and drag coefficients; $\delta_f = 10°$.

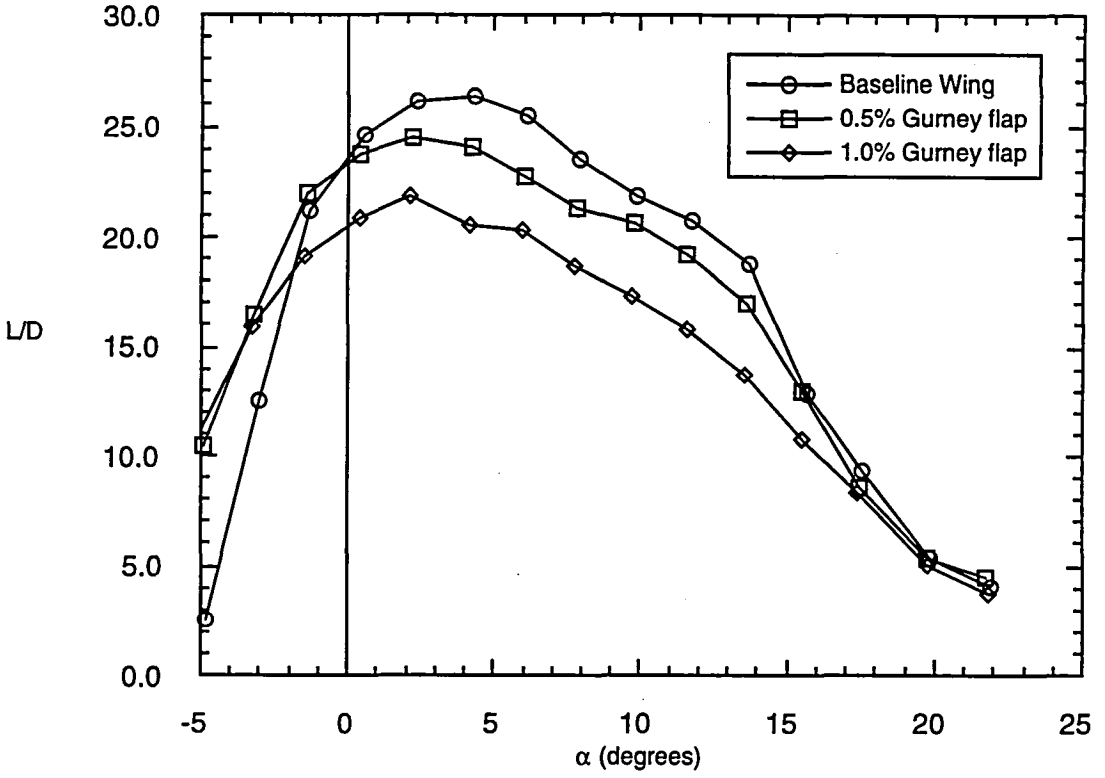

Figure 44. Effect of Gurney flap Configuration 1 on the lift-to-drag ratio; $\delta_f = 10°$.

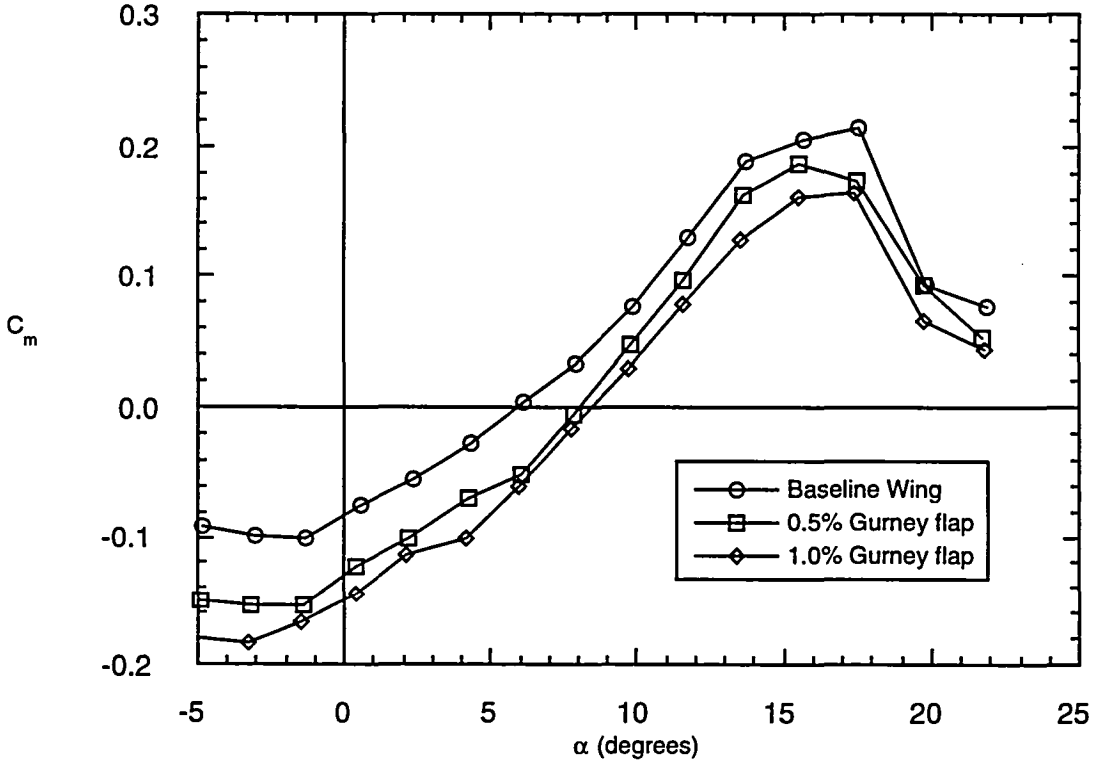

Figure 45. Effect of Gurney flap Configuration 1 on the pitching moment coefficient; $\delta_f = 10°$.

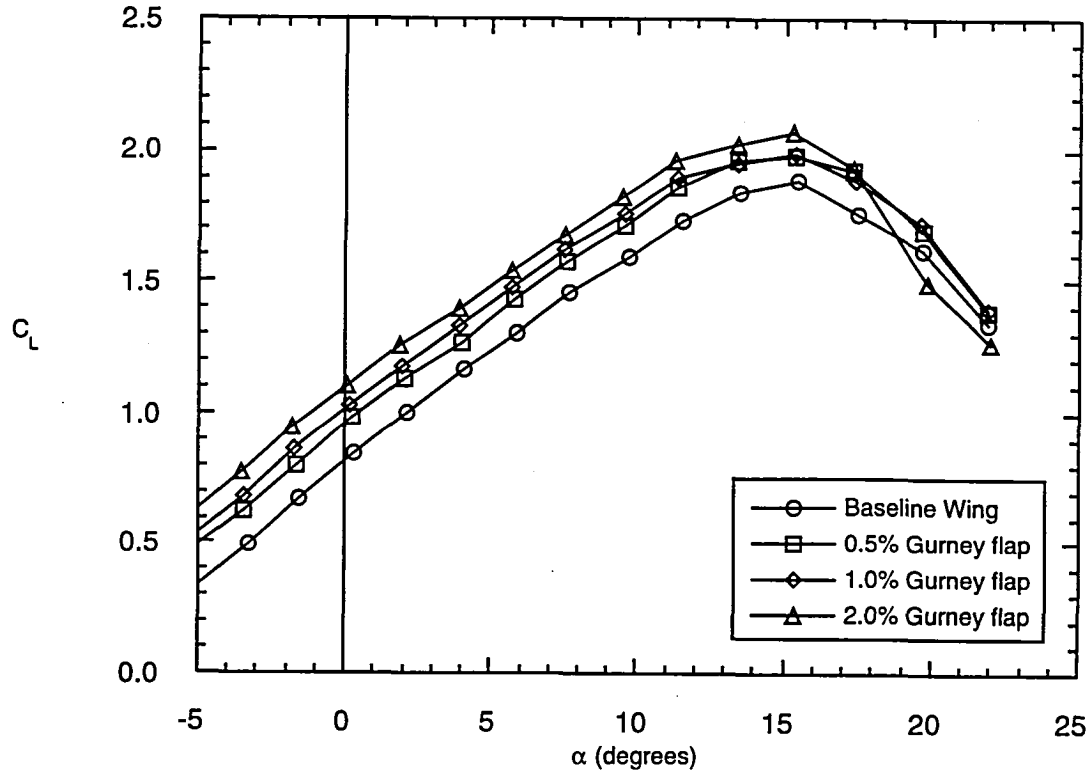

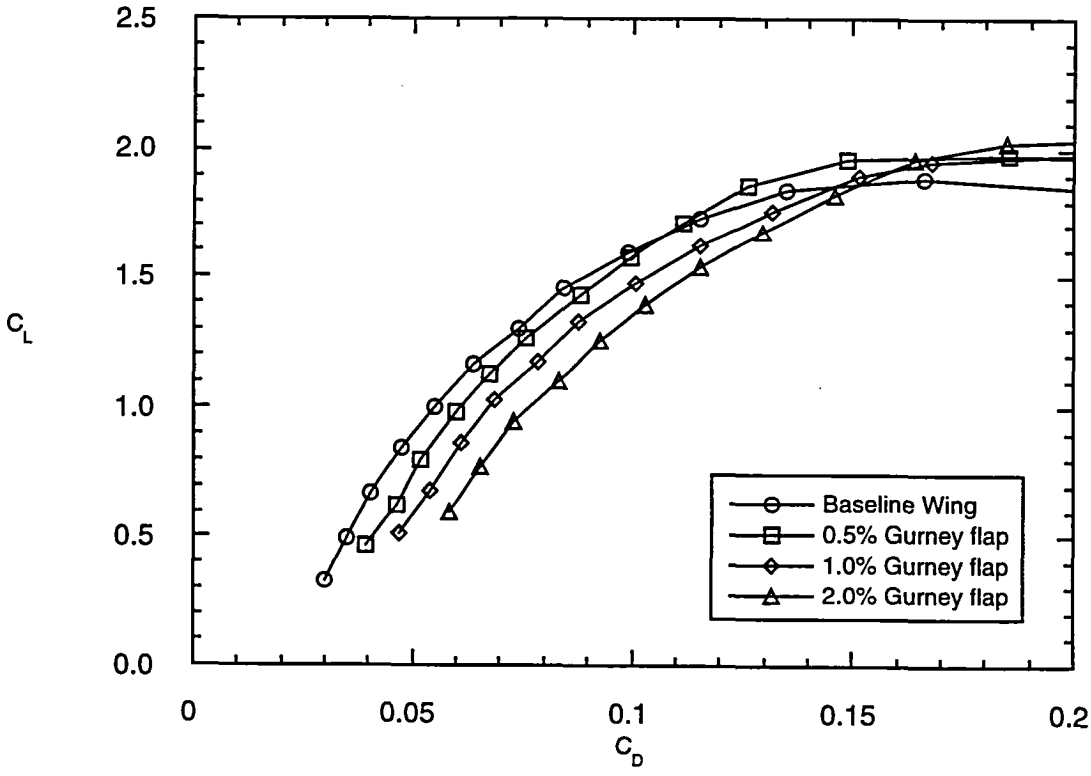

Figure 46. Effect of Gurney flap Configuration 1 on the lift and drag coefficients; $\delta_f = 20°$.

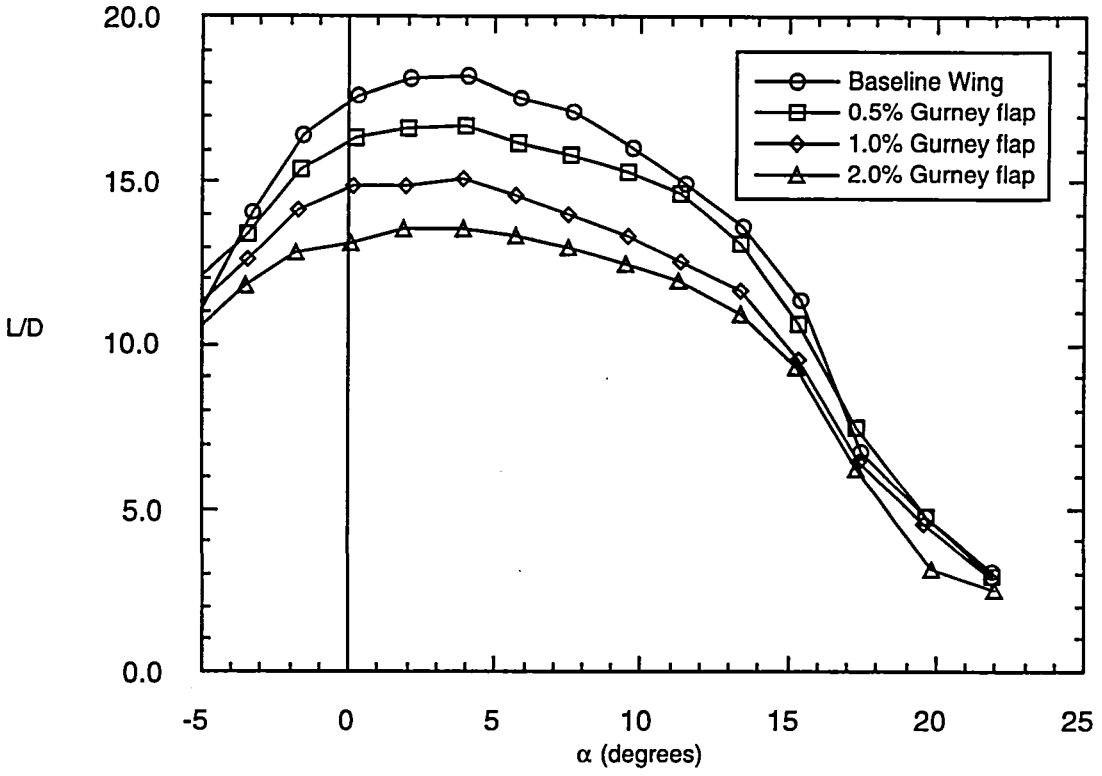

Figure 47. Effect of Gurney flap Configuration 1 on the lift-to-drag ratio; $\delta_f = 20°$.

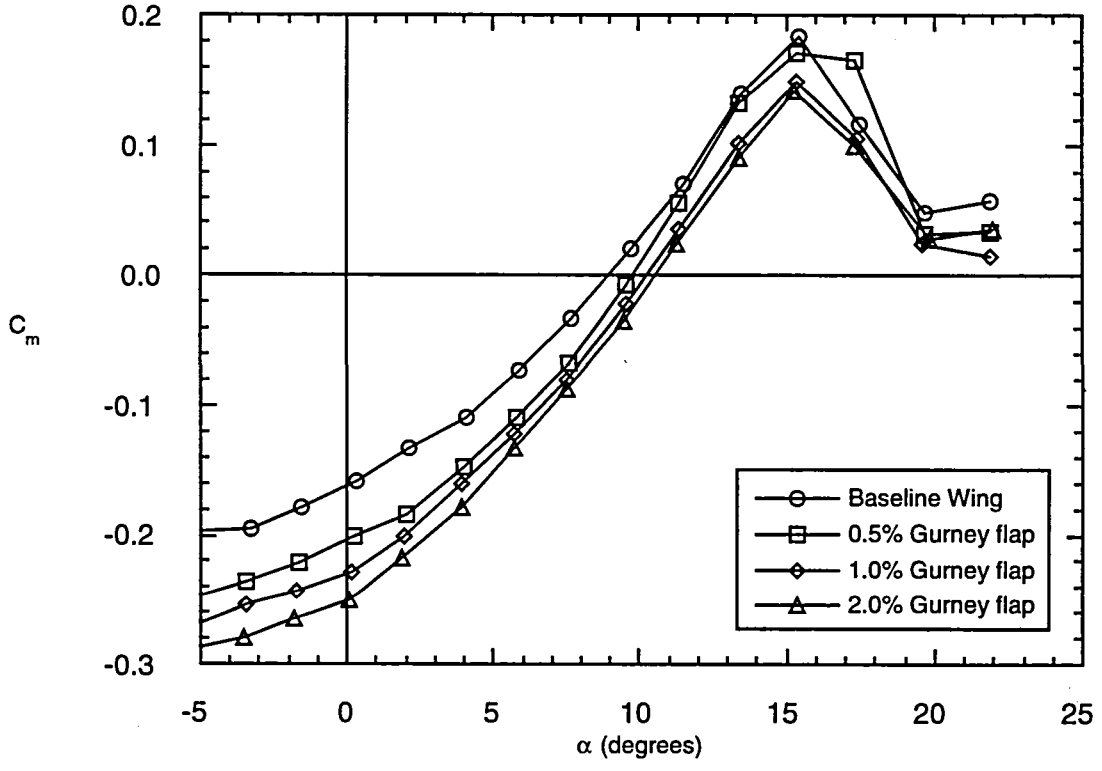

Figure 48. Effect of Gurney flap Configuration 1 on the pitching moment coefficient; $\delta_f = 20°$.

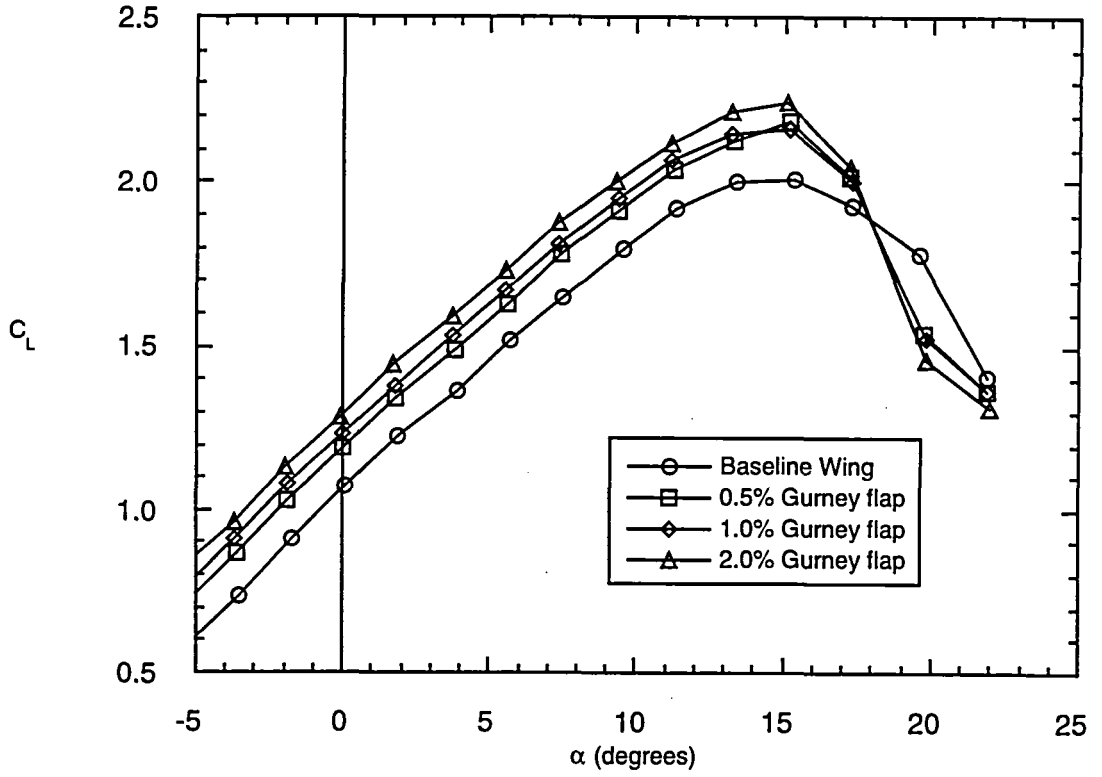

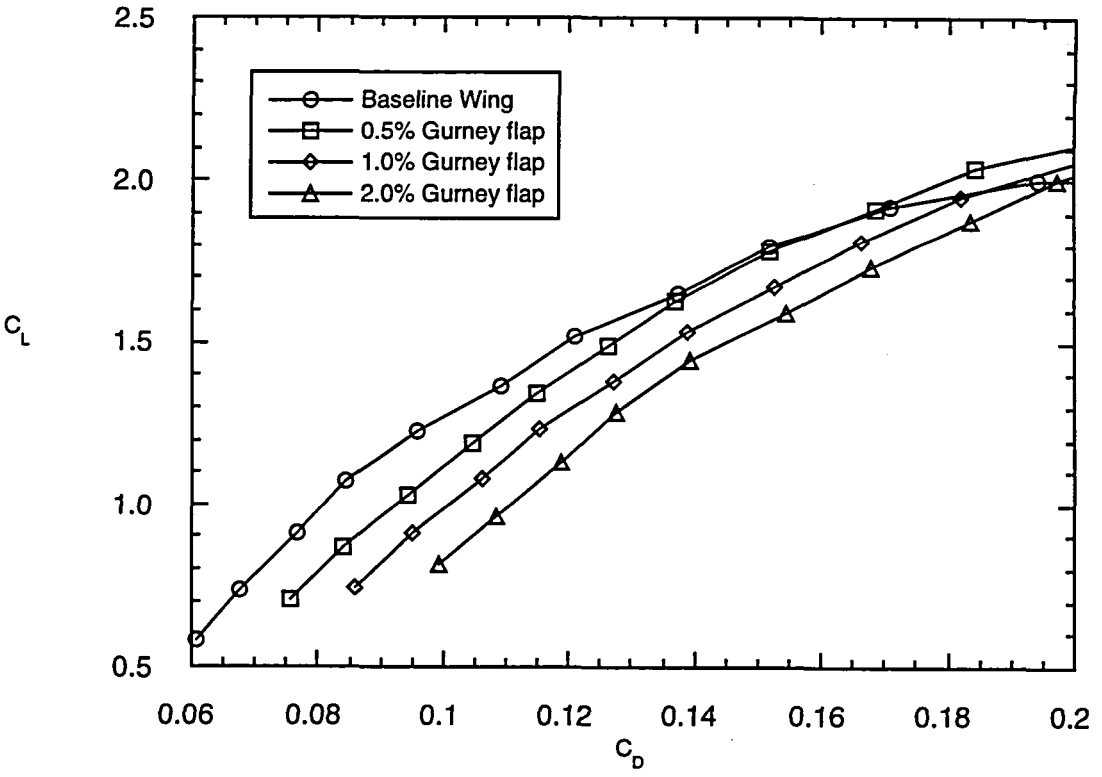

Figure 49. Effect of Gurney flap Configuration 1 on the lift and drag coefficients; $\delta_f = 30°$.

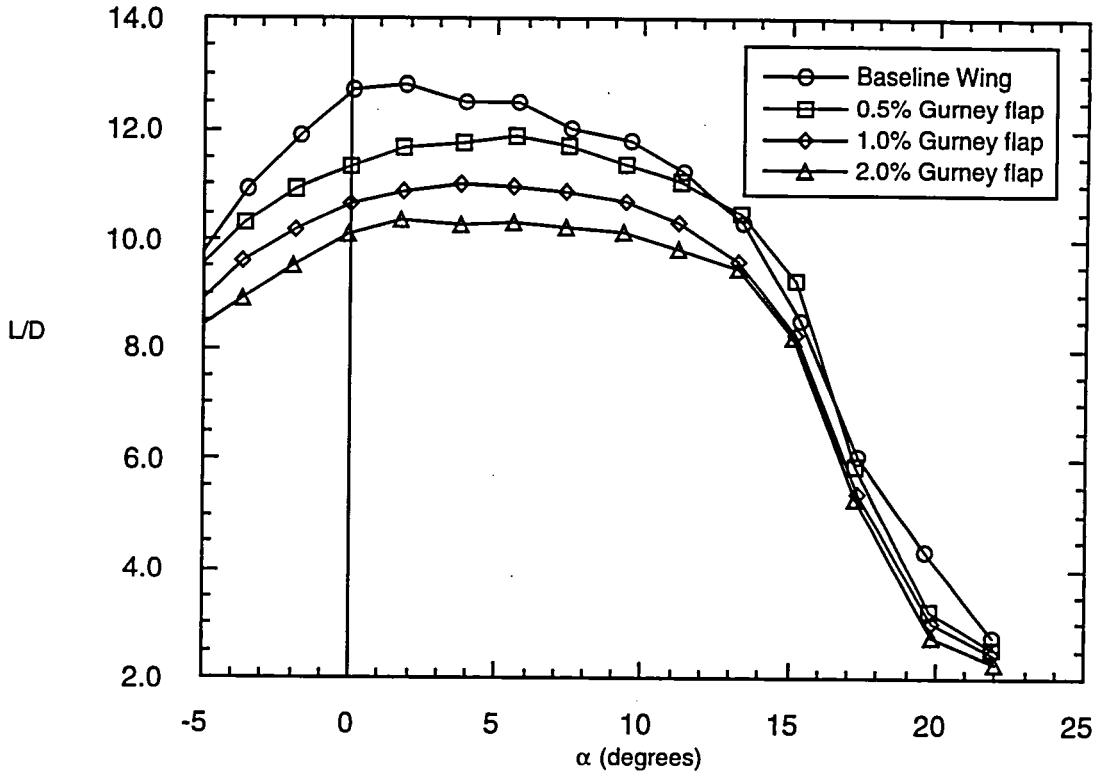

Figure 50. Effect of Gurney flap Configuration 1 on the lift-to-drag ratio; $\delta_f = 30°$.

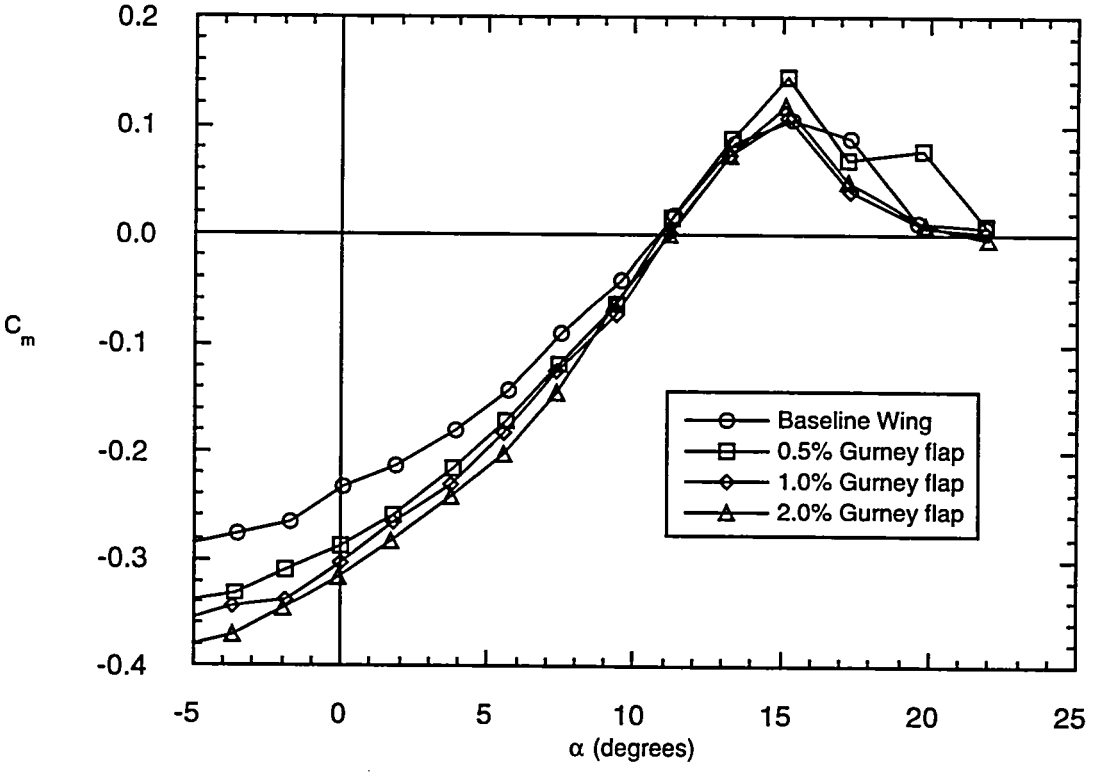

Figure 51. Effect of Gurney flap Configuration 1 on the pitching moment coefficient; $\delta_f = 30°$.

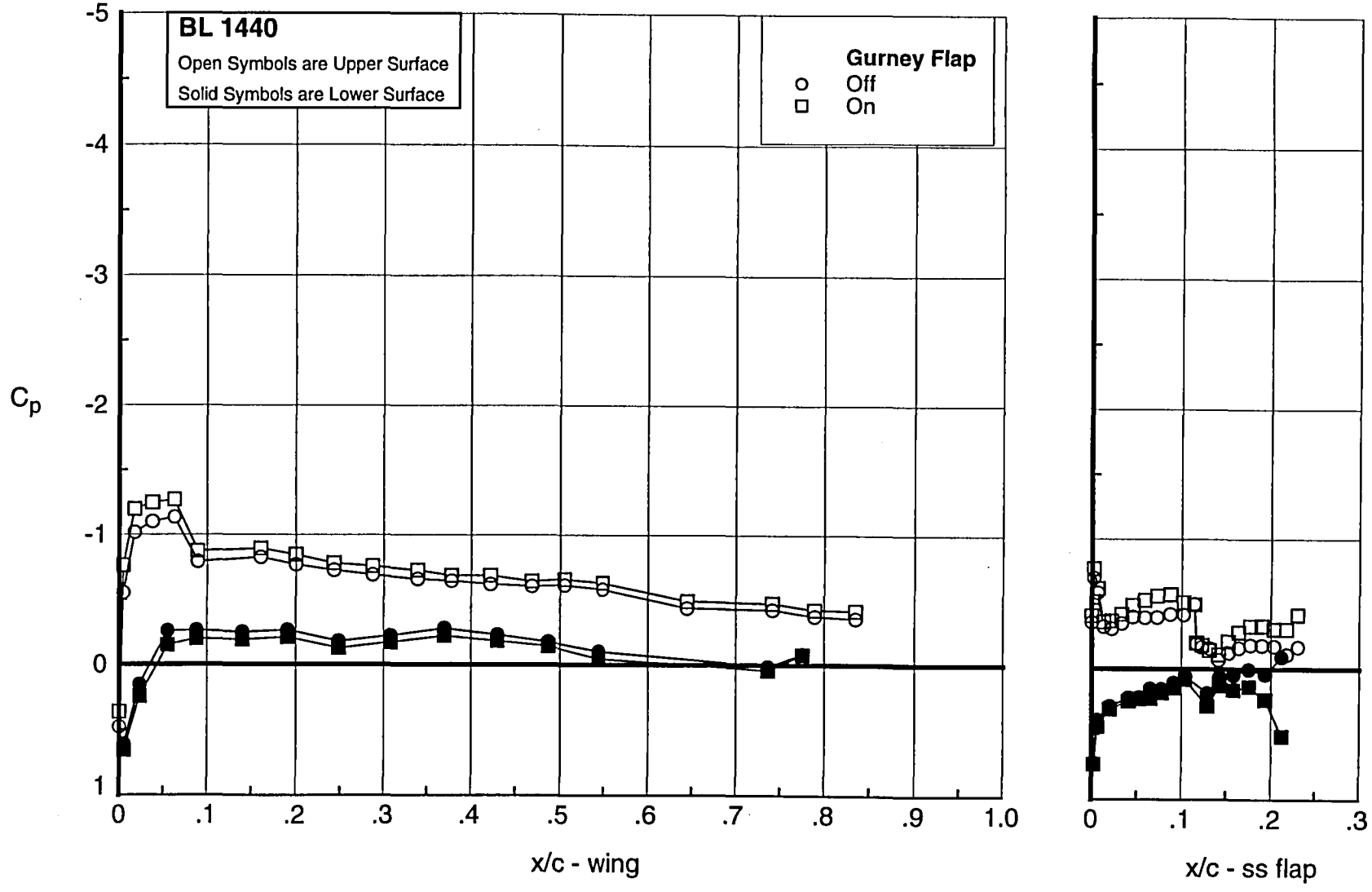

Figure 52. Effect of 0.5% Gurney flap at trailing edge of single-slotted flap on surface pressure; $\delta_f = 10^\circ$, $\alpha = 0.5^\circ$.

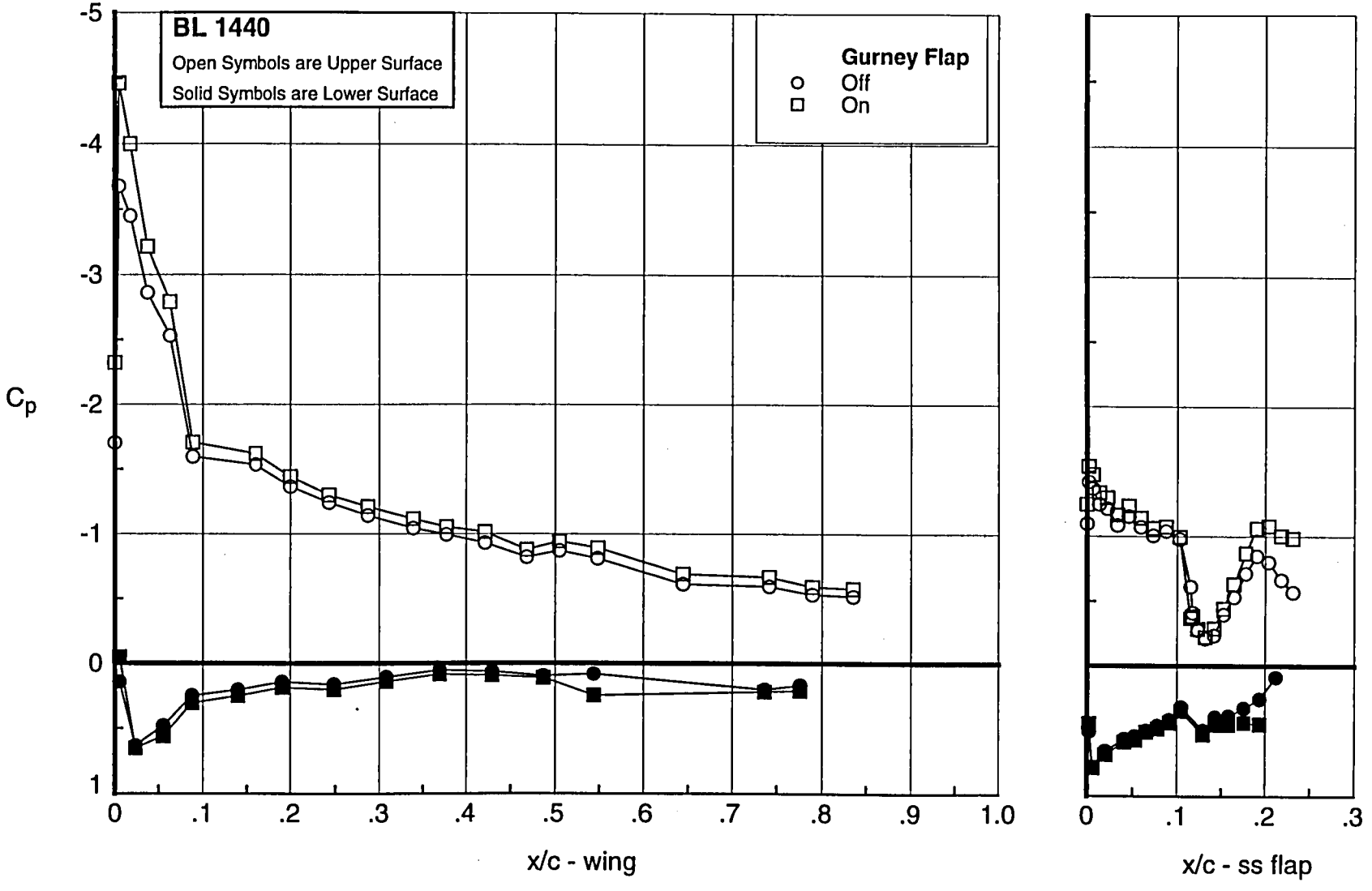

Figure 53. Effect of 0.5% Gurney flap at trailing edge of single-slotted flap on surface pressure; $\delta_f = 30^\circ$, $\alpha = 5.7^\circ$.

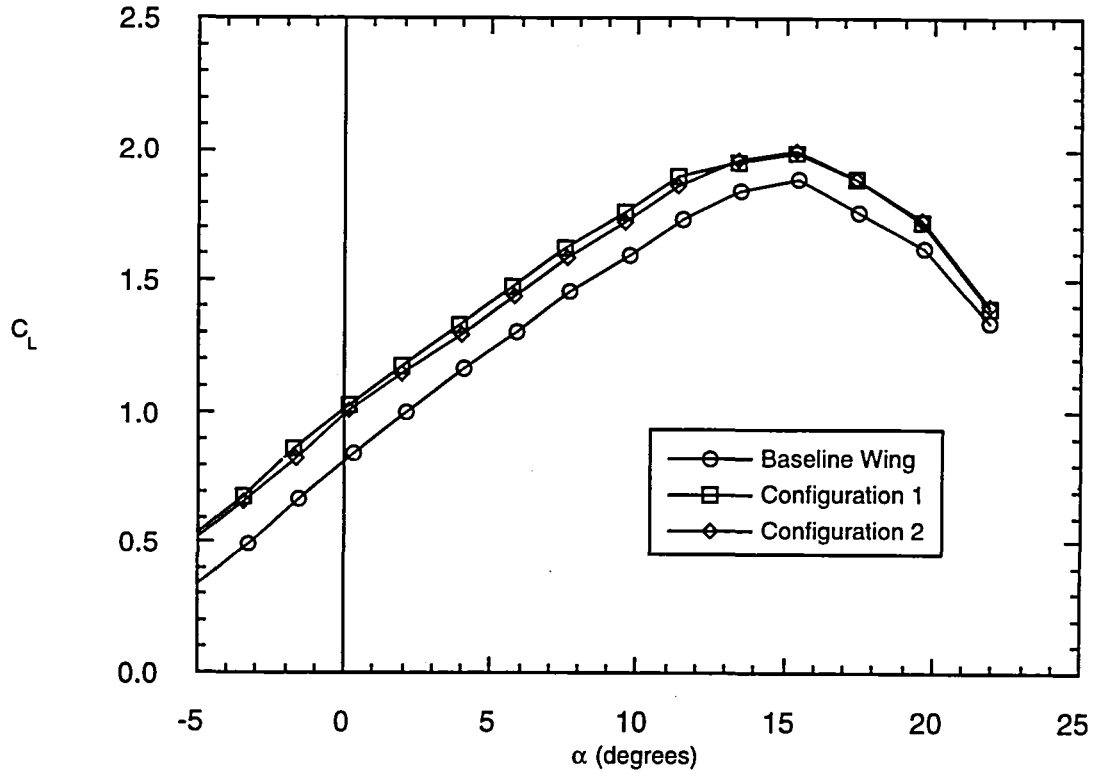

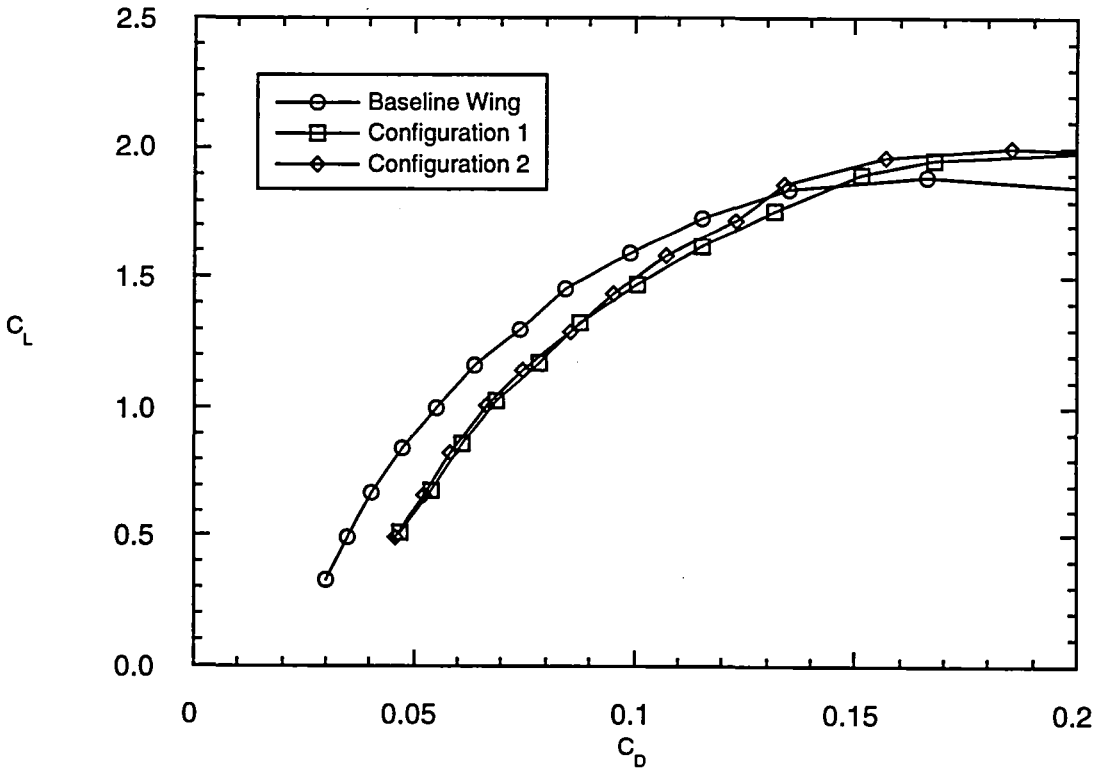

Figure 54. Effect of Gurney flap Configurations 1 and 2 on the lift and drag coefficients; $\delta_f = 20°$.

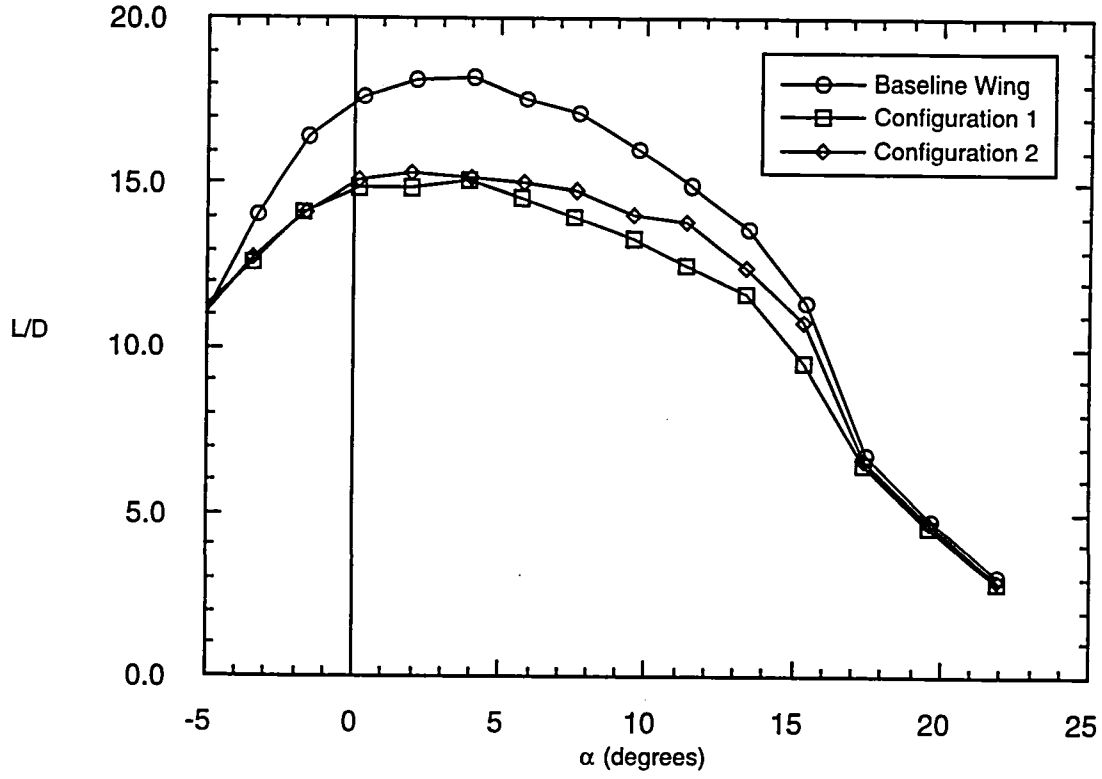

Figure 55. Effect of Gurney flap Configurations 1 and 2 on the lift-to-drag ratio; $\delta_f = 20°$.

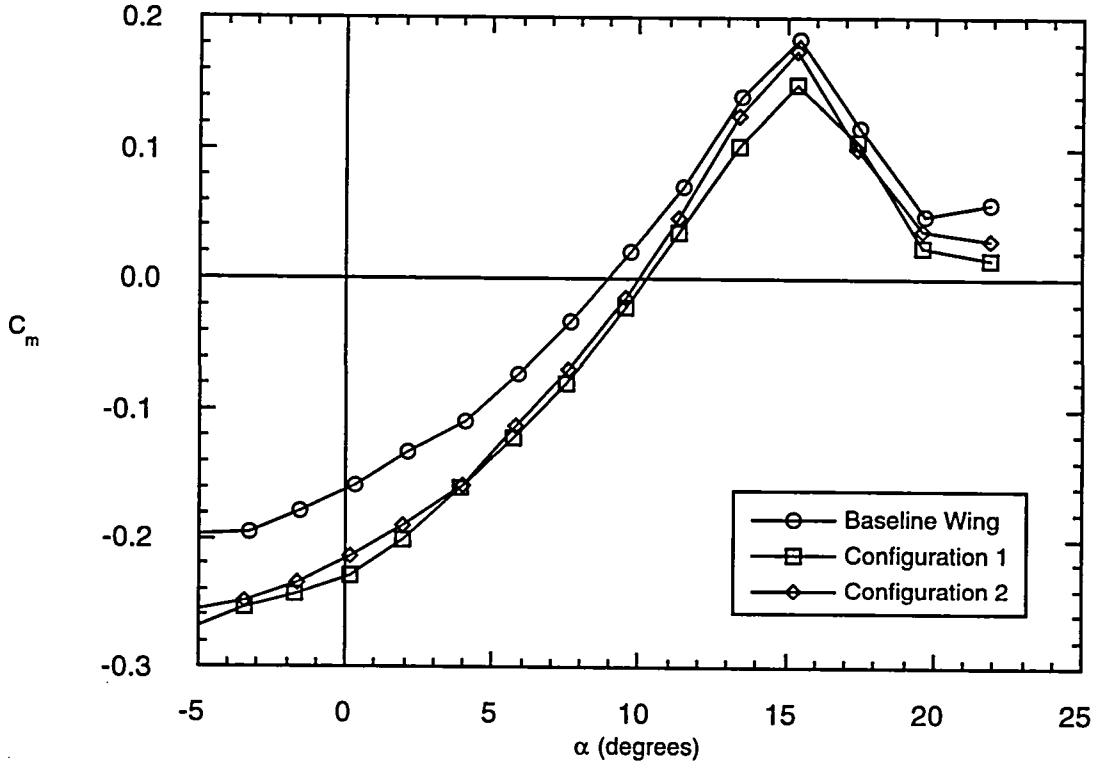

Figure 56. Effect of Gurney flap Configurations 1 and 2 on the pitching moment coefficient; $\delta_f = 20°$.

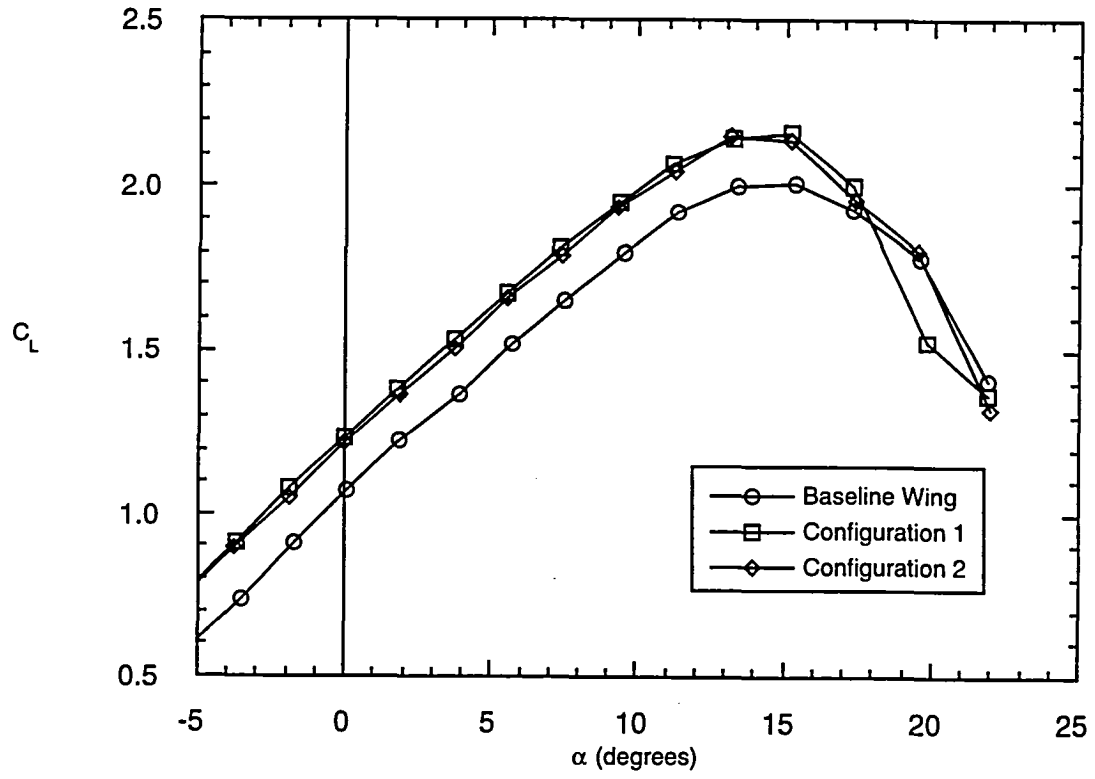

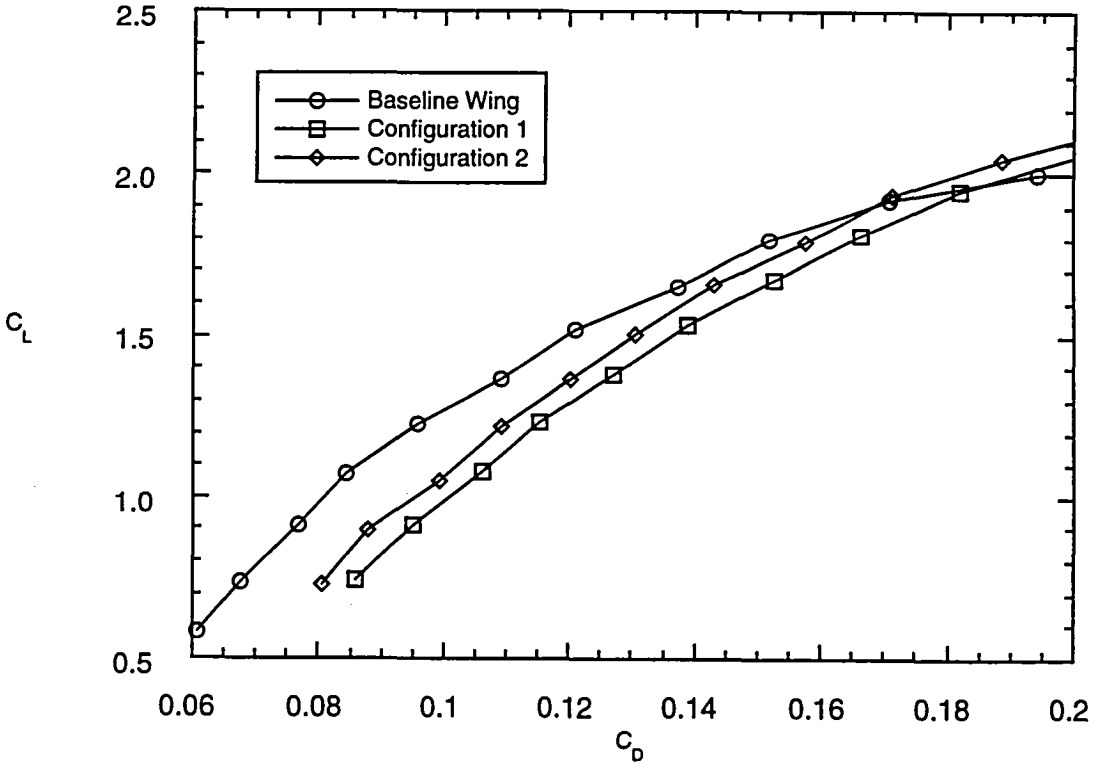

Figure 57. Effect of Gurney flap Configurations 1 and 2 on the lift and drag coefficients; $\delta_f = 30°$.

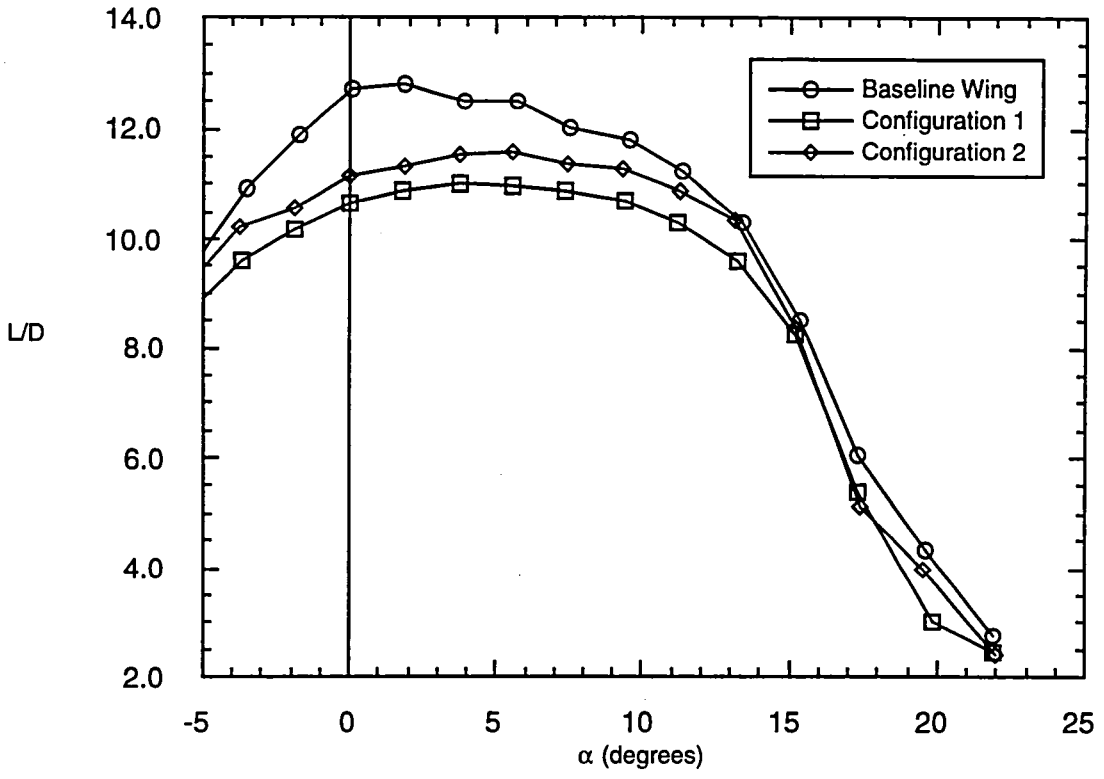

Figure 58. Effect of Gurney flap Configurations 1 and 2 on the lift-to-drag ratio; $\delta_f = 30°$.

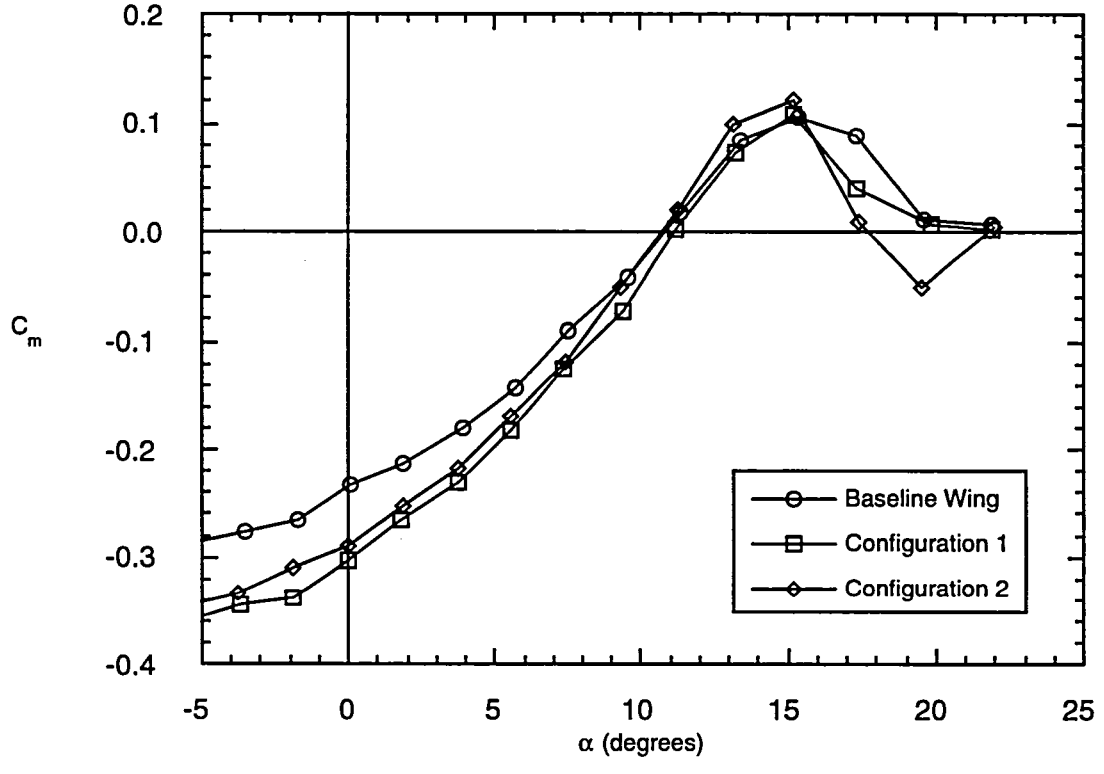

Figure 59. Effect of Gurney flap Configurations 1 and 2 on the pitching moment coefficient; $\delta_f = 30°$.

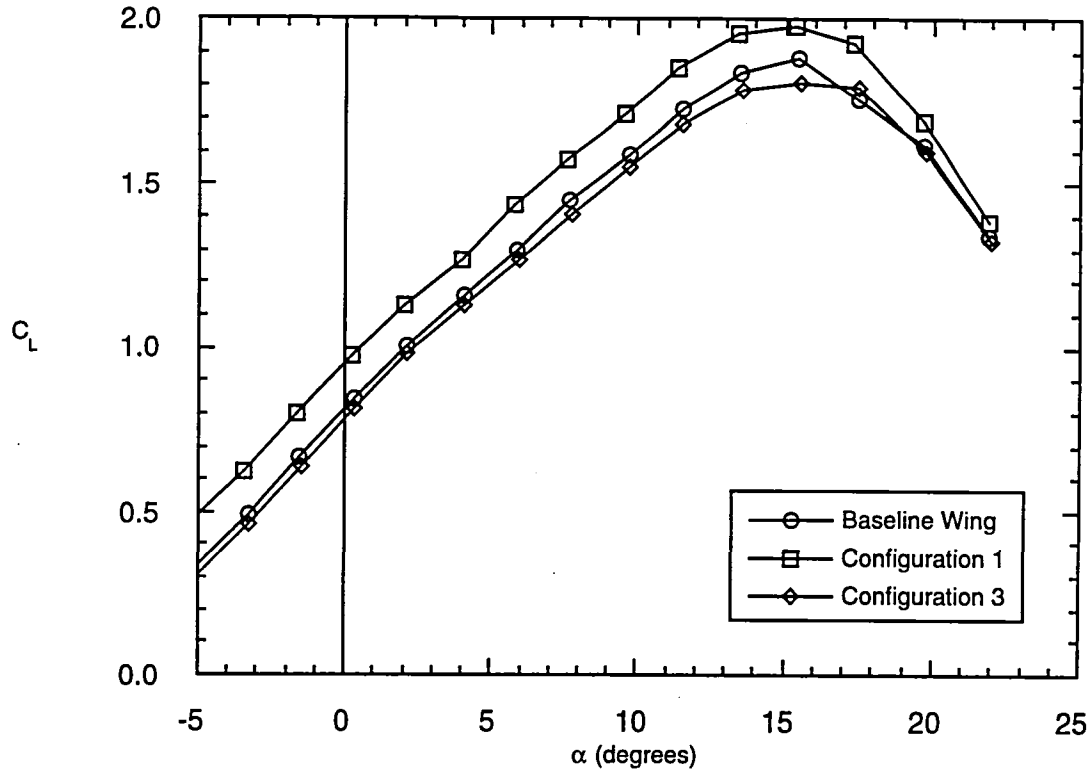

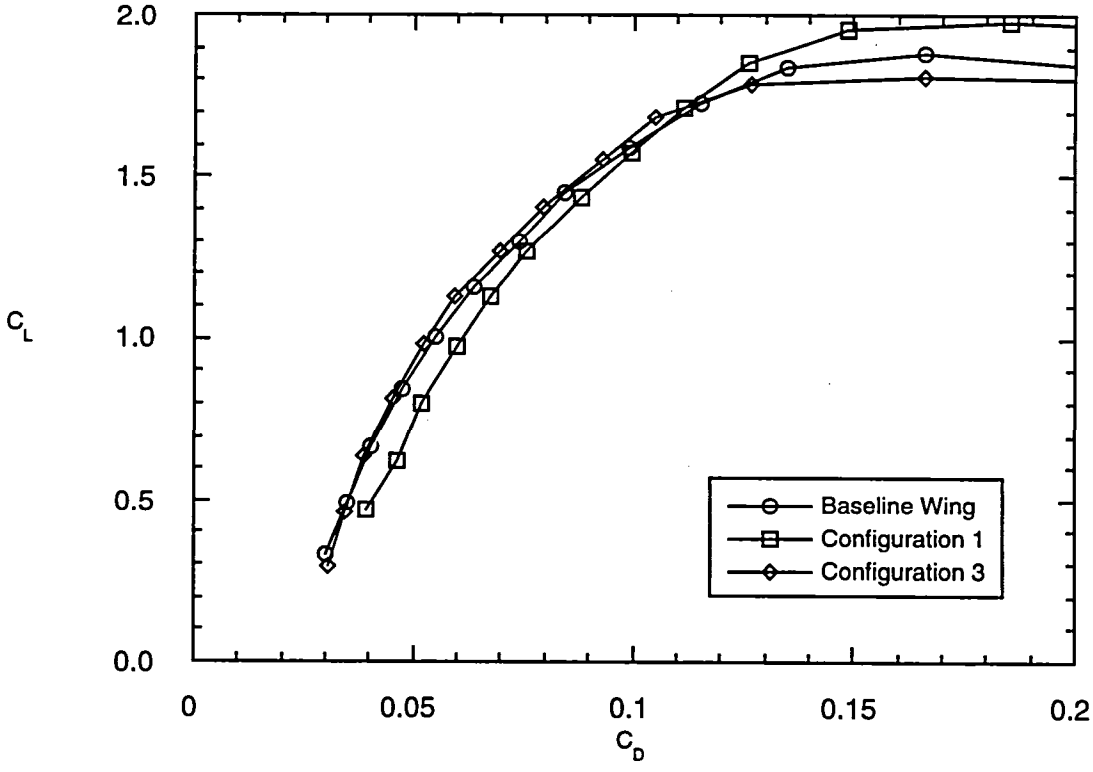

Figure 60. Effect of Gurney flap Configurations 1 and 3 on the lift and drag coefficients; $\delta_f = 20°$.

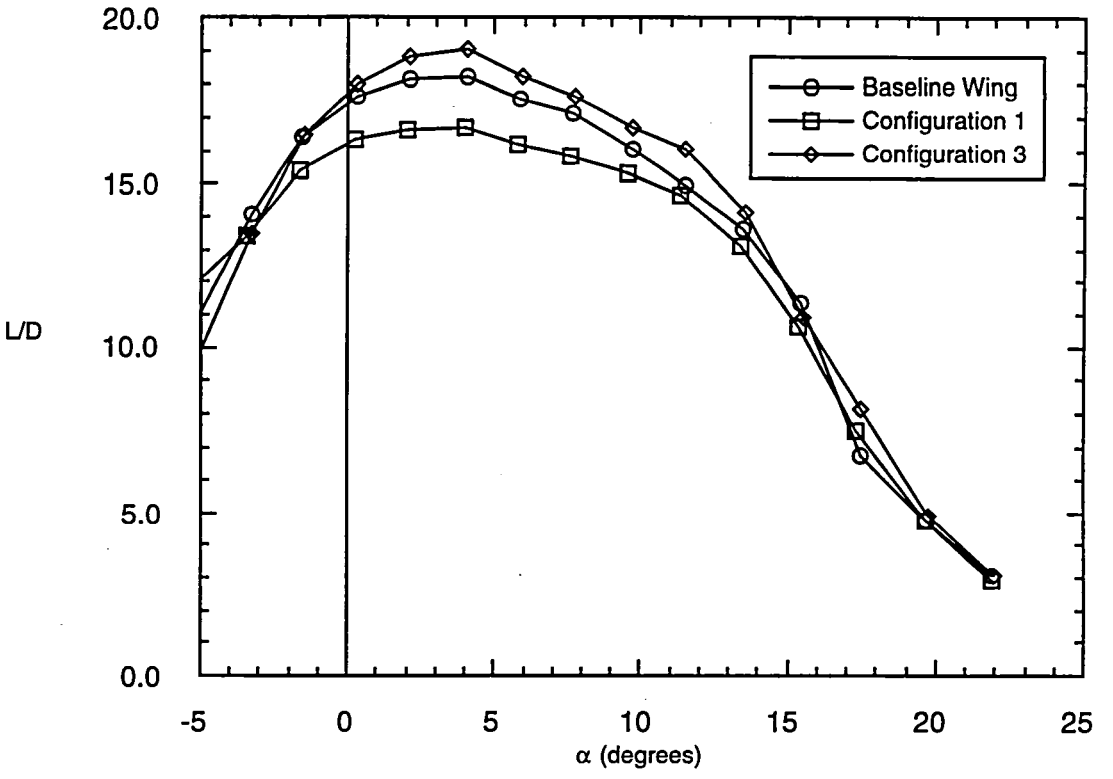

Figure 61. Effect of Gurney flap Configurations 1 and 3 on the lift-to-drag ratio; $\delta_f = 20°$.

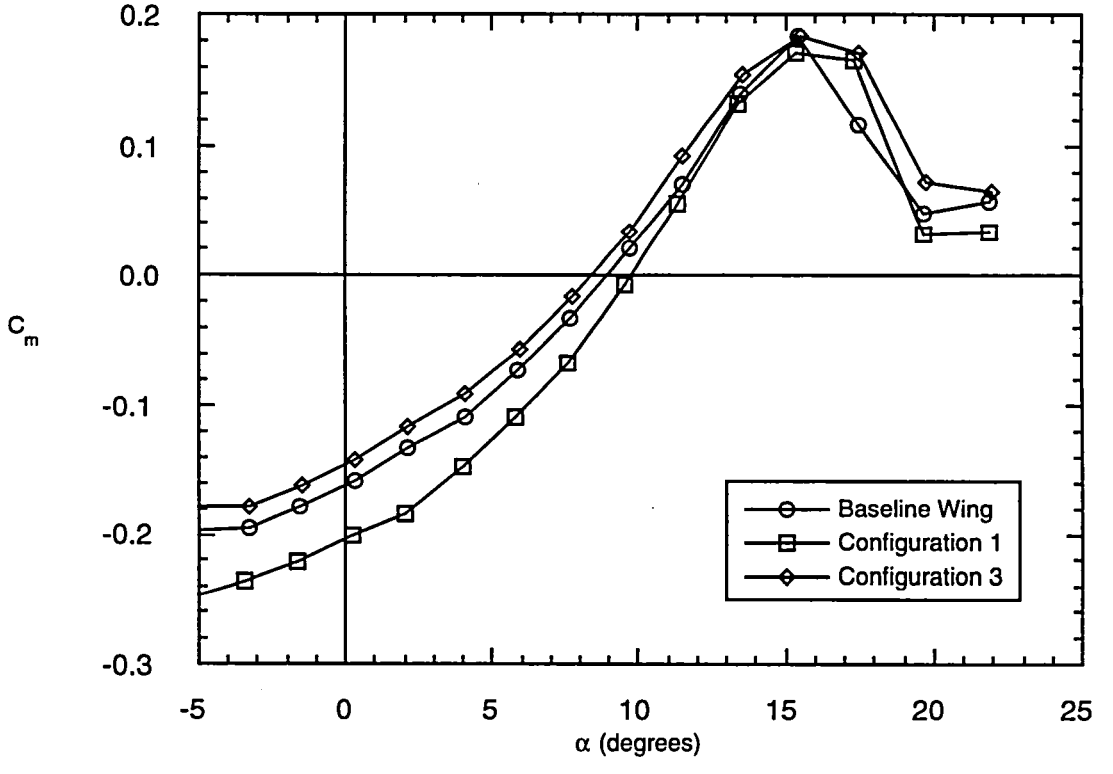

Figure 62. Effect of Gurney flap Configurations 1 and 3 on the pitching moment coefficient; $\delta_f = 20°$.

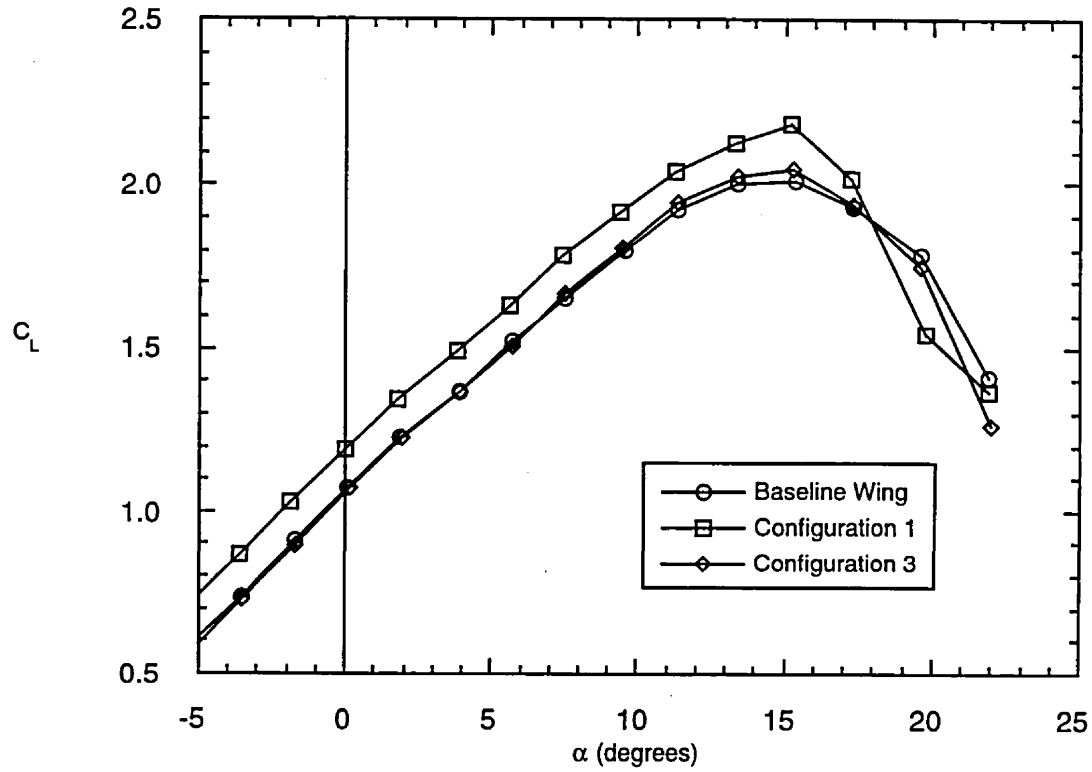

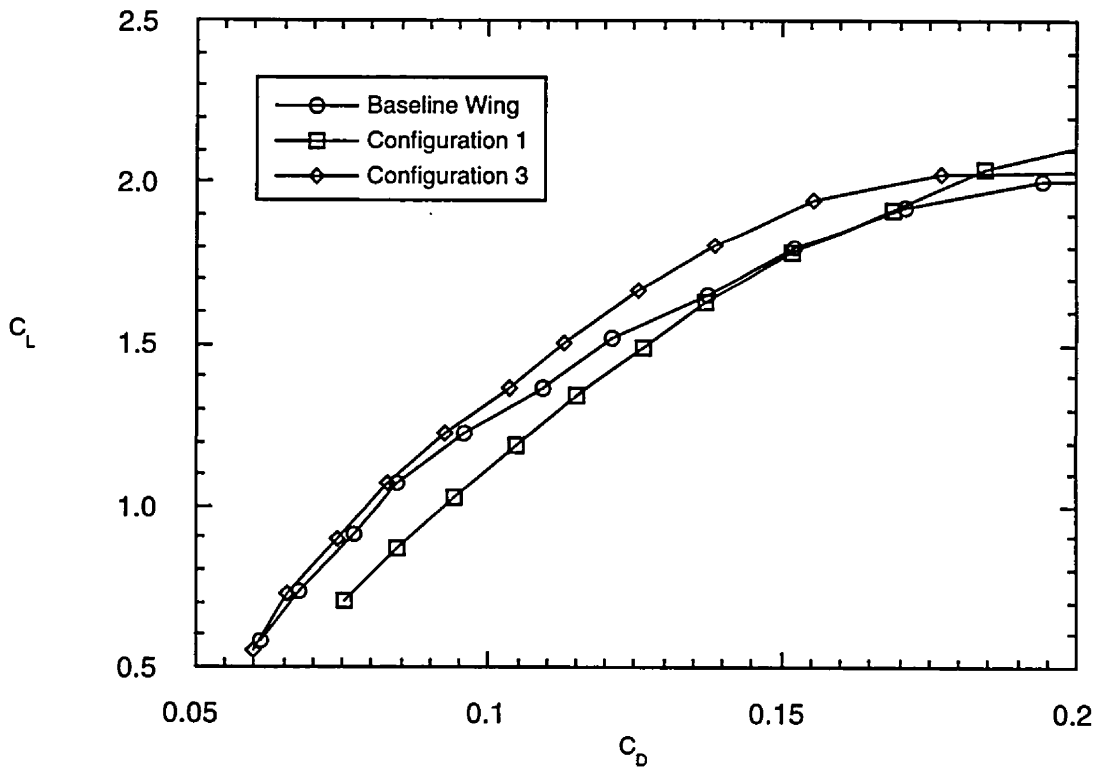

Figure 63. Effect of Gurney flap Configurations 1 and 3 on the lift and drag coefficients; $\delta_f = 30°$.

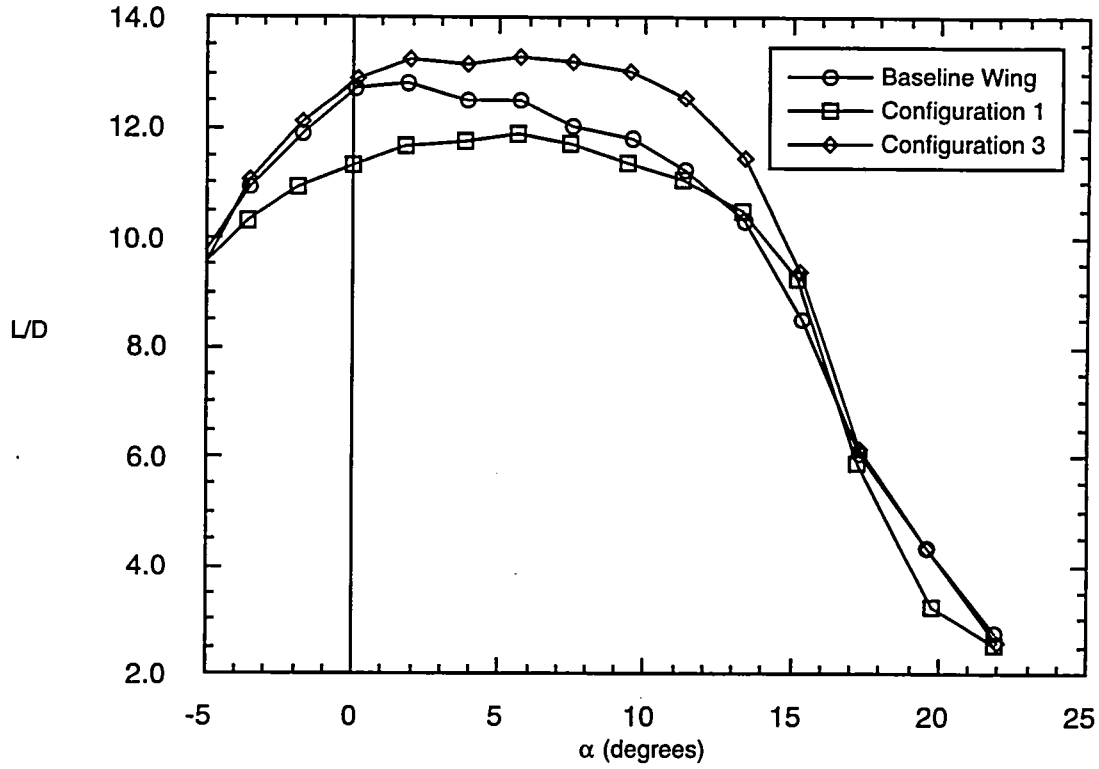

Figure 64. Effect of Gurney flap Configurations 1 and 3 on the lift-to-drag ratio; $\delta_f = 30°$.

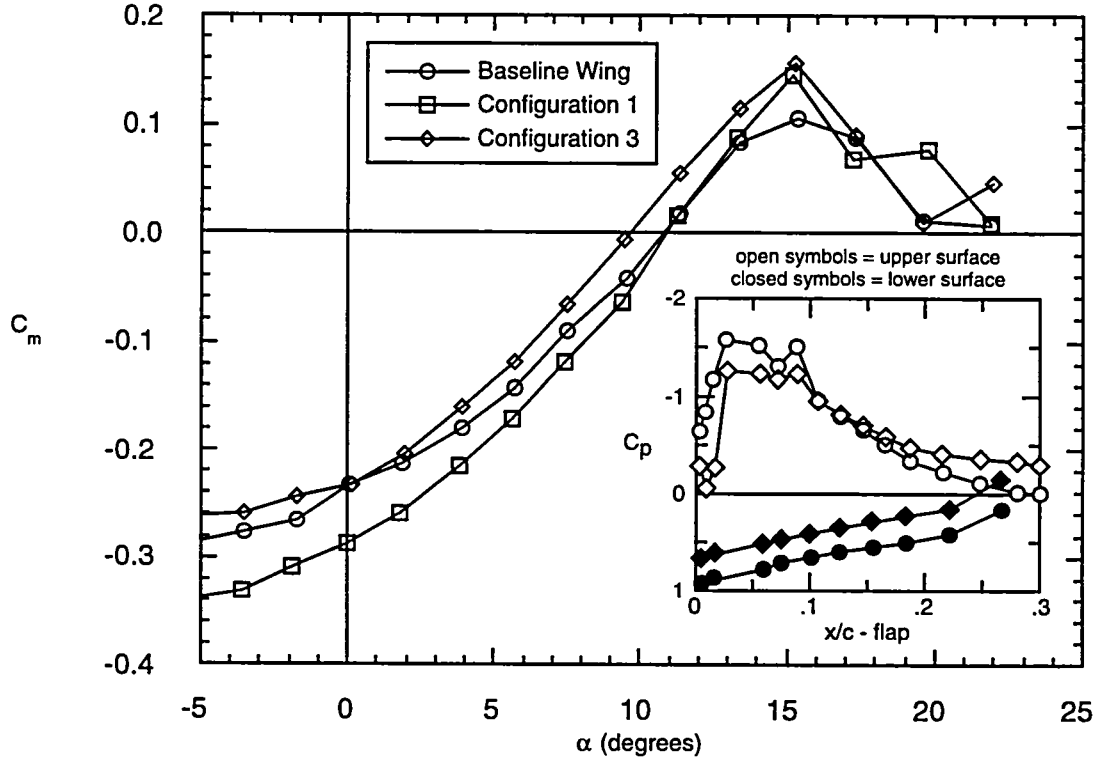

Figure 65. Effect of Gurney flap Configurations 1 and 3 on the pitching moment coefficient; $\delta_f = 30°$.

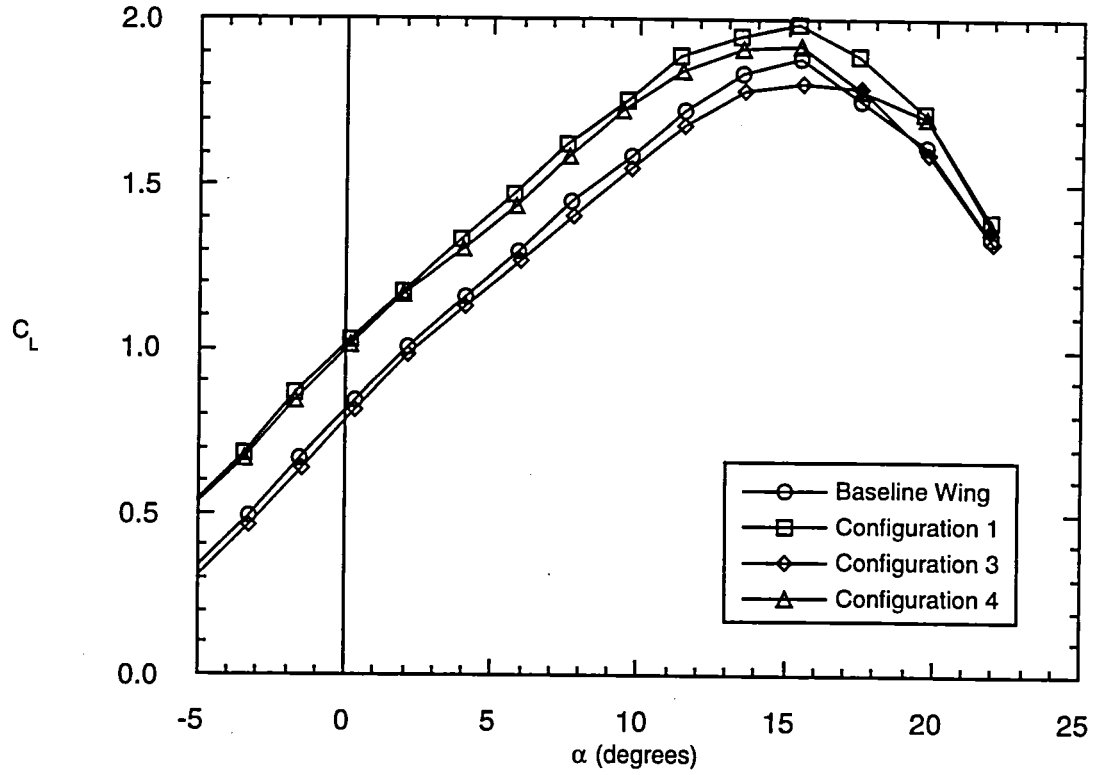

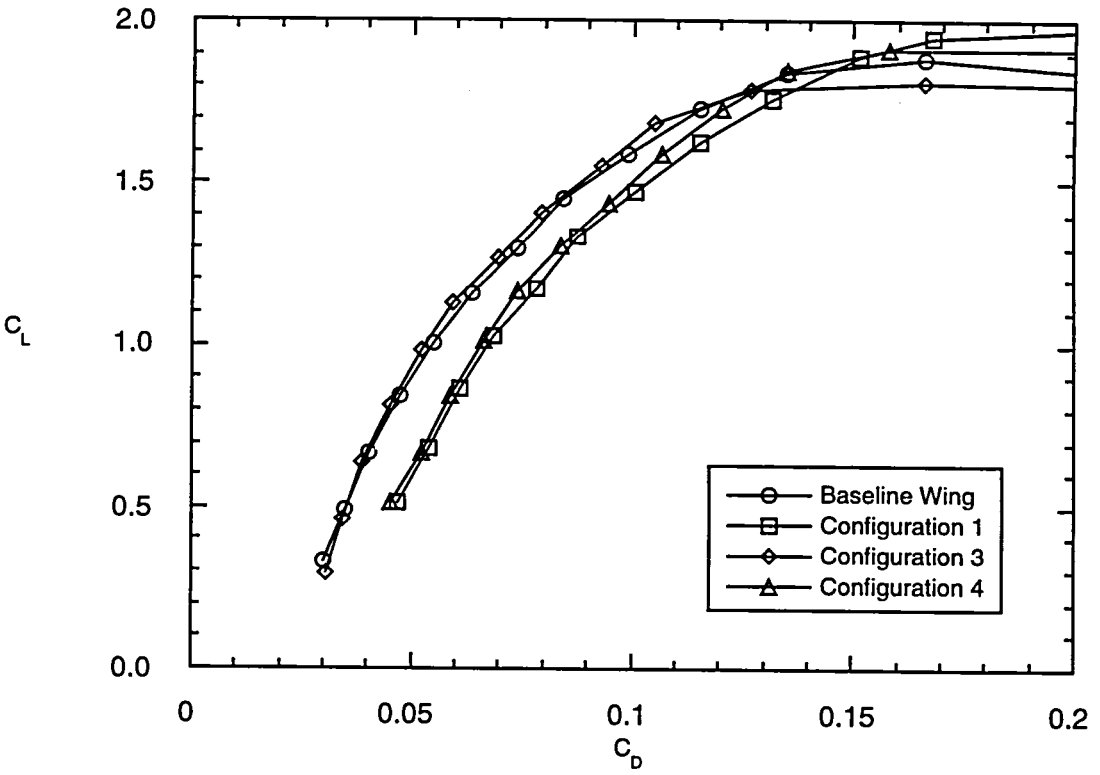

Figure 66. Effect of Gurney flap Configurations 1, 3, and 4 on the lift and drag coefficients; $\delta_f = 20°$.

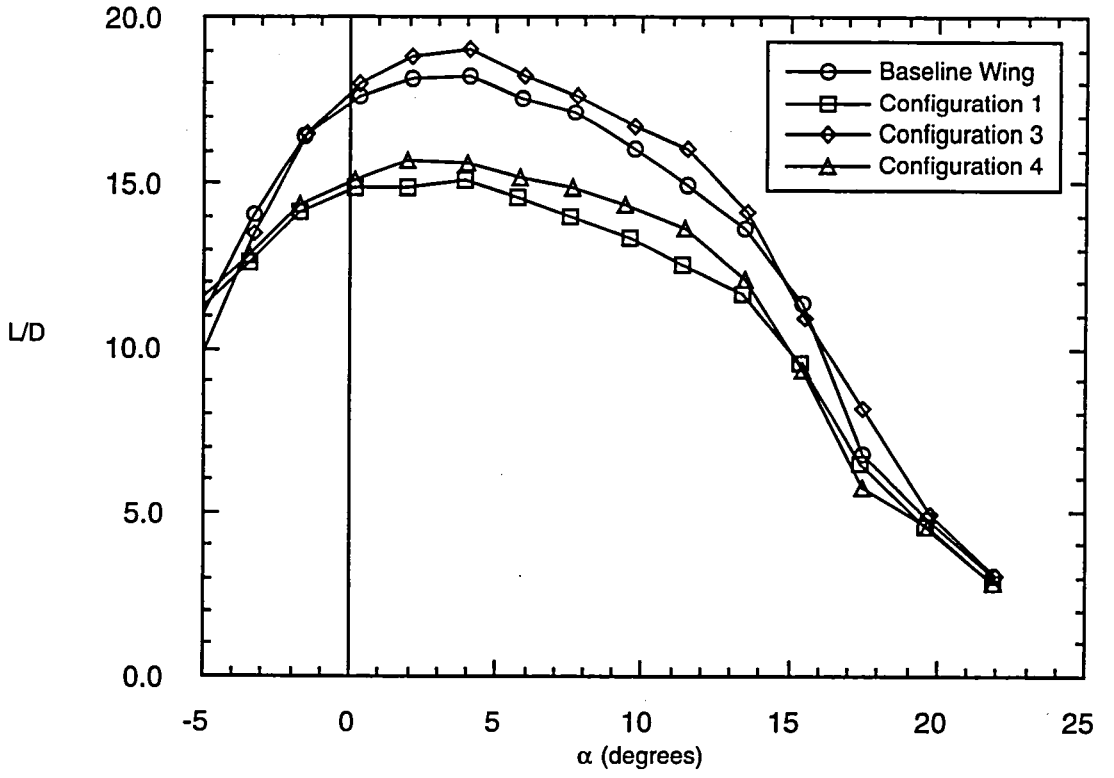

Figure 67. Effect of Gurney flap Configurations 1, 3, and 4 on the lift-to-drag ratio; $\delta_f = 20°$.

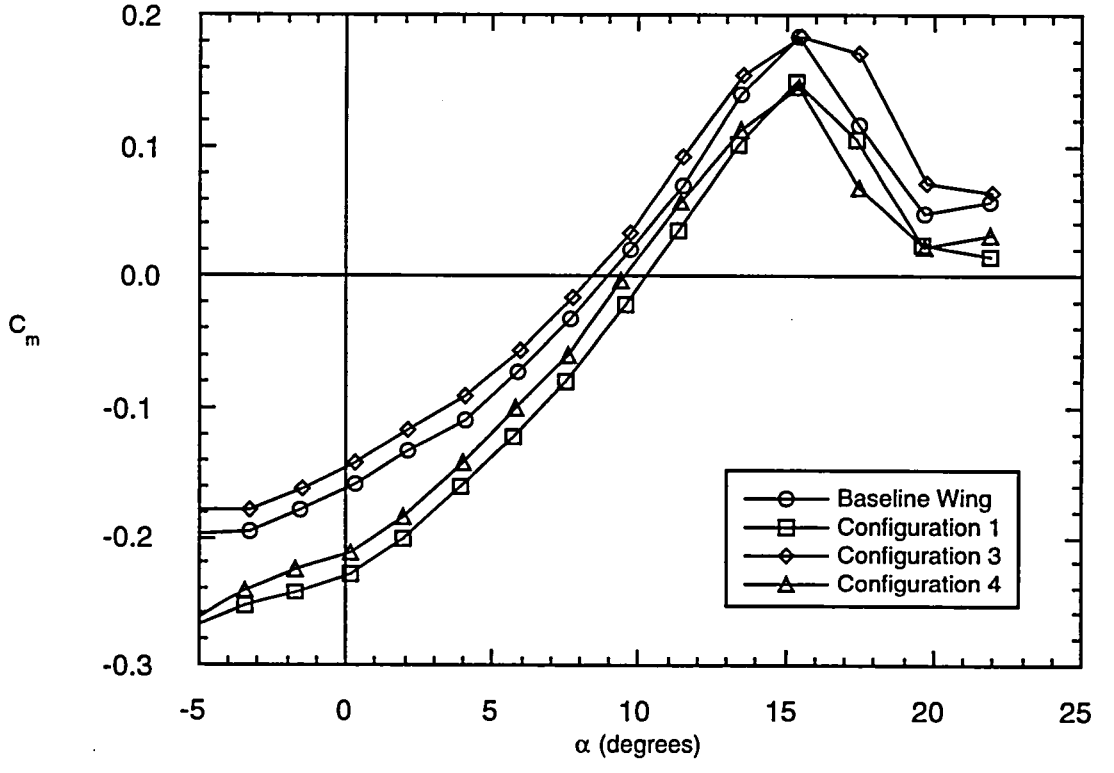

Figure 68. Effect of Gurney flap Configurations 1, 3, and 4 on the pitching moment coefficient; $\delta_f = 20°$.

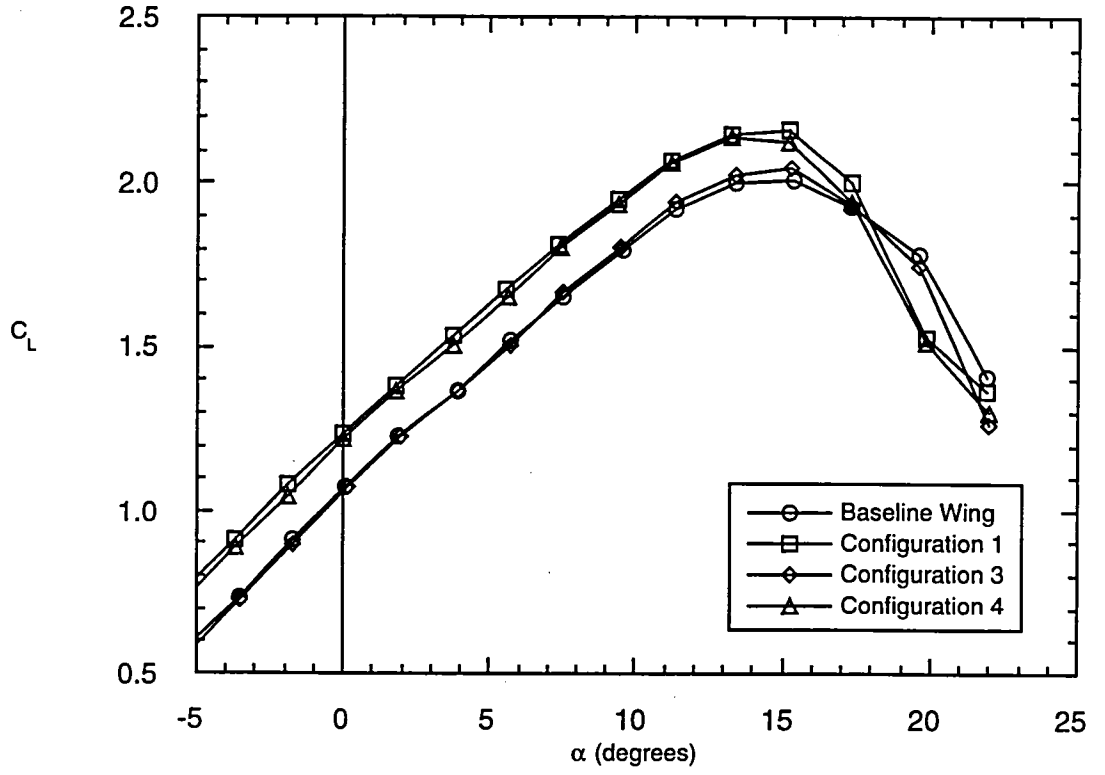

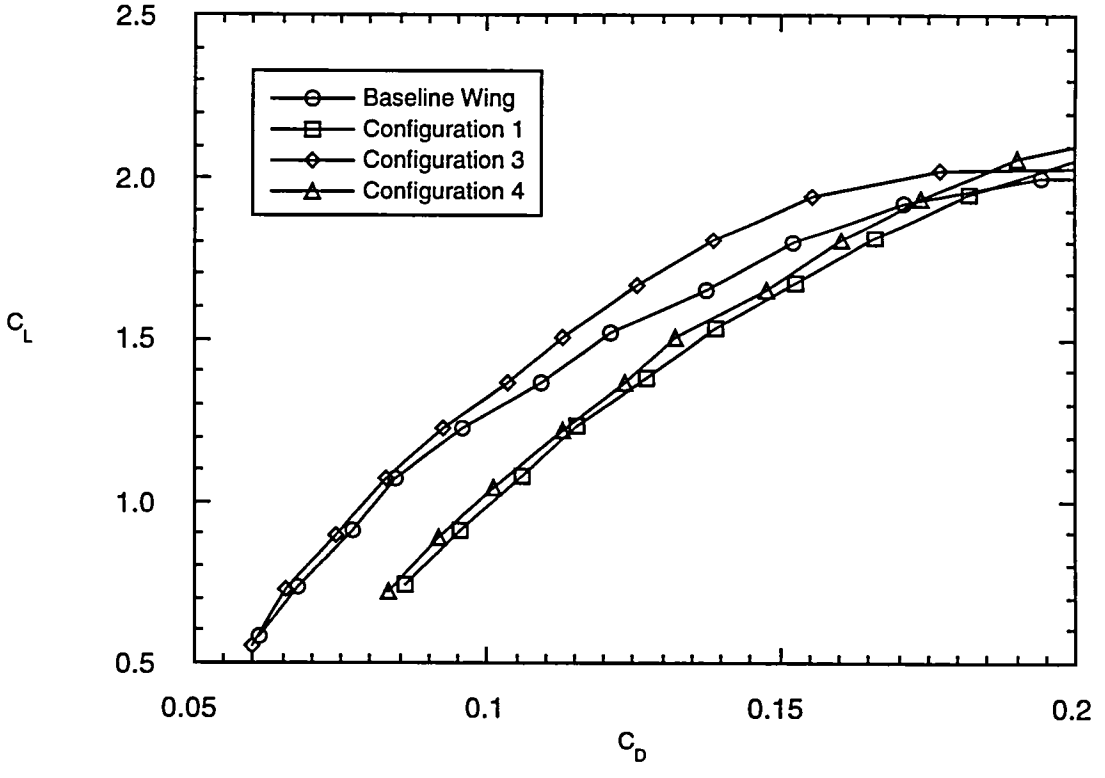

Figure 69. Effect of Gurney flap Configurations 1, 3, and 4 on the lift and drag coefficients; $\delta_f = 30°$.

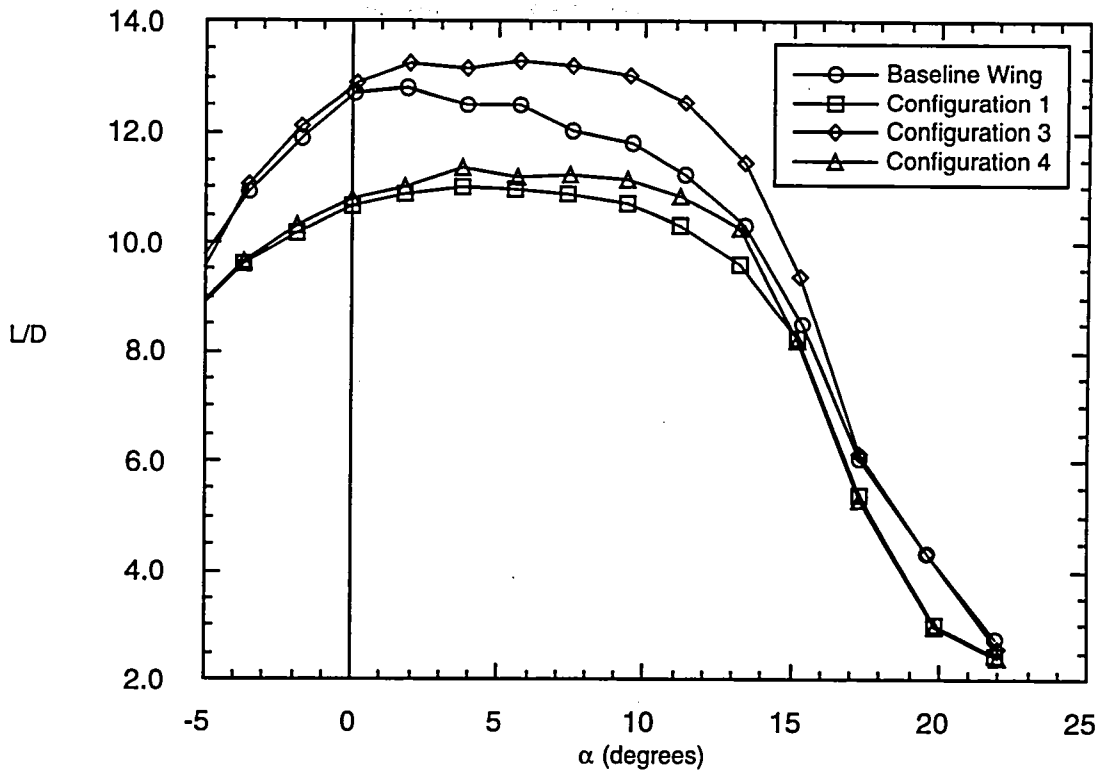

Figure 70. Effect of Gurney flap Configurations 1, 3, and 4 on the lift-to-drag ratio; $\delta_f = 30°$.

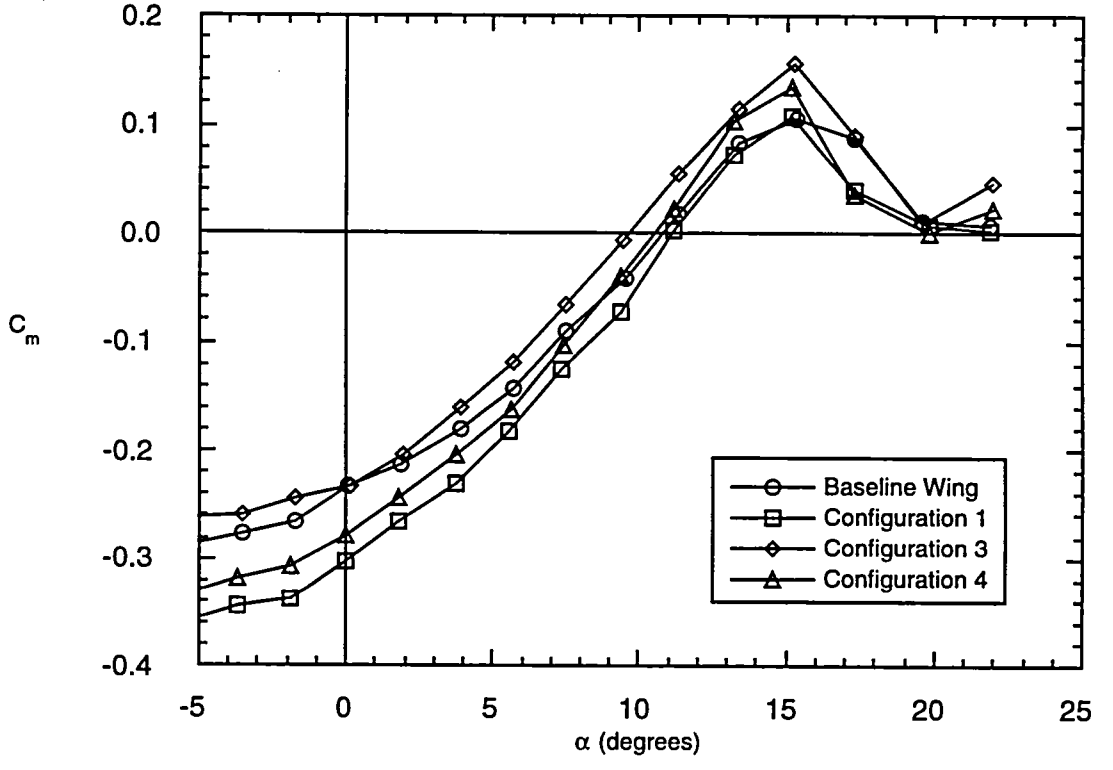

Figure 71. Effect of Gurney flap Configurations 1, 3, and 4 on the pitching moment coefficient; $\delta_f = 30°$.

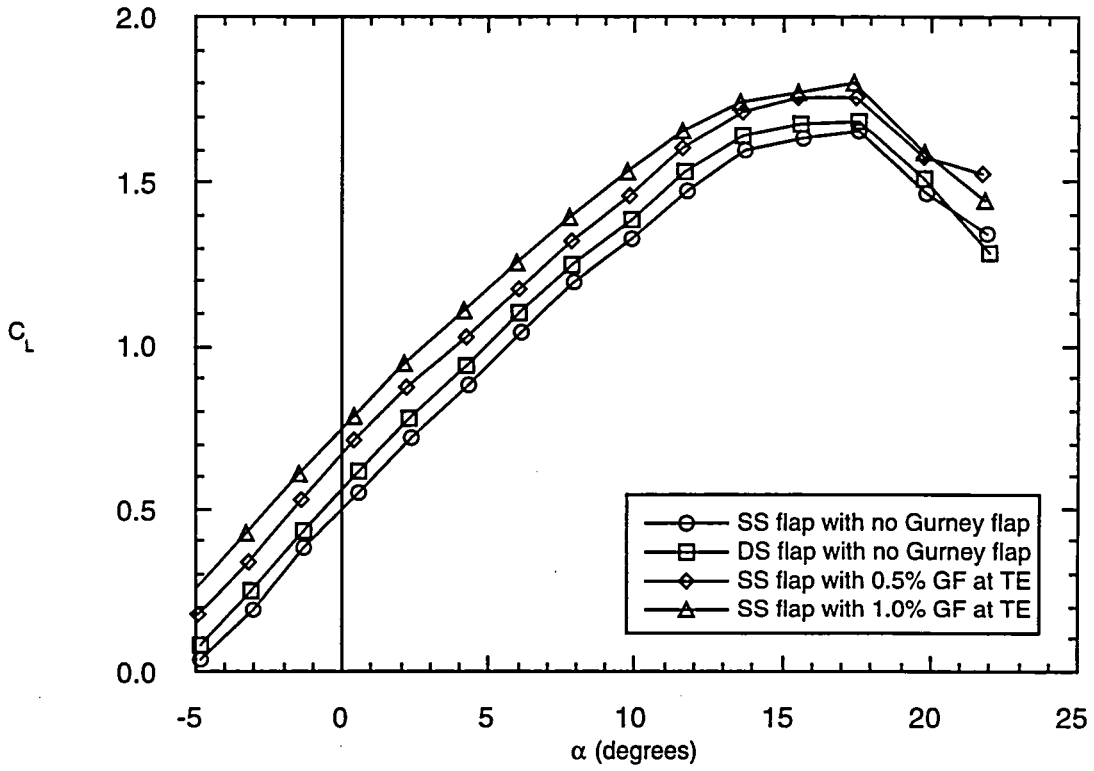

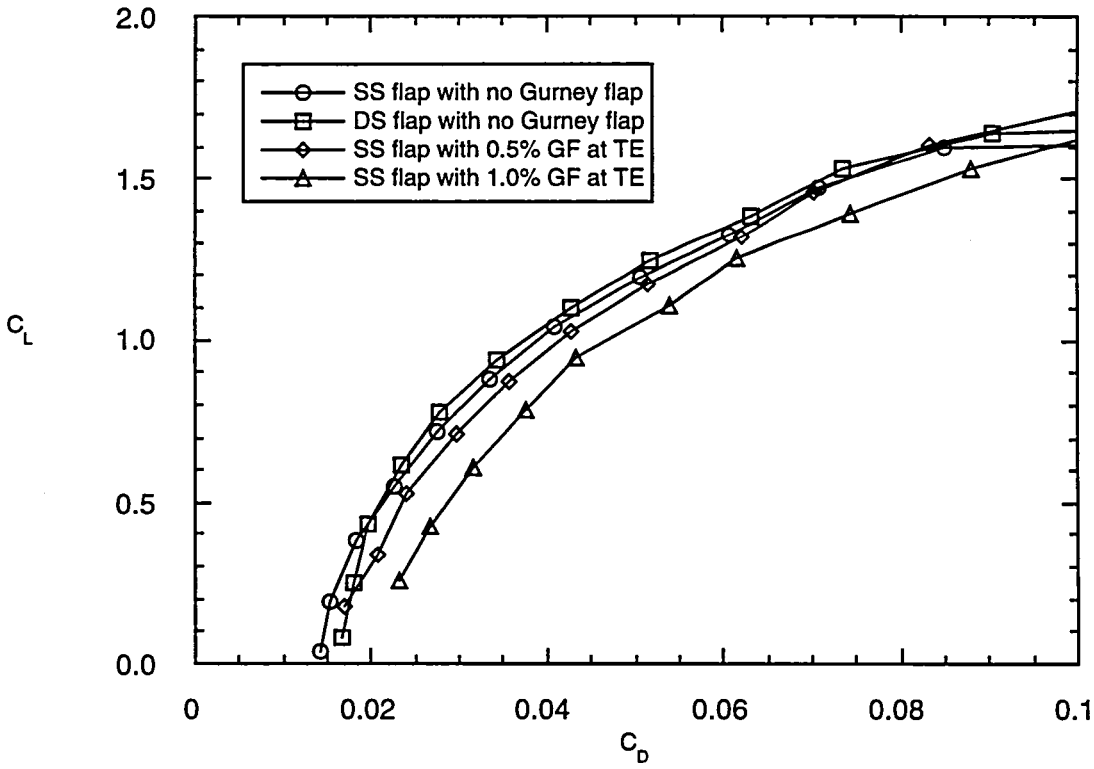

Figure 72. Comparison of the single-slotted flap and double-slotted flap (with no Gurney flap) effects to the 0.5% Gurney flap and 1.0% Gurney flap (in Configuration 1) effects on the lift and drag coefficients; $\delta_f = 10°$.

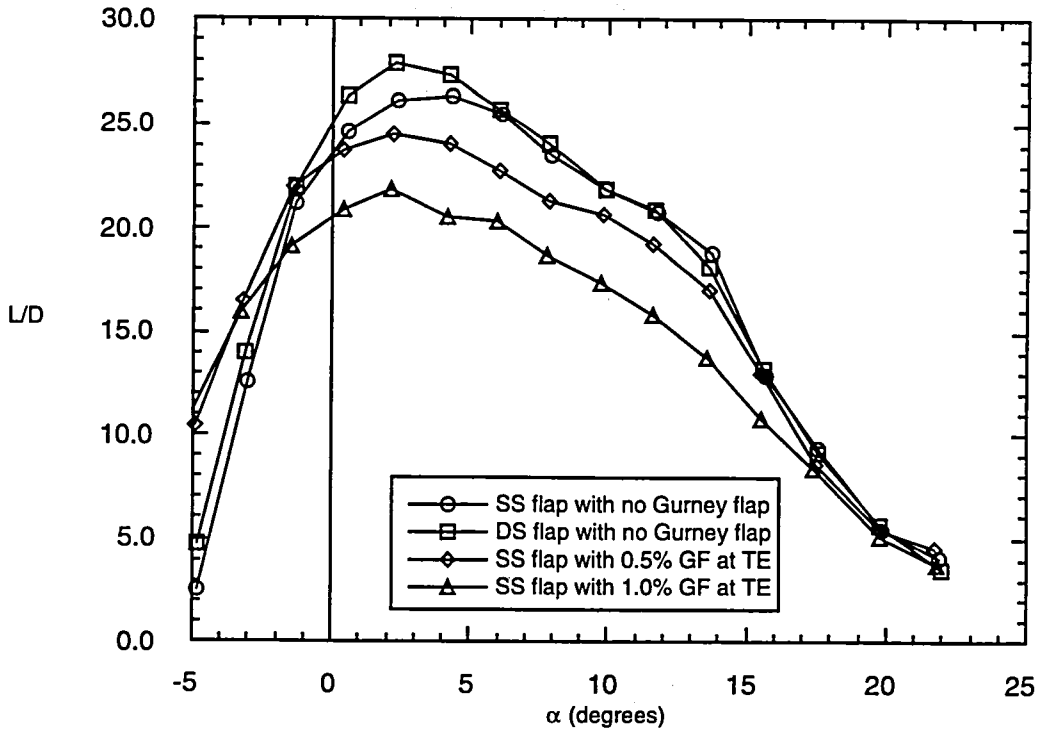

Figure 73. Comparison of the single-slotted flap and double-slotted flap (with no Gurney flap) effects to the 0.5% Gurney flap and 1.0% Gurney flap (in Configuration 1) effects on the lift-to-drag ratio; $\delta_f = 10°$.

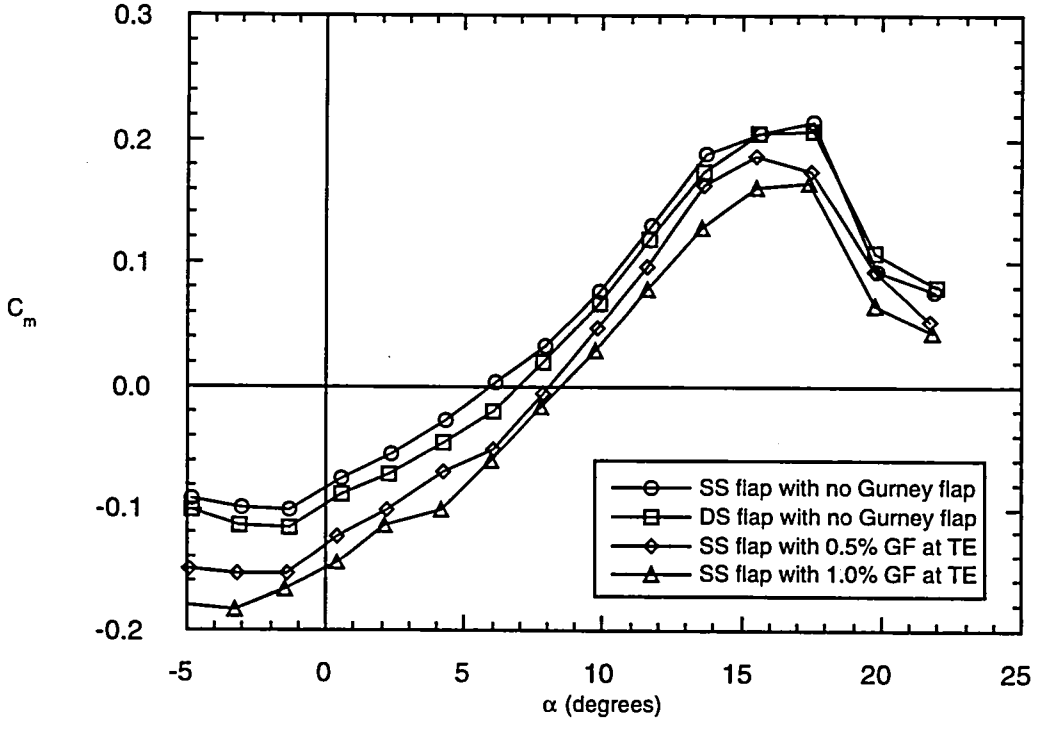

Figure 74. Comparison of the single-slotted flap and double-slotted flap (with no Gurney flap) effects to the 0.5% Gurney flap and 1.0% Gurney flap (in Configuration 1) effects on the pitching moment coefficient; $\delta_f = 10°$.

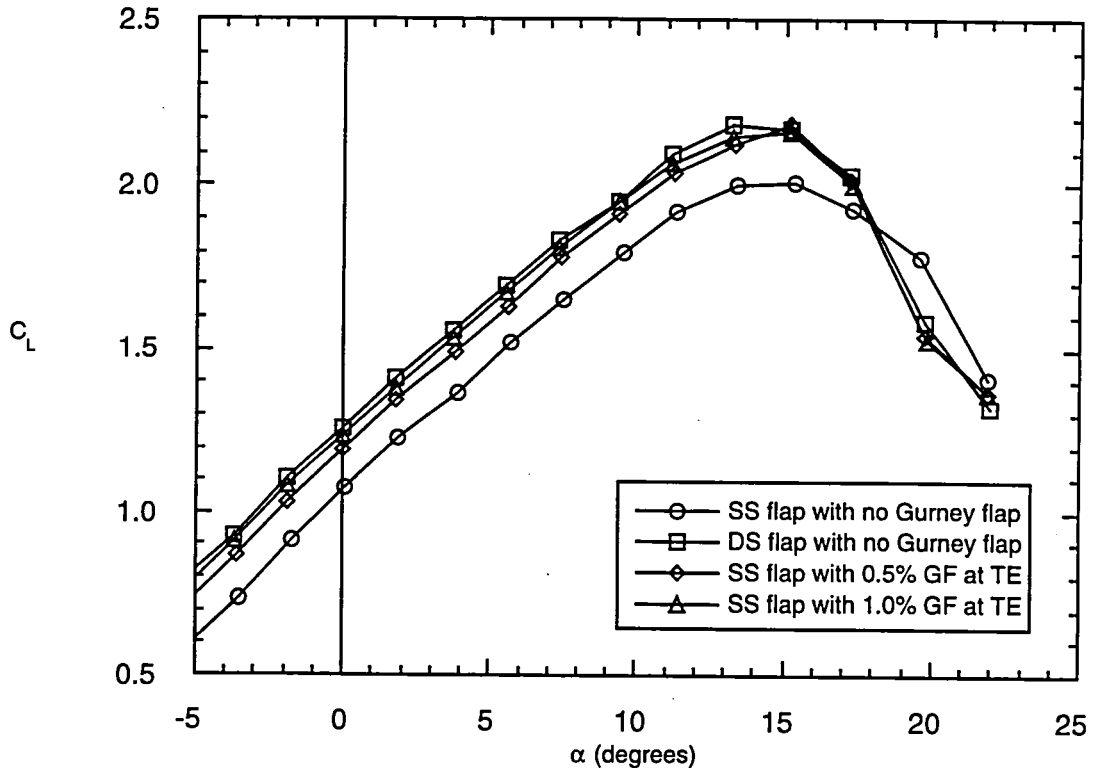

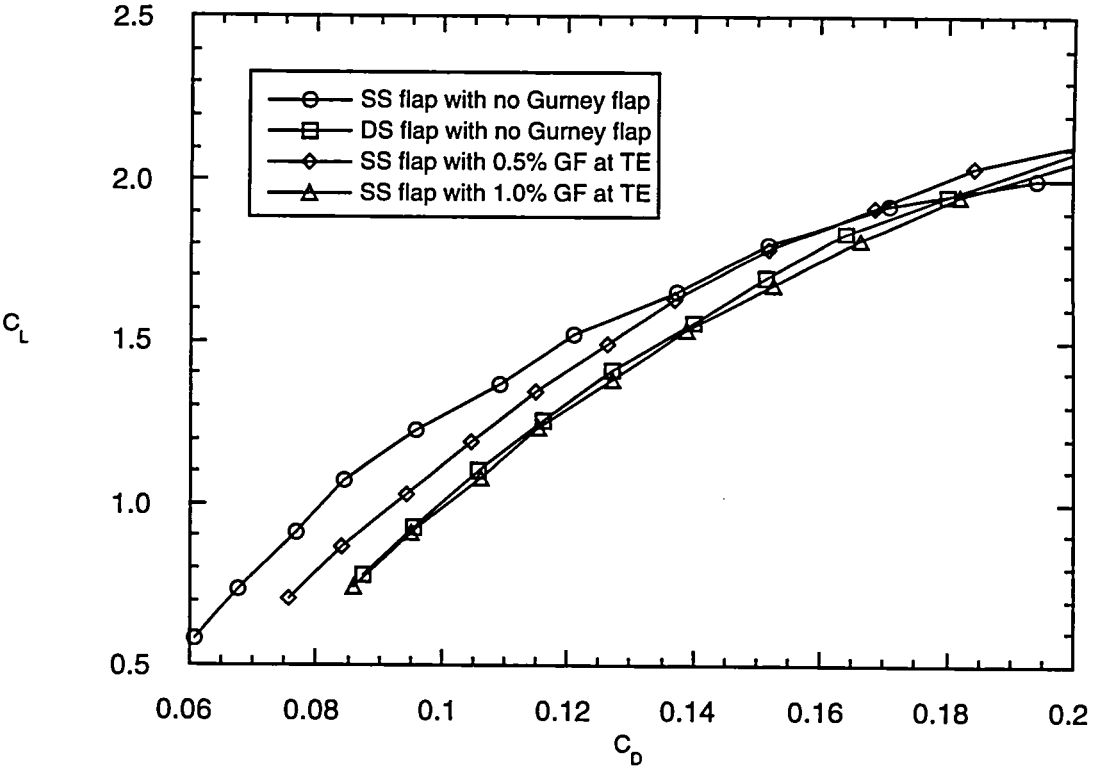

Figure 75. Comparison of the single-slotted flap and double-slotted flap (with no Gurney flap) effects to the 0.5% Gurney flap and 1.0% Gurney flap (in Configuration 1) effects on the lift and drag coefficients; $\delta_f = 30°$.

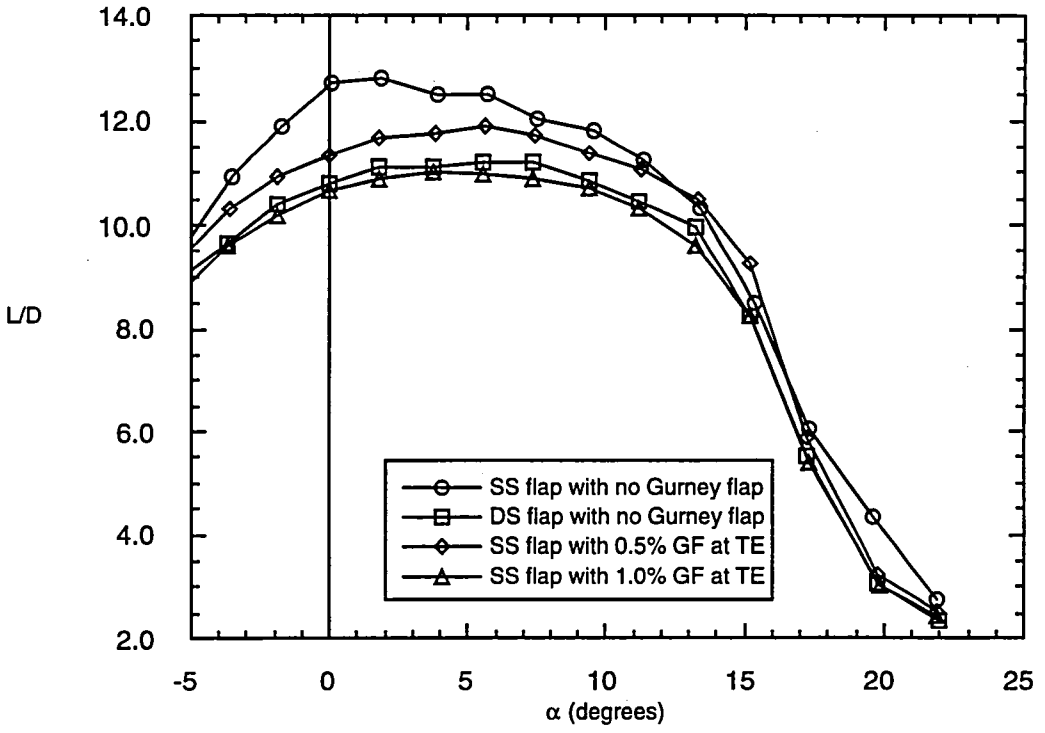

Figure 76. Comparison of the single-slotted flap and double-slotted flap (with no Gurney flap) effects to the 0.5% Gurney flap and 1.0% Gurney flap (in Configuration 1) effects on the lift-to-drag ratio; $\delta_f = 30°$.

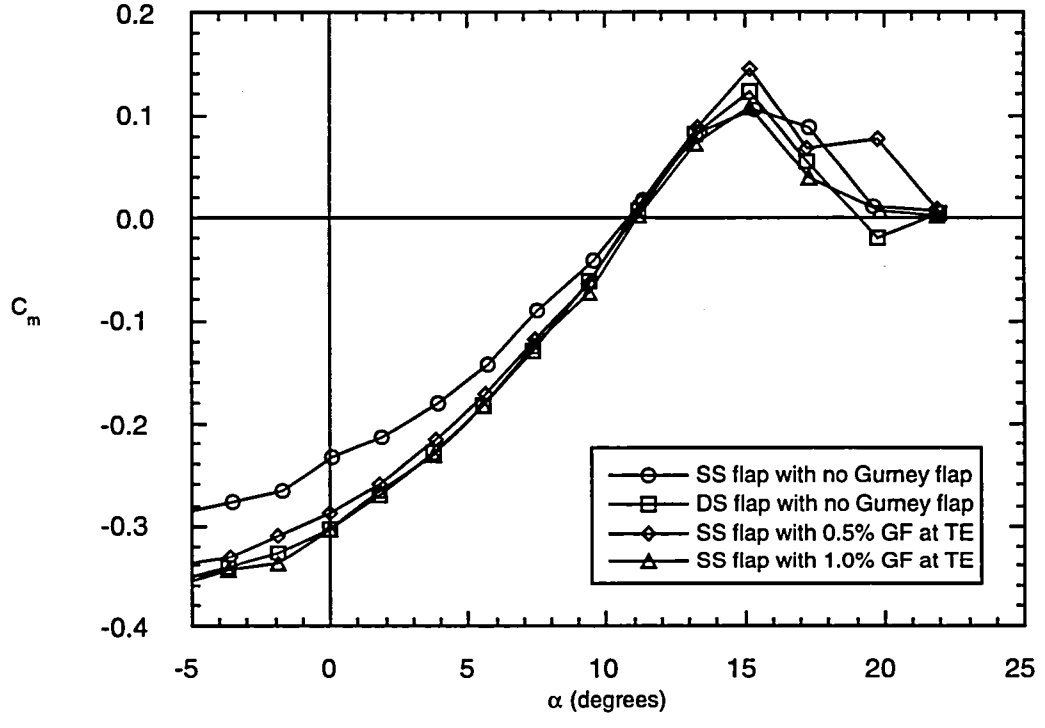

Figure 77. Comparison of the single-slotted flap and double-slotted flap (with no Gurney flap) effects to the 0.5% Gurney flap and 1.0% Gurney flap (in Configuration 1) effects on the pitching moment coefficient; $\delta_f = 30°$.

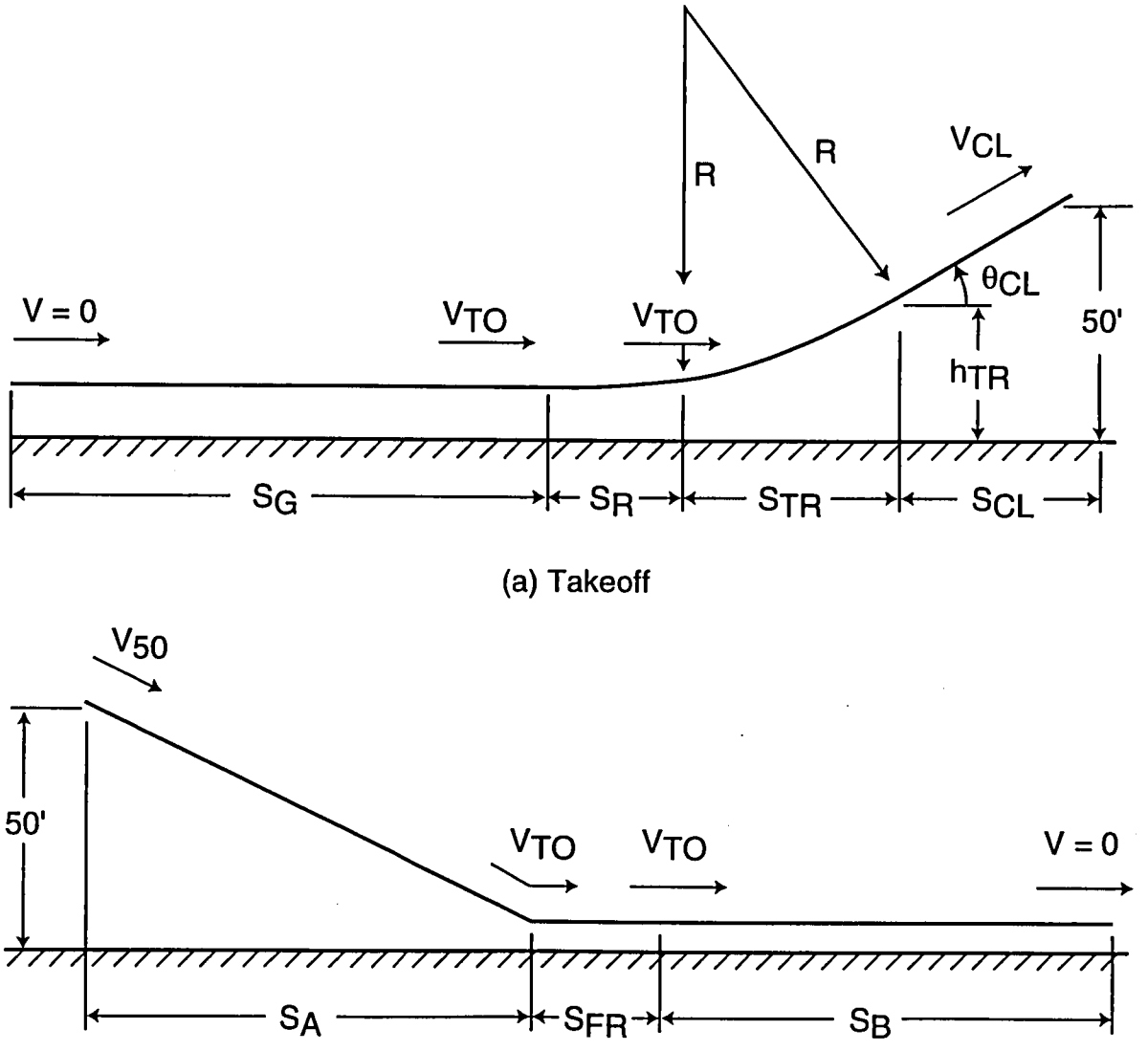

Figure 78. Schematic of takeoff and landing distances for an aircraft over a 50-foot obstacle (reference 26).

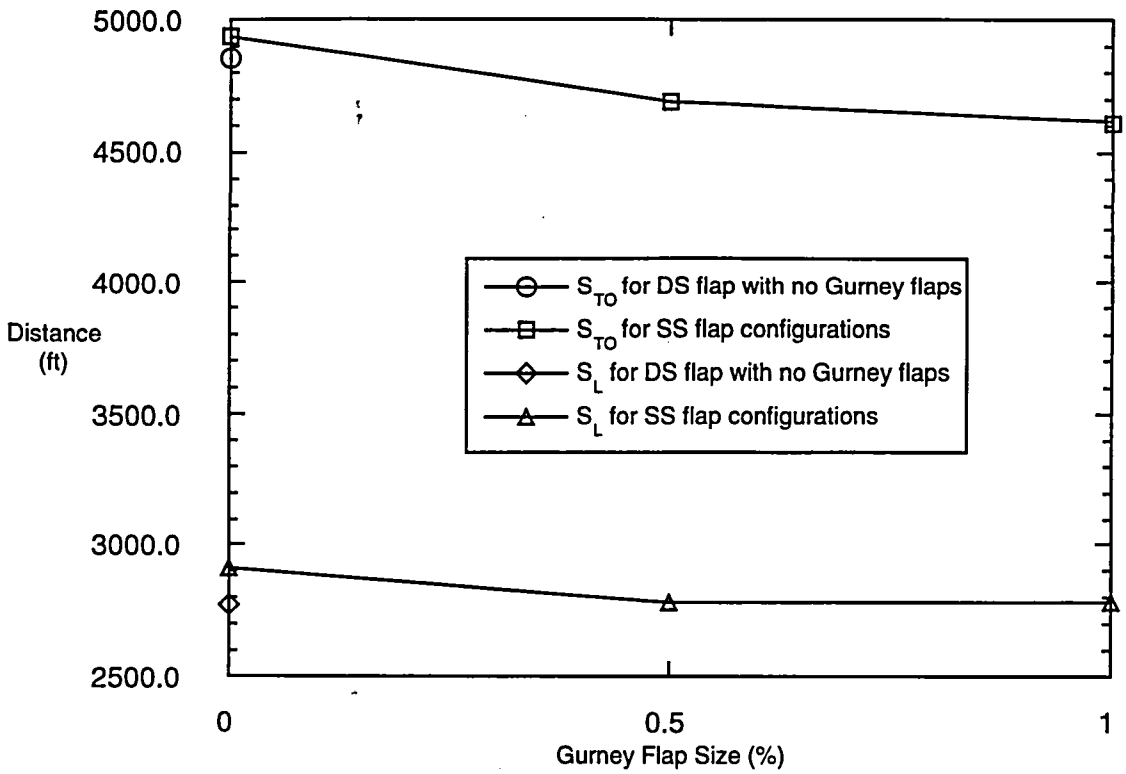

Figure 79. Takeoff and landing distance performance analysis.

NASA Technical Library
3 1176 01422 7145

DO NOT REMOVE SLIP FROM MATERIAL

Delete your name from this slip when returning material to the library.

NAME	DATE	MS
~~L. Wood~~	~~5-98~~	~~280~~
~~Dan Neuhart~~	~~12/04~~	~~170~~

NASA Langley (Rev. Dec. 1991) RIAD N-75